Summer 8-14-2015

Characteristics of Exocytosis and Endocytosis in Photoreceptors

Karlene M. Cork
University of Nebraska Medical Center

CHARACTERISTICS OF EXOCYTOSIS AND ENDOCYTOSIS IN PHOTORECEPTORS

By

Karlene Cork

A DISSERTATION

Presented to the Faculty of

the University of Nebraska Graduate College

in Partial Fulfillment of the Requirements

for the Degree of Doctor of Philosophy

Pharmacology and Experimental Neuroscience

Under the Supervision of Professor Wallace B. Thoreson, Ph.D.

University of Nebraska Medical Center
Omaha, Nebraska

July, 2015

Supervisory Committee:
Keshore Bidasee, Ph.D.
Anna Dunaevsky, Ph.D.
Myron L. Toews, Ph.D.

Acknowledgements

I would like to thank my mentor, Dr. Wallace B. Thoreson, for his guidance and support throughout my graduate study. Thanks also to members of the Thoreson laboratory for assistance including Dr. Minghui Chen and Dr. Matthew Van Hook. I would also like to thank my dissertation committee members, Dr. Keshore R. Bidasee, Dr. Anna Dunaevsky, and Dr. Myron L. Toews, for their suggestions on my research work.

Table of Contents

Table of Figures

CHARACTERISTICS OF EXOCYTOSIS AND ENDOCYTOSIS IN PHOTORECEPTORS

Karlene M. Cork, Ph.D.

University of Nebraska, 2015

Supervisor: Wallace B. Thoreson, Ph.D.

Photoreceptors signal changes in light intensity to downstream retinal neurons through the exocytosis of glutamate-containing synaptic vesicles. The maintenance of the vesicle exocytosis and endocytosis process is essential for ongoing synaptic signaling. This study investigated the properties of exocytosis and endocytosis in photoreceptors and their role in ongoing neurotransmission.

I used electrophysiology and imaging techniques to study the properties of vesicle exocytosis and endocytosis in photoreceptors. First, we examined baseline release in photoreceptors that occurs in the absence of depolarizing stimulation. We measured mEPSCs in whole cell patch clamp recordings from horizontal cells. After inhibiting Ca^{2+} influx and efflux and increasing intracellular Ca^{2+} buffering, we found that mEPSCs persisted, indicating that a portion of the baseline release occurs by a Ca^{2+}-independent mechanism. Presynaptic recordings from rods and cones confirmed that glutamate release continues after Ca^{2+} is blocked. There was a decrease in frequency and amplitude of Ca^{2+}-independent events. Visualization of individual exocytosis events by TIRF microscopy showed that Ca^{2+}-independent release can occur at non-ribbon release sites. Following exocytosis, vesicles are retrieved by endocytosis and reenter the vesicle cycle. We measured exocytosis and endocytosis from membrane capacitance changes evoked by depolarizing steps in voltage clamped rods. Endocytosis in rods was rapid relative to other neurons with an average time constant of

<200 ms. The endocytosis kinetics in rods slowed with more vesicle exocytoisis and greater Ca^{2+} influx.

Together these studies identified the sites and vesicle pools involved in Ca^{2+}-independent baseline release from photoreceptors and found that endocytosis kinetics in rods are rapid and depend upon endocytic load and local Ca^{2+} levels.

Chapter 1

Exocytosis and endocytosis maintain neurotransmission by photoreceptors

Photoreceptors in the retina are the initial site of light detection. Photoreceptors then transmit information about the light signal to second-order neurons within the retinal circuit through the exocytosis of glutamate-filled vesicles. To maintain signal transmission, neurons must sustain release of synaptic vesicles via exocytosis for long periods of time (Beutner et al., 2001; Wu et al., 2007; Alabi & Tsien, 2012). This process requires tight coupling between exocytosis and endocytosis (Gundelfinger et al., 2003; Haucke et al., 2011), with vesicles retrieved via endocytosis after their exocytosis (Pysh & Wiley, 1974; Miller & Heuser, 1984; LoGiudice & Matthews, 2007; Barg & Machado, 2008; Smith et al., 2008; Xue & Mei, 2011).

Maintaining neuronal signaling is central to many biological functions. The significance of this process is confirmed by studies showing that disrupting exocytosis and endocytosis, thereby impairing continued signal transmission, can lead to disease. Impairment in exocytosis has been found to contribute to a number of diseases. Knock-out models have shown that loss of central components of endocytosis including clathrin, AP2, epsin, and dynamin results in embryonic lethality. Less severe mutations in proteins involved in endocytosis have been linked to diseases (Smith et al., 2005; Keating, 2008; McMahon & Boucrot, 2011). The link between endocytosis impairment and neurological disorders includes Alzheimer ’s disease (Harold et al., 2009; Seshadri et al., 2010), Charcot-Marie-Tooth disease (Züchner et al., 2005), schizophrenia (Prabakaran et al., 2004; Clark et al., 2006; Pennington et al., 2008; English et al., 2009), and bipolar disorder (English et al., 2009; Saito et al., 2001). One specific endocytic protein linked to neurodegeneration is cysteine string protein α, a presynaptic vesicle protein that regulates endocytosis via interaction with dynamin 1 (Nosková et al.,

2011; Zhang et al., 2012). Another example is amphiphysin, a protein involved in recruiting dynamin to sites of endocytosis (David et al., 1996), which is associated with the CNS disorder stiff person syndrome (Krishna et al., 2012; Hansen et al., 2013).

Eye-specific disease has also been linked to proteins involved in early steps of the endocytic pathway (Erdmann et al., 2007). For example, Lowe Syndrome is characterized by major abnormalities of the nervous system and the eyes including cataracts and in some instances glaucoma (Kawano et al., 1998). Our study investigates the mechanisms by which the vesicle cycle maintains neurotransmission and can thus provide insight into the functional basis of these diseases related to exocytosis and endocytosis dysfunction. This work addresses outstanding questions about neurotransmission by photoreceptors: Does Ca^{2+}-independent exocytosis from photoreceptors occur (Chapter 2)? What factors impact the kinetics of endocytosis in rods (Chapter 3)? Overall, we found that Ca^{2+} is involved in the regulation of both exocytosis and endocytosis in photoreceptors. Ca^{2+} may play a role the tight coupling between these two steps in the vesicle cycle, which is required for ongoing synaptic transmission.

1.1 Anatomy of the vertebrate retina

1.1a Overview of retinal anatomy

The retina is the light-sensitive nerve tissue that lines the back of the eye. The retina is made up of five major types of neurons, photoreceptors, bipolar cells, horizontal cells, amacrine cells, and retinal ganglion cells, arranged in layers (Fig 1.). The outer nuclear layer contains the cell bodies of the rod and cone photoreceptors. The outer plexiform layer contains the synapses between the photoreceptors and the horizontal and bipolar cells. The inner nuclear layer contains the cell bodies of the horizontal, bipolar, and amacrine cells. The inner plexiform layer contains the synapses between the bipolar cells and the amacrine and retinal ganglion cells. The ganglion cell layer contains the cell bodies of the retinal ganglion cells. Müller cells are the major glial cell type within the retina. The anatomy of the vertebrate retina is highly conserved. In our studies, we used the tiger salamander (*Ambystoma tigrinum*) retina as our model system, because the size of the salamander photoreceptors makes them amenable for electrophysiology and imaging experiments.

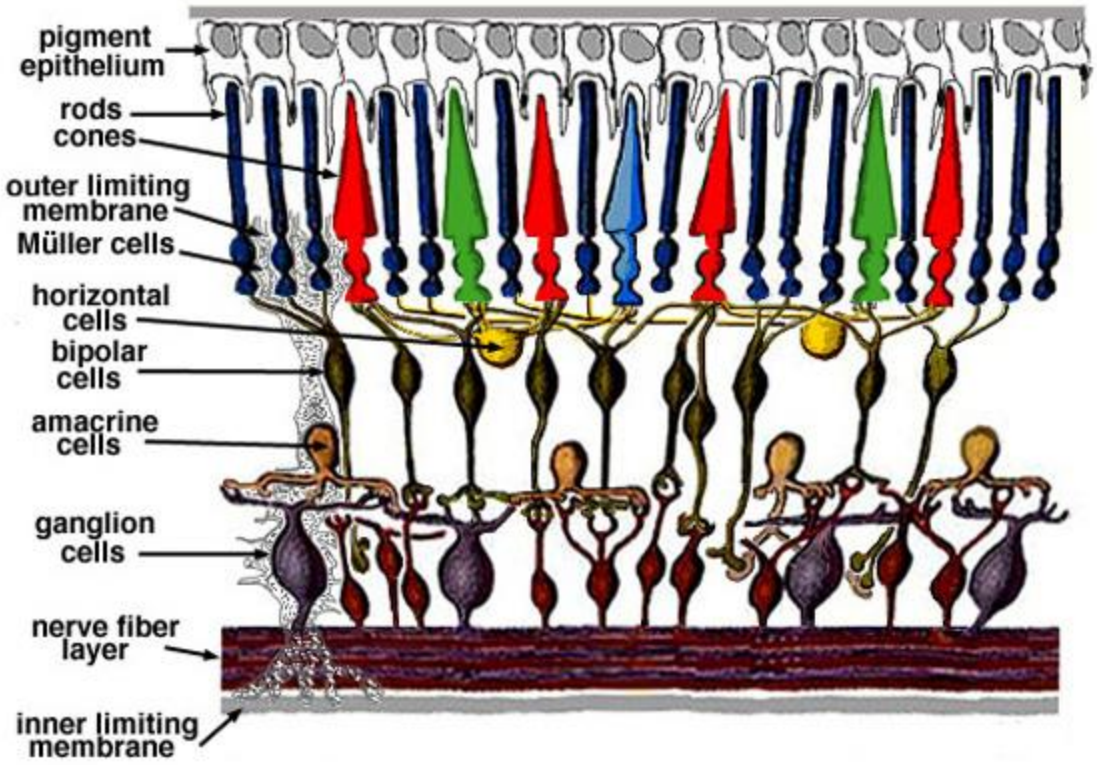

Figure 1: Retina organization.

The retina is made up of 5 major types of neurons: photoreceptors, bipolar cells, horizontal cells, ganglion cells, and amacrine cells. The retina has three layers of nerve cell bodies and two synaptic layers. The cell bodies of both rod and cone photoreceptors are located in the outer nuclear layer. The cell bodies of the bipolar, horizontal, and amacrine cells are located in the inner nuclear layer. The cell bodies of ganglion cells are located in the ganglion cell layer. The first synaptic layer is the outer plexiform layer where synapses between rod and cone photoreceptors and bipolar and horizontal cells are located. The second synaptic layer is the inner plexiform layer where synapses among bipolar, amacrine, and ganglion cells are located. The retinal pigment epithelium is a layer of cells that lies behind the retina and supports the function of the neuronal cells of the retina in many ways such as serving as part of the blood-retinal barrier and regenerating bleached photopigment. Müller glial cells extend vertically through all layers of the retina. Image from *Simple Anatomy of the Retina* by Helga Kolb, reproduced under a Creative Commons license.

1.1b Photoreceptor function and structure

Photoreceptors are categorized into rods and cones based on differences in their structure and function. Rods are involved in vision during dim-light conditions. Rods are extremely sensitive to light and are able to detect even single photons (reviewed by Sampath & Rieke, 2004). The rod cell is comprised of four main parts- outer segment, inner segment, cell body, and synaptic terminal. In the rod outer segment, the plasma membrane encloses a stack of disk-shaped organelles. The disk membrane is packed with rhodopsin, the rod visual pigment. The structure of the rod outer segments provides a large surface area to increase the efficiency of light absorption, which is especially important in low-light conditions. A thin cilium connects the rod outer and inner segments, which form two functionally distinct regions within the rod. The inner segment contains the mitochondria, ribosomes, and membranes for rhodopsin and other protein synthesis. The cell body contains the nucleus. The synaptic terminal is the site at which rods synapse with second order neurons- horizontal and bipolar cells.

Cones are less sensitive in low-light levels than rods and are primarily involved in vision in bright light conditions. Cones have faster kinetics during phototransduction allowing perception of finer details and more rapid changes in images than in rod based vision. Cones are also the cell type responsible for color vision based on different cone opsin photopigments. The different opsins found in different cone types are sensitive to different wavelengths of light. In humans, there are three cone subtypes: S, which are sensitive to short “blue” wavelengths; M, which are sensitive to middle “green” wavelengths; and L, which are sensitive to long “red” wavelengths (Schnapf et al., 1988). The structure of cones differs slight from rods, with cones typically having smaller outer segments. The pigment-containing disks in cones are formed by invaginations of the

plasma membrane, unlike the fully enclosed rod disks. As in rods, cones form synapses with second-order neurons.

1.1c Horizontal and bipolar cells

Horizontal and bipolar cells are the second neurons in the visual pathway after photoreceptors. Horizontal cells (HC), whose cell bodies are in the inner nuclear layer, are inhibitory interneurons that receive synaptic input from photoreceptors in the outer plexiform layer. When photoreceptors release glutamate, the HC response is mediated by its AMPA type postsynaptic ionotropic glutamate receptors. When light stimulation causes a reduction in the glutamate release from photoreceptors, HCs hyperpolarize due to a reduction in AMPA receptor activation. With the exception of certain types of fish HCs that have NMDA receptors, other types of glutamate receptors have not been found on HCs in the adult retina (Yang et al., 1998; Thoreson & Witkovsky, 1999; Cadetti et al., 2005). HCs also make reciprocal inhibitory synapses onto cones and bipolar cells. Although GABA is the primary neurotransmitter released by HCs, the inhibitory feedback onto cone terminals does not appear to be due to GABA but to other mechanisms such as protons (Thoreson & Mangel, 2012).

Most mammals have two subtypes of HCs classified based on whether or not the HC has an axon (Edqvist et al., 2008), both of which hyperpolarize to light within the visible spectrum. A third HC subtype has been identified that depolarizes to certain wavelengths of light and hyperpolarizes in response to other wavelengths of light. This third color-opponent HC subtype is found in many other species (Mariani, 1987; Kolb et al., 1994; Cuenca et al., 2000; Connaughton et al., 2004), although not salamander (Lasansky & Vallerga, 1975; Zhang et al., 2006). In our experiments, we did not

distinguish between HC subtypes when performing electrophysiology recordings, and therefore, likely recorded from multiple HC subtypes.

In addition to synaptic connections to photoreceptors, HCs are also coupled to one another by gap junctions (O'Brien et al., 2006). Functionally, the extensive electrical coupling between HCs is the basis of their large receptive fields. The extent of HC coupling depends upon the adaptation state of the retina, with coupling maximized in dim light and diminished at higher and lower light levels (Dong & McReynolds, 1991; Xin & Bloomfield, 1999). HCs are coupled to adjacent HCs of the same functional class creating a network across the retina (Hankins, 1995). Since HCs contact multiple photoreceptors, typically both rods and cones, they are involved in spatial integration and regulation. Large receptive fields allow HCs to detect mean luminance across wide areas of the retina. Inhibitory feedback from HCs to cones and bipolar cells subtracts this average luminance from signals relaying information about localized changes in luminance (Thoreson & Mangel, 2012). Lateral feedback from HCs back to photoreceptors cells modifies their release properties. One significant role of this negative feedback is formation of center-surround receptive fields, which are involved in edge detection.

In experiments described later in this dissertation, HC to HC coupling can impact the ability to detect HC mEPSCs, because the coupling between cells impedes voltage clamping the HC membrane. Without quality voltage clamp of the HC, the membrane current change that occurs during a mEPSC is more difficult to detect especially if the amplitude of the mEPSC is small. In the retinal slice preparation used for most of these experiments, HC-HC coupling is typically reduced because connections between cells are physically severed during the tissue preparation.

Bipolar cells, whose cell bodies are also in the inner nuclear layer, form synapses in the outer plexiform layer with photoreceptors and horizontal cells. They also form synapses in the inner plexiform layer with ganglion and amacrine cells. The two synaptic regions of bipolar cells are essential for their function of transferring signals from photoreceptors to ganglion cells. Bipolar cells are classified into ON and OFF subtypes that respond in an opposite manner to glutamate released by photoreceptors. Glutamate causes ON-bipolar cells to depolarize and release glutamate, whereas OFF bipolar cells hyperpolarize and therefore release less glutamate (Euler et al., 2014). Within these two broad classes of ON and OFF bipolar cells, there are multiple different subtypes that are responsible for conveying information about different aspects of the visual scene. In salamander, there are at least 12 subtypes (Wu et al., 2000). In mammalian retina, there is also an additional rod bipolar cell subtype creating a total of 13 subtypes (Euler et al., 2014).

1.1d Glutamate receptors on horizontal and bipolar cells

Photoreceptors are the first cells in the visual pathway. After light stimulation is detected by the photoreceptors, their rate of continuous release of glutamate-filled vesicles is diminished. Following release of glutamate into the synapse, second order horizontal and bipolar cells detect changes in glutamate release through their glutamate receptors. The two main classes of glutamate receptors found on second-order neurons in the retina are ionotropic and metabotropic glutamate receptors. Ionotropic glutamate receptors form non-selective cation channels. Glutamate binding triggers opening of the channel pore, which is more permeable to Na^+ and K^+ than Ca^{2+}. Activation of ionotropic glutamate receptors thus leads to depolarization. Ionotropic glutamate receptors are present on horizontal cells and OFF-bipolar cells (DeVries & Schwartz, 1999; Shen et

al., 2004). There are three types of ionotropic glutamate receptors in the retina: AMPA receptors, kainate receptors, and NMDA receptors (Thoreson & Witkovsky, 1999; Yang, 2004). The evidence suggests that horizontal cells have only the AMPA type receptors (Yang et al., 1998; Thoreson & Witkovsky, 1999; Cadetti et al., 2005). OFF-bipolar cells can possess AMPA or kainate receptors (Cadetti et al., 2005; Lindstrom et al., 2014). The inactivation kinetics of different AMPA and kainate receptor subtypes help shape post-synaptic response kinetics (DeVries, 2000). In primate retina, transient signaling in the OFF pathway depends upon kainate but not AMPA receptors (Puthussery et al., 2014). In retinas of tetrapod vertebrates, NMDA receptors appear to be absent from horizontal and bipolar cells but are found only in third-order amacrine and ganglion cells (Thoreson & Witkovsky, 1999).

The second class of glutamate receptors in the retina is metabotropic glutamate receptors. Metabotropic glutamate receptors can produce membrane potential changes by acting through a G protein cascade to stimulate the opening or closing of ion channels. All eight subtypes of metabotropic glutamate receptors are expressed in retina, where they primarily serve a modulatory role as in other CNS neurons. The metabotropic glutamate receptor mGluR6 found on ON-bipolar cell dendrites post-synaptic to rods and cones is the only identified instance in the nervous system in which a metabotropic glutamate receptor is the primary signaling mechanism independent of involvement of ionotropic receptors (DeVries, 2000; Connaughton, 2007). The high affinity mGluR6 receptor acts via the G protein, G_o, to close TRPM1 non-selective cation channels (Koike et al., 2010; Morgans et al., 2010). This creates a sign-inverting synapse so that a light-induced reduction in glutamate release produces membrane depolarization in ON bipolar cells.

1.1e Amacrine and ganglion cells

Amacrine cells are lateral inhibitory neurons. In that sense, they function similarly to horizontal cells. Also like horizontal cells, many of them contain the inhibitory neurotransmitter GABA. Many others contain glycine. But there are many more subtypes of amacrine cells-at least 29 subtypes-than horizontal cells (Masland, 2012). The interactions among amacrine cells, bipolar cell terminals, and ganglion cell dendrites help to refine the visual image, encoding its features into at least 20 parallel pathways that are fed into the final retinal cell type, the retinal ganglion cell.

After receiving inputs from bipolar and amacrine cells, ganglion cells then transmit both image-forming and non-image-forming visual information to the brain. There are at least 20 types of retinal ganglion cells that appear to be specialized for transmitting information about different aspects of the visual world (Masland, 2012). These include ON, OFF, ON-OFF, sustained, and transient ganglion cell types. There are also ganglion cells with more elaborate receptive field properties such as directionally-selective cells that respond selectively to stimuli moving in a certain direction. There is also a population of intrinsically photosensitive retinal ganglion cells that can respond to light stimulation independently of the photoreceptors response (Ramsey et al., 2013). Unlike photoreceptors and second-order neurons, ganglion cells transmit information through spiking rather than graded changes in transmitter release. Visual information from the retina is then carried to the brain through the long axon of the ganglion cell that extends into midbrain nuclei including the lateral geniculate nucleus of the thalamus, the superior colliculus, the accessory optic system, the pretectum, and the hypothalamus (Robles et al., 2014).

1.2 Photoreceptor activity in darkness and in light

Both rods and cones convert light energy into changes in cell membrane potential that result in the transmission of electrical signals to downstream neurons in the visual pathway. This visual phototransduction is the process that allows vision to occur. Rods and cones differ in their activity in darkness and in light due to their different sensitivities. Rods undergo phototransduction in even very low-light conditions (Fig. 2), whereas cones undergo phototransduction more so in brighter light conditions.

In darkness, there is a high concentration of cGMP in the photoreceptor cell. The cGMP binds cyclic-nucleotide gated Na^+ channels causing the channels to open. This allows Na^+ ions to flow into the cell producing a photoreceptor resting membrane potential in darkness of about -40 mV. The depolarizing flow of Na^+ into the rod in darkness is known as the dark current (Dowling, 1987). Absorption of photons causes photoreceptors to hyperpolarize, producing graded changes in the membrane potential, which modulates their rate of tonic glutamate release. Retinal, also known as vitamin A aldehyde, is the photopigment in rods. When a photon of light hits the outer segment it can be absorbed by the chromophore 11-cis retinal causing photoisomerization to all-trans retinal. The 11-cis retinal form has a kinked conformation, whereas the all-trans retinal form is a straight chain. The conversion to all-trans retinal causes a conformational change in the G protein-coupled receptor rhodopsin to the active form metarhodopsin. Then, activation of metarhodopsin induces GDP to dissociate from the G protein alpha subunit, transducin (G_t), and be replaced by GTP. This in turn allows dissociation of the GTP-bound transducin, which activates cGMP phosphodiesterase to hydrolyze cGMP to 5'-GMP. This results in a decrease in the concentration of cGMP, so cyclic nucleotide-gated Na^+ channels close. The ongoing K^+ current hyperpolarizes the photoreceptor. The hyperpolarizing change in membrane voltage increases the

probability that voltage-gated Ca^{2+} channels will be in the closed conformation, thereby reducing the concentration of intracellular Ca^{2+} present to trigger vesicle exocytosis. With increasing light intensity the release of glutamate by rods is reduced, and at brighter light levels there is a decrease in glutamate release by cones as well.

Following phototransduction, the photopigment must be converted back to its original unbleached form before it can be used again to detect photons. Interestingly, pigment regeneration is not performed in the photoreceptor cells but requires export of bleached pigment to neighboring cells where it is then converted back to the unbleached all-trans form. In the classic visual cycle 11-cis retinal is generated from all-trans retinal in the retinal pigment epithelium. Cones also have an additional cone-specific process in which isomerization of all-trans retinol occurs in Müller cells, facilitating rapid regeneration of cone pigment (Tang et al., 2013). This pathway is essential for the cones to rapidly respond to changes in stimulation.

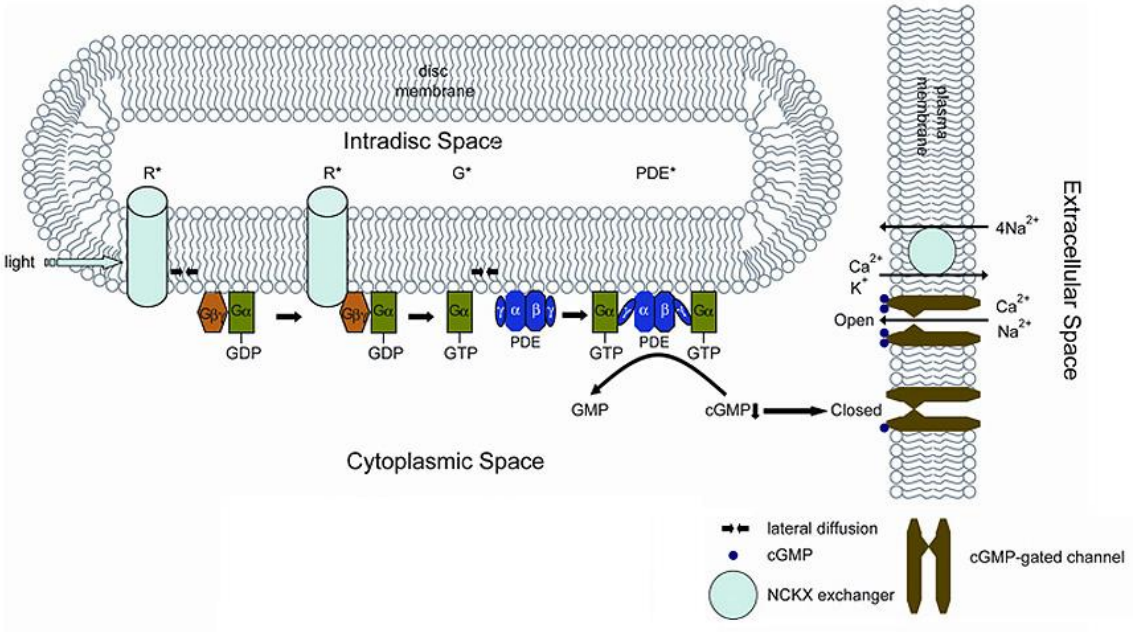

Figure 2: Rod phototransduction cascade.

A photon of light is absorbed in the rod outer segment. Activated rhodopsin then activates heterotrimeric G protein catalyzing the exchange of GDP for GTP. This produces the active form of the GTP-bound G protein. Two GTP-bound G proteins bind the two inhibitory γ subunits of phosphodiesterase (Deterre et al., 1988), which releases the catalytic α and β subunits. The activated phosphodiesterase catalyzes the hydrolysis of cGMP leading to a decrease in the cytoplasmic free cGMP. When the concentration of free cGMP is reduced cGMP-gated channels on the plasma membrane close. This channel closure blocks the influx of cations into the outer segment, reducing the circulating dark current. Image from *Phototransduction in rods and cones* by Yingbin Fu, reproduced under a Creative Commons license

1.3 Synaptic vesicle exocytosis and endocytosis in photoreceptors

1.3a Photoreceptor vesicle pool

Photoreceptors can sustain a very high rate of continuous vesicle exocytosis indefinitely during darkness. At conventional synapses, exocytosis occurs phasically in response to action potentials (LoGiudice & Matthews, 2007; Waites & Garner, 2011). Under dark conditions, photoreceptors in the retina have a relatively depolarized membrane potential, sustaining release for hours at a time with each cell capable of releasing over 6,000 vesicles per minute (Thoreson, 2010). To maintain this high rate of continuous release, photoreceptor synapses contain a much larger pool of releasable vesicles than conventional CNS neuronal synapses. Conventional neurons typically possess ~100 vesicles and most of these are relatively immobile (Hilfiker et al., 1999; Holt et al., 2004). By contrast, photoreceptors synapses contain nearly 100,000 vesicles and ~85% are freely mobile and participate in exocytosis (Rea et al., 2004; Sheng et al., 2007). Like a number of other sensory neurons, photoreceptors have adaptations including synaptic ribbons and large vesicle pools that facilitate long periods of exocytosis.

1.3b Photoreceptor synaptic ribbon

To maintain signaling during long periods of depolarization such as occurs in prolonged darkness at night, photoreceptors must sustain a high level of ongoing exocytosis. To achieve this end, photoreceptors and a number of other sensory neurons including retinal bipolar cells, pineal photoreceptors, cochlear hair cells, vestibular hair cells, lateral line organ hair cells, and electroreceptors possess specialized protein

structures known as synaptic ribbons (Matthews & Fuchs, 2010). In photoreceptor and bipolar cell terminals, the ribbon has a plate-like shape whereas it is more spherical in hair cell terminals. In both rod and cone photoreceptors the ribbon is 30-40 nm wide and 200-400 nm high (reviewed by Heidelberger et al., 2005; Sterling & Matthews, 2005; Schmitz, 2009). Rod ribbons are longer on average than cone ribbons (rod ribbons 800-1500 nm long, cone ribbons 200–700 long). Rod terminals in mammals typically have one synaptic ribbon, whereas rod terminals in amphibians can have multiple ribbons (Carter-Dawson & LaVail, 1979; Townes-Anderson et al., 1985). Cone terminals in both mammals and amphibians are larger and can have a dozen or more ribbons. Each individual photoreceptor ribbon runs along the synaptic ridge on top of the arciform density. The Ca^{2+} channels are located in the synaptic membrane beneath the arciform density. Synaptic vesicles are tethered to the ribbon.

RIBEYE is the primary protein that makes up the ribbon (Matthews and Fuchs, 2010). The RIBEYE protein is made up of two domains (Schmitz et al., 2000). The A domain is specific for ribbons and mediates assembly of RIBEYE into the ribbon structure. The B domain is the same as C-terminal binding protein B, which is a transcriptional repressor related to 2-hydroxyacid dehydrogenase. The B domain binds NAD+ with high affinity.

The protein that tethers vesicles to the ribbon has not yet been identified but may involve Rab3a (Tian et al., 2012). Voltage-gated L-type Ca^{2+} channels are localized beneath the synaptic ribbon likely through protein-protein interactions. In salamander rods, 95% of the Ca^{2+} channels are located in the terminal (Xu & Slaughter, 2005)) and most of those are clustered beneath the ribbon (Nachman-Clewner et al., 1999; tom Dieck et al., 2005; Choi et al., 2008; Mercer & Thoreson, 2011). Upon depolarization, the voltage-gated Ca^{2+} channels open. The influx of Ca^{2+} triggers release of the readily

releasable pool of vesicles which contact the plasma membrane at the base of the ribbon (Snellman et al., 2011). With additional stimulation, additional vesicles on the ribbon descend down to release sites at the ribbon base. The sustained rate of release from cones is limited by the rate of vesicle delivery to these release sites (Jackman et al., 2009). While cones appear to release vesicles exclusively at ribbons (Snellman et al., 2011), rods are also capable of substantial vesicle release at non-ribbon sites, triggered by Ca^{2+}-induced Ca^{2+} release (CICR) from endoplasmic reticulum stores (Krizaj et al., 1999; Cadetti et al., 2006; Suryarnaryanan & Slaughter, 2006; Babai et al., 2010; Chen et al., 2013,2014).

The synaptic ribbon is believed to play a role in maintaining neurotransmission, though its exact function in photoreceptors and in other neurons is still being investigated. Originally, the ribbon was proposed to function as a conveyor belt delivering synaptic vesicles to the release sites (Bunt, 1971). Later, it was shown that movement of vesicles on the ribbon is not ATP-dependent (Heidelberger et al, 2002) and is likely due to passive diffusion (Graydon et al., 2014). The ribbon may be involved in concentrating vesicles through protein-protein interaction (Prescott & Zenisek, 2005). By facilitating delivery of vesicles to release sites (Jackman et al., 2009), the ribbon may also make release more consistent. Regularizing release would facilitate detection of single photons by post-synaptic neurons, which can be impeded by randomness in vesicle release rates (Schein & Ahmad, 2005). Ribbons localize synaptic vesicles to the active zone where vesicle exocytosis occurs. Through this localization ribbons are likely to play a role in positional priming, bringing synaptic vesicles into close proximity with Ca^{2+} channels. Therefore, when the Ca^{2+} channels open, the small domains of high Ca^{2+} concentration that form can trigger exocytosis of nearby vesicles tethered to the ribbon. Ribbons may also play a role in molecular priming (Snellman et al., 2011), making

vesicles competent for release, for instance by facilitating changes in protein conformation needed for efficient exocytosis.

1.3c The invaginating synaptic cleft in photoreceptors

The photoreceptor synaptic contact with the dendrites of second order horizontal and bipolar cells occurs in an invaginated cleft in the photoreceptor terminal (Fig. 3; Dowling & Werblin, 1969; Lasansky, 1973; Haverkamp et al., 2000). Bipolar cell dendrites terminate directly opposite the vesicle release sites at the base on the photoreceptor ribbon. Horizontal cell dendrites are located laterally from the release sites. In rods, there are usually two rod bipolar cell dendrites at the center of the invagination and two lateral HC dendrites. In cones, there is typically one ON-bipolar cell dendrite at the center of the invagination flanked by two HC dendrites. Other bipolar cells can make basal junctions with the cone on the under surface of the cone pedicle near the edges of the invagination. Unlike mammalian retina, in the salamander retina that was used for these studies, the central contact is more often an OFF-bipolar cell and the basal junctions are more often ON-bipolar cells (reviewed in van Hook & Thoreson, 2014).

The HC dendrites are located laterally on either side of the central bipolar cell dendrites. The glutamate receptors are localized to the tips of the HC and bipolar cell dendrites. The difference in position of the bipolar cell and HC dendrites relative to the sites of glutamate release impacts the mEPSCs measured in the two cell types. The amplitudes of mEPSCs vary among different post-synaptic neurons. The variability cannot be fully explained by differences in the sizes of synaptic vesicles (Miller et al. 2001), though there may be differences in the amount of glutamate loaded into individual vesicles (Bartoletti and Thoreson, 2011). Different types of glutamate receptors on

different post-synaptic bipolar and horizontal cells might also contribute to differences in post-synaptic responses. Differences in diffusional distance from release sites to the bipolar and horizontal cell dendrites due to the architecture of the invaginating synapse are also likely to play a role (DeVries et al., 2006). HC dendrites are in closer proximity to the glutamate release sites than the bipolar cell dendrites, so they will be exposed to highly concentrated, localized, and brief increases in glutamate rapidly following release. HC glutamate receptors are only about 15-50 nm from release sites (Rao-Mirotznik et al., 1998). The increase in glutamate at the HC receptors following vesicle release thus rises high and falls rapidly. Glutamate levels at HC dendrites may exceed 1 mM (Kim & Miller, 1993; Cadetti et al., 2008). The HC glutamate receptors have low affinity and fast dissociation binding characteristics (Rao-Mirotznik et al., 1998). During light stimulation and sustained depolarization the response of HCs that contact rods but not cones is strongly influenced by the level of residual glutamate remaining in the cleft (Cadetti et al., 2008).

Glutamate must diffuse further within the cleft before reaching the bipolar cell dendrites, so bipolar cells detect more dilute, diffuse, and prolonged increases in glutamate following release. Depending on the subtypes of bipolar cell, glutamate receptors may be as close as 130 nm from release sites but as far away as 1840 nm, much further than HC receptors (Calkins et al., 1996; Rao-Mirotznik et al., 1998). The increase in glutamate at the bipolar cell receptors following vesicle release is thus lower and decreases more slowly (DeVries et al., 2006). The bipolar cell glutamate receptors have high affinity and likely slower dissociation binding characteristics (Rao-Mirotznik et al., 1998).

The invagination at the rod synapses is typically deeper than the invagination at the cone synapses. There is evidence that the difference in the synaptic cleft between

rods and cones is functionally significant. In rods, the deeper invagination may prevent spillover of transmitter to neighboring cells, so that single photon responses from individual rods can be detected (Rao-Mirotznik et al., 1998). In contrast, it has been found that during a light response, glutamate released by one cone can spill over to neighboring cones, which may mediate a spatially distributed positive feedback (Szmajda & Devries, 2011).

A.

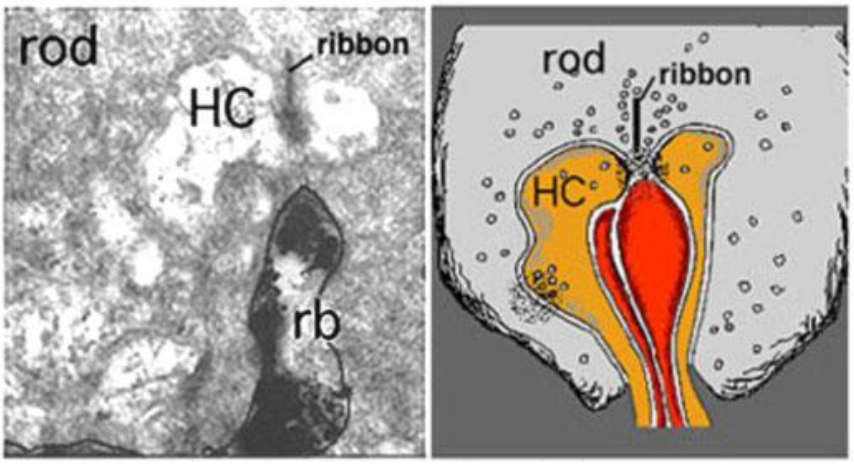

B.

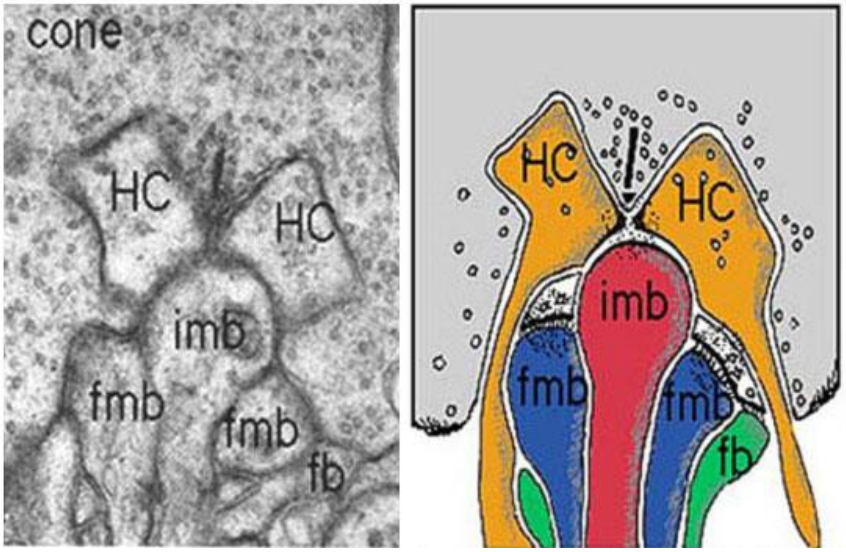

Figure 3: Structure of the rod and cone invaginating synapses.

A single synaptic ribbon with vesicles tethered along the sides of the ribbon is depicted for each photoreceptor type. The ribbon appears as a thin dark strip in these cross sectional views. A. Electron microscopy and schematic of the mammalian rod synaptic triad. The three cell types are the rod, the horizontal cell axon terminals (HC), and the rod bipolar cell dendrite (rb). Processes from two horizontal cells and two rod bipolar cells are seen in the invaginating cleft. B. Electron microscopy and schematic of the mammalian cone synaptic triad. The three cell types are the cone, the horizontal cell dendrite (HC), and the bipolar cells – the invaginating midget bipolar dendrite (imb), the flat midget bipolar (fmb), and the flat diffuse bipolar dendrite (fb). Image from *Photoreceptors* by Helga Kolb, reproduced under a Creative Commons license.

Glutamate transporters also play a role in shaping glutamate dynamics within the synaptic cleft. Within the retina, excitatory amino acid transporters (EAATs) are responsible for uptake of extracellular glutamate. EAATs are Na^+- and K^+-dependent membrane transporters. These transporters have two separate conductances when activated: a coupled Na^+,H^+,K^+-dependent conductance that is necessary for the transporter to bind and translocate glutamate and a stoichiometrically uncoupled Cl^- conductance (Danbolt, 2001). There are five glutamate transporter subtypes EAAT-1 through EAAT-5. These high-affinity glutamate transporters are located on the terminals of photoreceptors and bipolar cells, as well on Müller glia surrounding the synaptic cleft (Eliasof et al., 1998; Burris et al., 2002). In photoreceptors, the glutamate transporters are localized at the base of the synaptic terminal outside the cleft (Hasegawa et al., 2006; Rowan et al., 2010). The reuptake of glutamate by EAATs in photoreceptors produces anion currents that can be used to detect glutamate release presynaptically (Picaud et al., 1995; Szmajda & Devries, 2011). In studies described later in this thesis, we exploit this property of glutamate transporter currents in our studies of baseline release by photoreceptors (Chapter 2).

Glutamate uptake into rod and cone photoreceptors is mediated by different EAAT subtypes, which is likely to contribute to differences in the kinetics of glutamate transmission between the two photoreceptor types (Rauen et al. 2004). In cones, EAATs maintain a low level of tonic glutamate in darkness preventing synaptic depression and play a role in encoding light offset signals (Rowan et al., 2010).

Different EAAT subtypes in rods and cones probably play a role in differential modulation of synaptic activity in rods and cones. Glutamate transporters are also present on retinal Müller cells (Yang & Wu, 1997). However, the processes of Müller cells in salamander do not enter the cone invaginated cleft (Lasansky, 1973). Because

of their spatial separation from the synapse, Müller cells are unlikely to be involved in rapid regulation of synaptic transmission.

1.3d Evoked and spontaneous exocytosis in photoreceptors

Exocytosis from photoreceptors involves both evoked and spontaneous types of release. Evoked release is Ca^{2+}-dependent and occurs following the opening of L-type Ca^{2+} channels, or in rods by CICR. In photoreceptors, the Ca^{2+} channels are clustered beneath the synaptic ribbon adjacent to ribbon-associated synaptic vesicles. Localized domains of high Ca^{2+} trigger fusion of the synaptic vesicles. Experiments with the rapid Ca^{2+} chelator BAPTA suggest that Ca^{2+} channels are located less than 100 nm from release sites and that nanodomains of high Ca^{2+} control exocytosis from photoreceptors (Mercer et al., 2011). Compared to release at other synapses, vesicle release from photoreceptors is highly Ca^{2+}-sensitive. At most synapses, Ca^{2+} levels must attain high micromolar levels to trigger release, but photoreceptor release can be driven by much lower Ca^{2+} levels with a threshold of about 400 nM (Rieke & Schwartz, 1996; Thoreson et al., 2004; Shen et al., 2007; Duncan et al., 2010). Photoreceptors also exhibit a lower cooperativity of about 2 Ca^{2+} ions compared to 5 ions at most other synapses. Opening of the voltage-gated L-type Ca^{2+} channels typically occurs after cell depolarization. When the cell is depolarized, there is a high probability that the Ca^{2+} channels will be in the open conformation, allowing Ca^{2+} influx into the synaptic terminal. However, even when the cell is not depolarized there is still low probability occurrence of stochastic Ca^{2+} channels openings that could trigger exocytosis. In our studies, we have defined any exocytosis that occurs due to the opening of Ca^{2+} channels following cell depolarization as evoked release. Conversely, we defined spontaneous release as release occurring independently of cell depolarization. There is evidence for Ca^{2+}-independent

spontaneous release in other neurons including CA3 neurons (Scanziani et al., 1992). However, spontaneous release can also include Ca^{2+}-dependent release that is not triggered by Ca^{2+} channel openings but instead is driven by basal intracellular Ca^{2+} levels (Goswami et al., 2012).

Different presynaptic mechanisms and postsynaptic targets may separate spontaneous and evoked neurotransmission (Kavalali, 2015). The mechanisms that drive spontaneous exocytosis are not as well characterized as those mechanisms that allow evoked exocytosis. However, one mechanisms that is believed to drive spontaneous exocytosis is thermodynamically driven changes in the conformation of proteins involved in exocytosis such as SNAREs that occasionally cause exocytosis independent of Ca^{2+}. Functionally, spontaneous release may regulate synaptic plasticity and homeostasis. For instance, in other neurons baseline release has been shown to facilitate maintenance of synaptic connections and potentiation of post-synaptic receptors (McKinney el al., 1999; Kombian et al., 2000; Carter & Regehr, 2002; Sutton et al., 2006). The evidence increasingly suggests that spontaneous release may have a functionally significant role in neuronal signaling.

In rods and cones, exocytosis is maintained continuously in both light and dark conditions, although it diminishes in light when photoreceptors hyperpolarize. Our results show that baseline release from photoreceptors in light-adapted conditions includes both evoked release dependent upon Ca^{2+} influx and Ca^{2+}-independent spontaneous release (Chapter 2). In rods, Ca^{2+} released from internal Ca^{2+} stores such as the endoplasmic reticulum can drive evoked baseline exocytosis (Chen et al., 2014). Baseline exocytosis can also involve Ca^{2+}-independent spontaneous release. In chapter 2, the process of baseline exocytosis in photoreceptors is characterized and its mechanisms are tested experimentally.

1.3e Exocytic proteins in photoreceptors

Synaptic vesicle exocytosis involves the interaction of multiple proteins. Fusion of the vesicle membrane with the synaptic membrane is mediated by the SNARE (soluble NSF attachment protein receptor) complex, which is a four-helix bundle. The SNARE complex includes proteins associated with the target membrane, in this case the photoreceptor synaptic membrane, known as t-SNAREs, and proteins associated with the vesicle membrane, v-SNAREs (Ungar & Hughson, 2003; Chapman, 2008). The t-SNARES in photoreceptors are SNAP-25, which contributes two helices to the SNARE complex, and syntaxin-3, which contributes one helix (Sherry et al., 2006; Kwok et. al., 2008). Photoreceptor synapses have syntaxin-3, whereas syntaxin-1 is the typical subtype found at other synapses. In addition to serving as part of the core SNARE complex, there is evidence that SNAP-25 can also be associated with vesicles near the ribbon and potentially promotes vesicle priming or compound fusion prior to exocytosis (Morgans et al., 1996). The V-SNARE in photoreceptors is synaptobrevin 2/3, also known as vesicle-associated membrane protein 2/3 (VAMP 2/3), which contributes one helix to the SNARE complex (Kwok et. al., 2008).

Ca^{2+}-dependent exocytosis is regulated by calcium sensors that mediate SNARE complex-dependent fusion. The Ca^{2+} sensor facilitates vesicle fusion by binding to phospholipids and the fusion machinery. Synaptotagmin has been identified as the Ca^{2+} sensor in a number of cells types and its mechanism of action has been characterized. When Ca^{2+} binds to the C2 domains of synaptotagmin 1 this enhances binding to syntaxin and drives membrane fusion (Rizo & Rosenmund, 2008). The identity of the Ca^{2+} sensor in photoreceptors is not known, but some of its properties have been determined. As described in the previous section, the photoreceptor Ca^{2+} sensor has a

high affinity for Ca^{2+} with a threshold of 400 nm and low cooperativity of about two Ca^{2+} ions relative to other synapses (Thoreson et al., 2004). The unique properties of the photoreceptor Ca^{2+} sensor could be because the Ca^{2+} sensor is another type or isoform of synaptotagmin or could result from the action of other accessory proteins that interact with the SNARE complex.

1.3f Endocytosis in photoreceptors

Following exocytosis, vesicles are retrieved by endocytosis. Endocytosis is important for maintaining the structure of the synapse and synaptic exocytosis over both short and long time periods (LoGiudice & Matthews, 2007). Because of the high rate of vesicle exocytosis in rods especially in darkness, rapid endocytosis may be even more critical in rod synapses than at conventional synapses. In the short term, disruption of endocytosis could lead to a decrease in the neuron's ability to respond to a given input (von Gersdorff and Matthews, 1994*a*; Sun et al., 2002; Kuromi and Kidokoro, 2005). While it has been established that endocytosis is necessary to maintain synaptic exocytosis, the mechanisms by which endocytosis facilitates ongoing release are not fully understood. One function of endocytosis is to prevent depletion of the vesicle pool. Particularly in neurons with a small vesicle pool during periods of high stimulation of exocytosis, the vesicle pool would be rapidly depleted without endocytosis. Endocytosis returns vesicles to the synaptic terminal where they can rejoin the vesicle cycle. These vesicles can then be refilled with glutamate and be re-released by exocytosis during subsequent stimulation.

Three main mechanisms of endocytosis have been identified in other cell types:

clathrin-mediated endocytosis, kiss-and-run endocytosis, and bulk endocytosis. Clathrin-mediated endocytosis involves the formation of a clathrin protein lattice around the vesicle prior to endoctyosis. Assembly of this clathrin coat takes time, so this mode of endocytosis is typically thought to be slow, on the order of tens of seconds (Jockush et al., 2005). However, there is evidence that this process can be primed by use of other forms of clathrin, the presence of partially preformed lattices, or the involvement of accessory proteins, thus speeding clathrin-mediated endocytosis (Pelassa et al., 2014). However, thus far there is no evidence to suggest that clathrin can mediate very rapid modes of endocytosis occurring in less than 1 second. The kiss-and-run endocytosis mechanism has been suggested as a possible form of very rapid endocytosis (Zenisek et al., 2002; Llobet et al., 2003). In kiss-and-run endocytosis a transient pore forms between the vesicle and the plasma membranes, but the two membranes do not completely fuse. Neurotransmitter can be released through this pore before the pore closes and the vesicle returns to the cell cycle. In bulk endocytosis a larger than single vesicle-sized portion of synaptic membrane is retrieved (Holt et al., 2003; Coggins et al., 2007). After endocytosis of this larger endosome, individual vesicles bud off and rejoin the vesicle pool. Bulk endocytosis occurs when there is a high rate of exocytosis, as occurs with strong and prolonged stimulation.

In chapter 3, we characterize endocytosis in rod photoreceptors. We found that endocytosis occurs with a time constant of < 200 ms, which is rapid relative to the rate of previously identified modes of endocytosis. The rate of endocytosis is dependent upon the amount of exocytosis that occurs: with more release, the time course of endocytosis slows. The rate of endocytosis is also dependent on the amount of Ca^{2+} influx into the synaptic terminal: with higher concentrations of Ca^{2+}, the time course of endocytosis slows.

1.4 Ca^{2+} in photoreceptors

1.4a Photoreceptor synaptic Ca^{2+}

Ca^{2+} regulation is essential for photoreceptor function and integrity. Both excessively low and excessively high intracellular Ca^{2+} concentrations can damage photoreceptors (Fain, 2006). The outer and inner segments of the photoreceptors differ in function and also in their Ca^{2+} regulation (Thoreson et al., 1997; Krizaj & Copenhagen, 2002). The inner segment, which includes the synaptic terminal, is the functional region relevant for synaptic transmission. At the synapse, Ca^{2+} drives the photoreceptor response to changes in light stimulation by modulating the vesicle release rate. The amount of intracellular Ca^{2+} depends on the stimulation state of the photoreceptors.

In darkness, photoreceptors have a relatively depolarized membrane potential of about -40 mV. Voltage-gated L-type Ca^{2+} channels open allowing Ca^{2+} to move down its concentration gradient into the synaptic terminal. This leads to an increase in Ca^{2+} concentration in the terminal to about 400 nM (Rieke & Schwartz, 1996, Szirka & Krizaj, 2006; Choi et al., 2008; Mercer et al., 2011). In the dark state, there is a dynamic equilibrium between the concentration of Ca^{2+} outside the cell which is typically about 2 mM and the concentration of Ca^{2+} in the photoreceptor. The intracellular Ca^{2+} concentration is prevented from becoming as high as the extracellular Ca^{2+} concentration, because a too high Ca^{2+} concentration within the cell would lead to toxicity. The kinetics of Ca^{2+} removal from the synapse determines the kinetics of exocytosis (Rieke & Schwartz, 1996). Ca^{2+} also plays a role in maintaining equilibrium in the polarization state of the membrane by activating outward K^+ and Cl^- conductances.

Upon stimulation by light, the phototransduction cascade causes hyperpolarization of the cell resulting in closure of the voltage-gated Ca^{2+} channels. As the Ca^{2+} channels close, influx of Ca^{2+} into the synapse is diminished. As light stimulation increases and intracellular Ca^{2+} subsequently decreases, the rate of vesicle exocytosis decreases. In bright light, the cytoplasmic Ca^{2+} concentration in the inner segment is low, between 100 and 200 nM (Szikra & Krizaj, 2006; Mercer et al., 2011).

Multiple mechanisms are involved in controlling the Ca^{2+} concentration in the photoreceptors. The intracellular Ca^{2+} concentration is reduced as residual cytoplasmic Ca^{2+} is effluxed from the synapse or sequestered into intracellular Ca^{2+} stores (Krizaj & Copenhagen, 2002). High affinity mechanisms for Ca^{2+} efflux maintain the tight coupling between intracellular Ca^{2+} concentration and membrane potential. Efflux occurs mainly via plasma membrane Ca^{2+} ATPases (Krizaj & Copenhagen, 1998; Morgans et al., 1998). Cones also have Na^{+}/Ca^{2+} exchangers at their active zones that facilitate rapid reductions in Ca^{2+} concentration during light adaptation to increase the speed of the cone light response (Johnson et al., 2007). Ca^{2+} extrusion in the outer segment is also performed by Na^{+}/Ca^{2+} exchangers (Thoreson et al., 1997; Krizaj & Copenhagen, 1998). Sites of Ca^{2+} sequestration include the endoplasmic reticulum (ER) and mitochondria. Uptake of Ca^{2+} by the ER is ATP-dependent and mediated by the sarcoplasmic-endoplasmic reticulum calcium ATPase (Ungar et al., 1984). In photoreceptors, the principal SERCA subtype is type 2 (Krizaj, 2005; Szikra & Krizaj, 2007). The ER is a dynamic site of Ca^{2+} storage, and Ca^{2+} can also be released from the ER when the cell is stimulated. The functional impact of Ca^{2+} release from the ER is discussed below. Mitochondria are present in the terminals of mammalian photoreceptors, and while their primary role appears to be to provide the ATP needed for active extrusion of Ca^{2+} from

the terminal (Zenisek & Matthews, 2000), in conditions of high Ca^{2+} concentration, mitochondria can themselves sequester Ca^{2+} (Wan et al., 2012).

1.4b Photoreceptor exocytosis can be driven by Ca^{2+}

Ca^{2+} influx at the photoreceptor synapse can trigger evoked release of synaptic vesicles from the synaptic ribbon. Voltage-gated Ca^{2+} channels (VGCCs) are the primary means of Ca^{2+} influx into the photoreceptor terminal. Voltage-gated Ca^{2+} channel 1.4 is the major type of VGCC in photoreceptors (Lee et al., 2015). In the retina, the voltage-gated Ca^{2+} channel is made up of a pore-forming α1 subunit and auxiliary β2 and α2δ4 subunits (Ball et al., 2002; Qin et al., 2002; Wycisk et al., 2006). Opening of the Cav1.4 channels is highly efficient at triggering release of synaptic vesicles from the photoreceptor ribbon, with the opening of fewer than three channels on average being sufficient to drive exocytosis (Bartoletti et al., 2011).

Because Ca^{2+} influx occurs through VGCCs, the amount of Ca^{2+} influx into the cell depends upon the membrane potential. The voltage at which photoreceptor Ca^{2+} currents achieve half-maximal activation is approximately -39 mV, similar to the dark resting membrane potential (Babai & Thoreson, 2009). Because the midpoint is the steepest region of the sigmoidal Ca^{2+} current activation curve, small changes in Ca^{2+} channel activation near the dark potential can result in large, functionally significant changes in synaptic release. Because membrane depolarization increases the open probability of the Ca^{2+} channels, this allows greater Ca^{2+} influx. The peak activation of VGCCs is achieved at membrane potentials above -20 mV. While overall cytosolic Ca^{2+} remains low relative to other neural synapses (Krizaj, 2012), small domains of high Ca^{2+} concentration near the Ca^{2+} channels drive release of the synaptic vesicles located in close proximity at the base of the ribbon (Cadetti et al., 2006; Choi et al., 2008). Many

factors including protons, divalent cations, and anions have been shown to modulate Ca^{2+} channel gating and permeability (Barnes & Kelly, 2000) and thus the rate of vesicle exocytosis. For example, increases in pH increase synaptic efficacy (Harsanyi & Mangel, 1993). Other neuromodulators including zinc, glutamate, dopamine, adenosine, cannabinoids, somatostatin, insulin, nitric oxide, retinoids, and polyunsaturated fats can also change the Ca^{2+} current (reviewed by Heidelberger et al., 2005).

In synaptic terminals of rod photoreceptors, Ca^{2+} influx through Ca^{2+} channels can also trigger Ca^{2+}-induced Ca^{2+} release (CICR) from internal stores (Križaj et al., 1999; Cadetti et al., 2006; Suryanarayanan & Slaughter, 2006; Babai et al., 2010; Chen et al. 2013, 2014). CICR does not appear to be present in the terminals of cones (Cadetti et al., 2006). In rods, there is ER located in the inner segment region near the synaptic terminal (Babai et al., 2010). Ca^{2+} influx mobilizes Ca^{2+} from the ER via ryanodine receptors (Krizaj et al., 2003). There is a retina-specific isoform of the ryanodine receptor, RyR2 (Shoshan-Barmatz et al., 2005, 2007). Release of Ca^{2+} from the ER can trigger additional vesicle release (Krizaj et al., 1999; Suryarnaryanan and Slaughter, 2006; Cadetti et al, 2006; Babai et al., 2010) including exocytosis from non-ribbon sites in rods (Chen et al., 2013, 2014). ER Ca^{2+} at the terminal can be replenished by diffusion of Ca^{2+} through the ER from soma to terminal (Chen et al., 2014). During maintained depolarization, store-operated channels in the plasma membrane allow Ca^{2+} entry that elevates cytoplasmic Ca^{2+} that is used to replenish ER Ca^{2+} (Molnar et al., 2012). The slower kinetics of CICR-mediated release contribute to overall slower release kinetics at rod synapses compared to cone synapses which in turn parallel the slower light response kinetics of rods (Schnapf & Copenhagen, 1982).

1.4c Ca^{2+} and endocytosis in photoreceptors

While the role of Ca^{2+} in driving exocytosis is well established, less is known about the role of Ca^{2+} in the next and final phase of the vesicle cycle, endocytosis. Evidence from another sensory synapse, the cochlear hair cell, indicates that Ca^{2+} can contribute to compensatory endocytosis with an increase in the fast mode of endocytosis with high intracellular Ca^{2+} concentrations (Beutner et al., 2001). In cone photoreceptors, Ca^{2+} concentration did not impact the time constant of endocytosis, but did enhance endocytic overshoot (Van Hook & Thoreson, 2012). Ca^{2+} is involved in exocytosis and likely in endocytosis in photoreceptors. Ca^{2+} may play a role in linking these two steps in the vesicle cycle. In chapter 2, we examine the role that Ca^{2+} plays in driving baseline release from photoreceptors. In chapter 3, we examine how Ca^{2+} impacts the kinetics of vesicle endocytosis in rods.

Chapter 2

Properties of spontaneous vesicle release by rod and cone photoreceptors

Abstract

In addition to evoked release, neurons can release vesicles spontaneously without stimulation. We studied mechanisms and sites of baseline release by photoreceptors. To measure baseline release, we performed whole cell recordings from horizontal cells (HCs), which receive inputs from rod and cone photoreceptors, in a slice preparation of tiger salamander retina. We detected miniature excitatory post-synaptic currents (mEPSCs) in light-adapted HCs when no stimulation was applied to promote exocytosis. Blocking Ca^{2+} influx with Cd^{2+} or lowering extracellular Ca^{2+} reduced the frequency and amplitude of mEPSCs, indicating that many mEPSCs are evoked by Ca^{2+} entry. Event frequency was not diminished by increasing intracellular Ca^{2+} buffering with EGTA-AM, even in the presence of Cd^{2+}. These data indicate that some baseline release is due to Ca^{2+}-independent, spontaneous release. We measured quantal release of glutamate presynaptically from glutamate transporter anion currents. These were also reduced in amplitude by Cd^{2+}, indicating that the change in mEPSC amplitude likely reflected smaller packets of glutamate release. Presynaptic current measurements also established that both rods and cones exhibit spontaneous Ca^{2+}-independent release. Evoked release in cones occurs only at ribbons and so it is likely that spontaneous release from cones also occurs at ribbons. Using total internal reflectance fluorescence (TIRF) microscopy to visualize individual vesicles loaded with pHrodo, we found that baseline release in rods occurred throughout the entire terminal, whereas evoked release was clustered close to Ca^{2+} entry sites near ribbons, suggesting that spontaneous release can occur at non-ribbon sites in rods.

2.1 Introduction

Neurons transmit signals to one another by the evoked release of vesicles, triggered by cell depolarization and resultant opening of voltage-gated Ca^{2+}channels (Katz, 1969; Llinás, 1991; Schweizer, 2006). But neurons are also capable of spontaneous release that does not require depolarization. The functional roles and mechanisms involved in spontaneous release are not as well understood as those of evoked release and appear to vary at different synapses (see reviews by Kaeser & Regehr, 2014; Kavalali, 2015).

There is evidence for both Ca^{2+}-dependent and Ca^{2+}-independent components to spontaneous release in various neurons. A number of studies have found that spontaneous release depends upon intracellular Ca^{2+}, although the source of Ca^{2+} can vary. Spontaneous release can be reduced substantially by introducing the Ca^{2+} chelators BAPTA or EGTA into neurons (Xu et al., 2009; Goswamit et al., 2012; Schneider et al., 2015). Ca^{2+} entry through a variety of Ca^{2+}-permeable ion channels can contribute to spontaneous release. Antagonism of voltage-gated Ca^{2+} channels in cortical and cerebellar neurons reduced spontaneous release by ~50% (Goswami et al., 2012; Williams et al., 2012). In brainstem neurons, influx through tonically active TRPV1 receptors accounted for a substantial fraction of spontaneous release (Shoudai et al., 2010; Peters et al., 2010). Activation of Ca^{2+}-permeable P2X2 receptors (Khakh, 2009) and release of intracellular Ca^{2+} from internal stores can also trigger spontaneous mEPSCs (Emptage et al., 2001; Xu et al., 2009). On the other hand, other studies show that spontaneous release does not always require elevation of intracellular Ca^{2+}. Blocking voltage-gated Ca^{2+} channels did not alter spontaneous release in CA3 neurons (Scanziani et al., 1992). In neocortical neurons, spontaneous release was found to

depend on Ca^{2+}-sensing G protein-coupled receptors that are activated by extracellular rather than intracellular Ca^{2+} (Vyleta & Smith, 2011).

In addition to employing different mechanisms, evoked and spontaneous release can occur at distinct sites. In hippocampal neurons, different populations of NMDA receptors respond to evoked and spontaneous release (Atasoy et al., 2008) suggesting spatial separation of the two forms of release. Imaging of release events at individual Drosophila neuromuscular junctions showed that evoked and spontaneous release can occur at spatially distinct synapses (Melom et al., 2013; Peled et al., 2014). TIRF imaging studies of single vesicle release at retinal bipolar cell synapses showed that evoked release events clustered near ribbons whereas spontaneous release events often occurred at non-ribbon sites (Zenisek, 2008).

In photoreceptors, evoked release is tightly coupled to the opening of L-type Ca^{2+} channels localized to confined domains beneath the synaptic ribbons (Nachman-Clewner et al., 1999; Morgans, 2001; Mercer et al., 2011). Due to the presence of open cyclic nucleotide-gated channels in the outer segment, the photoreceptor membrane potential rests around -40 mV in darkness. This relatively depolarized membrane potential stimulates Ca^{2+} channel openings that trigger release of ribbon-associated vesicles. In rods, but not cones, Ca^{2+} channel openings can also trigger non-ribbon release by activating Ca^{2+}-induced Ca^{2+} release (CICR) (Križaj et al., 1999; Cadetti et al., 2006; Suryanarayanan & Slaughter, 2006; Babai et al., 2010; Chen et al., 2014). Second-order horizontal and OFF-bipolar cells that receive synaptic inputs from photoreceptors show a high rate of miniature excitatory post-synaptic currents (mEPSCs) in darkness. Much of this baseline release is not truly spontaneous, but evoked by the opening of L-type Ca^{2+} channels at the relatively depolarized membrane

potential of photoreceptors in darkness. We thus prefer the term “baseline” rather than “spontaneous” when discussing release in the absence of Ca^{2+} channel blockers.

In the present study, we examined the contributions of Ca^{2+}-independent spontaneous release to baseline release by photoreceptors. It has been shown that a significant fraction of baseline release events persist after applying Co^{2+} in nominally Ca^{2+}-free conditions (Maple et al., 1994), suggesting a contribution from Ca^{2+}-independent spontaneous release. However, removal of extracellular Ca^{2+} causes membrane surface charge effects that can shift Ca^{2+} current activation to more negative potentials so that relatively large Ca^{2+} currents can be generated at the dark potential even in the presence of Co^{2+} (Piccolino et al., 1996; Piccolino & Pignatelli, 1996). We therefore tested the ability of 0.1 mM Cd^{2+} to inhibit mEPSCs in horizontal cells. We also inhibited Ca^{2+} influx through other ion channels by using a Ca^{2+}-free extracellular solution and we prevented release from internal stores by blocking ryanodine receptors. To test whether basal Ca^{2+} levels may be sufficient to stimulate spontaneous release, we lowered intracellular Ca^{2+} by incubating retinas with a cell-permeant Ca^{2+} buffer, EGTA-AM. In addition to measuring mEPSCs in horizontal cells, we examined release events presynaptically by measuring glutamate transporter anion currents in rods and cones. We found that there is a Ca^{2+}-independent component to baseline release from both rod and cone photoreceptors. Ca^{2+}-independent spontaneous release events were smaller in amplitude than evoked release events and showed a more rapid decline in the presence of a vesicular ATPase inhibitor, suggesting different vesicle pools are involved. We looked at the locations of release events in rods by visualizing the fusion of individual vesicles loaded with a fluorescent dye, 10-kD dextran-conjugated pHrodo, using TIRF microscopy. Our results suggest that spontaneous release can occur at both ribbon and non-ribbon sites.

2.2 Materials and methods

2.2a Retinal slice

Retinal slice preparations were made using the retinae of aquatic tiger salamanders (*Ambystoma tigrinum*; both sexes, 18-25 cm length; Charles Sullivan, Nashville, TN) following methods described by Van Hook and Thoreson (2013). The University of Nebraska Medical Center's Institutional Animal Care and Use Committee approved all experimental procedures. Salamanders were housed in a tank with the water maintained at 4-8 ºC on a 12 h:12 h light-dark cycle. Salamanders are sacrificed 1-2 hours after the beginning of subjective night following treatment with 0.25 g/L MS222 for 15 minutes. The eyes were then enucleated and the anterior segment and the lens were removed. A section of eyecup was placed vitreal side down onto a nitrocellulose membrane (5 x 10 mm; type AAWP, 0.8 µm pores; Millipore). The sclera, choroid and retinal pigment epithelium were gently separated from the retina under cold superfusate to isolate the retina. A razor blade tissue slicer (Stoelting Co.) was used to cut the isolated retina into 125-µm slices, which were then rotated 90 degrees and anchored to the recording chamber with vacuum grease. Dissections were performed under room lights. The retinal cells were visualized using an upright fixed-stage microscope (E600FN; Nikon) equipped with a long working distance, 60X, 1.0 NA water-immersion objective. The tissue was superfused at ~1 ml/min with an oxygenated amphibian saline solution containing the following (in mM): 111 NaCl, 2.5 KCl, 1.8 $CaCl_2$, 0.5 $MgCl_2$, 5 glucose, and 10 HEPES (pH 7.8; 240-245 mOsm). A 0 Ca^{2+} extracellular solution was prepared by adding 1 mM EGTA to a Ca^{2+}-free extracellular solution in order to buffer

any residual Ca^{2+}. In some instances other pharmacological agents were also added to the perfusion solution as detailed below.

2.2b Electrophysiology and mEPSC analysis

Whole-cell patch clamp recordings from postsynaptic horizontal cells (HCs) were made using the retinal slice preparation described above. Borosilicate glass pipettes (1.2 mm outer diameter, 0.9 mm inner diameter, with internal filament; World Precisions Instruments) were used to make recording pipettes with a Narishige PP-830 vertical puller to produce tips of 1-2 μm in diameter and resistance values between 12-20 MΩ. Pipettes were filled with a solution containing the following (in mM): 40 Cs glutamate, 50 Cs gluconate, 10 TEACl, 3.5 NaCl, 1 $CaCl_2$, 1 $MgCl_2$, 10 MgATP, 0.5 GTP, 5 EGTA, and 10 HEPES (pH 7.2; 235-240 mOsm). Huxley-Wall micromanipulators were used to position pipettes such that the tip contacted the cell body, which was identified morphologically based on position within the retinal layers. Once a giga-ohm seal was formed, gentle suction was used to rupture the patch. HCs were voltage clamped at -60 mV with a Multiclamp 700A amplifier (Axon Instruments), which was controlled using an Axon Instruments Digidata 1550 interface (Molecular Devices) and pClamp 10.4 software (Axon/Molecular Devices). Quantal mEPSCs in HCs were detected and analyzed using Minianalysis 6.0.7 (Synaptosoft, Inc., Decatur, GA). Events were detected using an amplitude threshold of 2 pA and an area threshold of 5 pC. After automated detection, each mEPSC was then evaluated individually by eye and the peak amplitude recalculated as necessary. Double peaks were analyzed using an algorithm within Synaptosoft that extrapolates the exponential decay of the first peak.

Presynaptic currents in rod and cone photoreceptors arising from activation of glutamate transporter currents were measured using a pipette solution contained 90 mM

potassium thiocyanate in place of the 40 mM Cs glutamate and 50 mM Cs gluconate (Picaud et al., 1995; Szmajda & Devries, 2011). Use of thiocyanate enhanced the anion currents associated with glutamate transporter activation. Photoreceptors were voltage clamped at -70 mV.

2.2c Imaging

For imaging experiments with total internal reflection fluorescence (TIRF) microscopy, isolated rod photoreceptors were used. The retina was dissected under infrared illumination and isolated in a solution containing the following (in mM): 116 NaCl, 2.5 KCl, 1.8 $CaCl_2$, 0.5 $MgCl_2$, 10 HEPES, and 5 glucose (pH 7.8). The tissue was kept in darkness to maintain rods in a depolarized state and incubated with a 10-kDa dextran-conjugated, pH-sensitive form of rhodamine (pHrodo, 500 µg/ml; Invitrogen) for 3 min at 20°C. This brief incubation period loads only a small fraction (~3%) of synaptic vesicles allowing individual vesicles to be visualized under TIRF illumination (Chen et al., 2013). After dye loading was complete, retinas were placed in a nominally Ca^{2+}-free saline solution and exposed to light to limit further vesicle cycling. Next, the retina was prepared for dissociation by incubation with papain (30 U/ml; Worthington) plus cysteine (0.2 mg/ml) in nominally Ca^{2+}-free amphibian saline for 35 min at 20°C. The tissue was then washed and triturated using a fire-polished Pasteur pipette. The cell suspension containing isolated rods was transferred onto 1.78 refractive index glass coverslips (Olympus) coated with Cell-Tak (3.5 µg/cm^2; BD Biosciences) 30 min prior to imaging. During the imaging experiments, the tissue was superfused with oxygenated amphibian saline solution at room temperature. Imaging was done using a 1.65 numerical aperture objective (Apo 100X oil; Olympus) with a solid-state laser at 561 nm wavelength (Melles Griot) illuminating the pHrodo-loaded vesicles. Fluorescence emission was filtered with

a 609 nm (54 nm wide) bandpass filter (Semrock) and collected by an electron multiplying CCD camera at 30–40 ms/frame (Hamamatsu ImageEM) with a pixel size of 80 nm/pixel. Data were acquired and analyzed using MetaMorph software (Molecular Devices).

Spontaneous release from rods was measured in standard amphibian saline solution with the addition of Cd^{2+} plus dantrolene to block Ca^{2+} channels. Alternatively, spontaneous release was measured in rods that were voltage clamped at -70 mV. In these same cells, Ca^{2+} imaging was then used to determine the sites of Ca^{2+} influx. In rod photoreceptors, the Ca^{2+} channels are clustered beneath the synaptic ribbons (Nachman-Clewner et al., 1999; tom Dieck et al., 2005; Choi et al., 2008; Mercer & Thoreson, 2011). As a result, sites of focal Ca^{2+} entry evoked by brief 50-ms depolarizing steps from -70 to -10 mV co-localize with the ribbons (Chen et al., 2013). Therefore, these sites of focal Ca^{2+} entry can be used as an indication of ribbon location, since ribbons in photoreceptors are difficult to visualize directly using TIRF microscopy, perhaps because of their distance from the plasma membrane (Chen et al., 2013). To image Ca^{2+} entry sites, fluo-5F (100 μM, K_d = 2.3 μM, Invitrogen) was added to the pipette solution. Ca^{2+} entry sites were defined as the sites of peak fluorescence increases evoked by 50-ms steps with $\Delta F/F > 0.5$. In some instances labeled vesicles approached the vesicle membrane but were not released. True release events were distinguished from non-release events based on the rapid decline in fluorescence following fusion and subsequent release of pHrodo. Release events were defined as a decline in peak fluorescence intensity of greater than 60% within two 40-ms frames with a total decrease in fluorescence of >90% relative to baseline. More details on the imaging technique can be found in Chen et al., 2013.

2.2d Pharmacology

Multiple pharmacological methods were used to study the Ca^{2+}-dependence of baseline release. Drug solutions were prepared in amphibian saline solution and superfused over the slice preparations unless otherwise noted. 100 µM cadmium (Cd^{2+}, Sigma Chemicals) was used to block influx through Ca^{2+} channels. 10 µM of the ryanodine receptor blocker dantrolene was used to block Ca^{2+} release from internal stores (Chen et al., 2014). Due to concerns about incomplete recovery after washout, each slice preparations was only exposed to Cd^{2+} one time, after which a new slice preparation was made for subsequent experiments. In some experiments, retinal slices were incubated with 100 µM EGTA-AM (Life Technologies) for 2 hours prior the start of the electrophysiology recordings to increase buffering of intracellular Ca^{2+}.

2.2e Analysis

Whole cell and paired recordings were analyzed with pClamp 10.4 software. Data were analyzed using GraphPad Prism 4 to determine the mean ± SEM. Statistical significance of differences between experimental conditions was determined using two-tailed independent or paired Student's t tests with $p < 0.05$. A Kolmogorov–Smirnov test (KS test) was used to compare cumulative frequency curves.

Amplitude histograms of mEPSCs were fit with a multiple Gaussian function where the integrals of the Gaussian fit were constrained to a binomial distribution using approaches described in detail by Freed and Liang (2014). The average quantal content of each mEPSC was calculated as $m = np/[1 - (1 - p)^n]$ where n = the number of release sites participating in release and p = release probability. In our fits, we constrained $n < 7$.

2.3 Results

2.3a HC mEPSCs persist when synaptic Ca^{2+} is reduced

The persistence of mEPSCs in bipolar cells following application of 2 mM Co^{2+} in nominally Ca^{2+}-free solution suggests that there may be a mechanism for Ca^{2+}-independent release of vesicles from photoreceptors (Maple et al., 1994). However, the effects of nominally Ca^{2+}-free solutions on membrane surface charge can enhance L-type Ca^{2+} currents in photoreceptors at or below the dark resting membrane potential. This allows functionally significant currents to persist in the presence of Co^{2+} (Piccolino et al., 1996; Piccolino and Pignatelli, 1996), raising concerns that Co^{2+} might not have completely blocked Ca^{2+} influx. CICR is also a major mechanism for controlling release from rods (Suranarayanan and Slaughter, 2006; Babai et al., 2010; Chen et al., 2014). We therefore tested effects on HC mEPSCs of inhibiting Ca^{2+} channels with Cd^{2+} (100 µM) and inhibiting CICR with dantrolene (10 µM). In light-adapted retinas under control conditions, we consistently detected mEPSCs in HCs arising from baseline release events. HCs receive both rod and cone inputs (Thoreson et al., 2002; Zhang et al., 2006), so mEPSCs detected in the HCs are typically a mix from both rods and cones. Fig. 4A shows a representative trace with multiple mEPSCs. Even in this light-adapted preparation, resting potentials of photoreceptors are likely to be sufficiently depolarized (-50 to -60 mV) to activate a fraction of the L-type Ca^{2+} channels in their synaptic terminals. If the baseline mEPSCs in control conditions were entirely due to Ca^{2+} and/or CICR, then application of Cd^{2+} plus dantrolene should completely abolish these events. Cd^{2+} (100 µM) completely blocked the rod Ca^{2+} current and dantrolene (10 µM) has been shown to block CICR in rods (Chen et al., 2014). We found that, although the frequency

diminished considerably, a large number of mEPSCs persisted in Cd^{2+} plus dantrolene. This is illustrated by a representative trace from the same cell in Fig. 4B. Fig. 4C and D show the mEPSC amplitude distributions for the records in Fig. 4 A and B, respectively. In addition to reducing frequency, application of Cd^{2+} plus dantrolene also reduced the average amplitude of mEPSCs relative to control conditions (Fig. 4 B and D, KS test $P < 0.001$).

Amplitude histograms in control conditions and in Cd^{2+} plus dantrolene could be fit by a sum of Gaussians where the integrals of the Gaussians are constrained to a binomial distribution (Singer et al., 2004; Freed & Liang, 2014). The quantal content of mEPSCs in control and Cd^{2+} plus dantrolene conditions did not differ significantly, averaging 1.13 ± 0.03 and 1.17 ± 0.05 respectively ($P = 0.34$ paired t-test, $N = 7$). These results suggest that a similar small number of events in both conditions arise from the simultaneous coordinated release of more than one vesicle. Thus, the smaller amplitude of mEPSCs in Cd^{2+} plus dantrolene is not due to a lower frequency of coordinated release events. Furthermore, these results suggest that the mechanisms responsible for this coordinated release did not differ for Ca^{2+}-dependent and Ca^{2+}-independent spontaneous release. We obtained poor fits to amplitude histograms when we constrained the mean quantal amplitude for control mEPSCs to the smaller value determined for Ca^{2+}-independent mEPSCs from the same cell. This indicates that the quantal amplitude of control baseline mEPSCs is not a multiple of the smaller amplitude Ca^{2+}-independent events observed in Cd^{2+}.

To compare kinetics of mEPSCs in control vs. Cd^{2+} plus dantrolene conditions, we analyzed ~100 well-isolated events in both conditions to determine their rise and decay time constants. In control, the rise time was 2.11 ± 0.03 ms and the decay averaged 2.94 ± 0.31 ms. The rise and decay times in Cd^{2+} plus dantrolene did not differ

significantly, averaging 2.09 ± 0.06 ms and 2.91 ± 0.34 ms respectively (rise P = 0.81, decay P = 0.88). The fact that the kinetics did not differ significantly suggests that the smaller size of Ca^{2+}-independent spontaneous release was not due to release at significantly more distant sites that would be expected to produce longer diffusional distances and/or greater electrotonic decay.

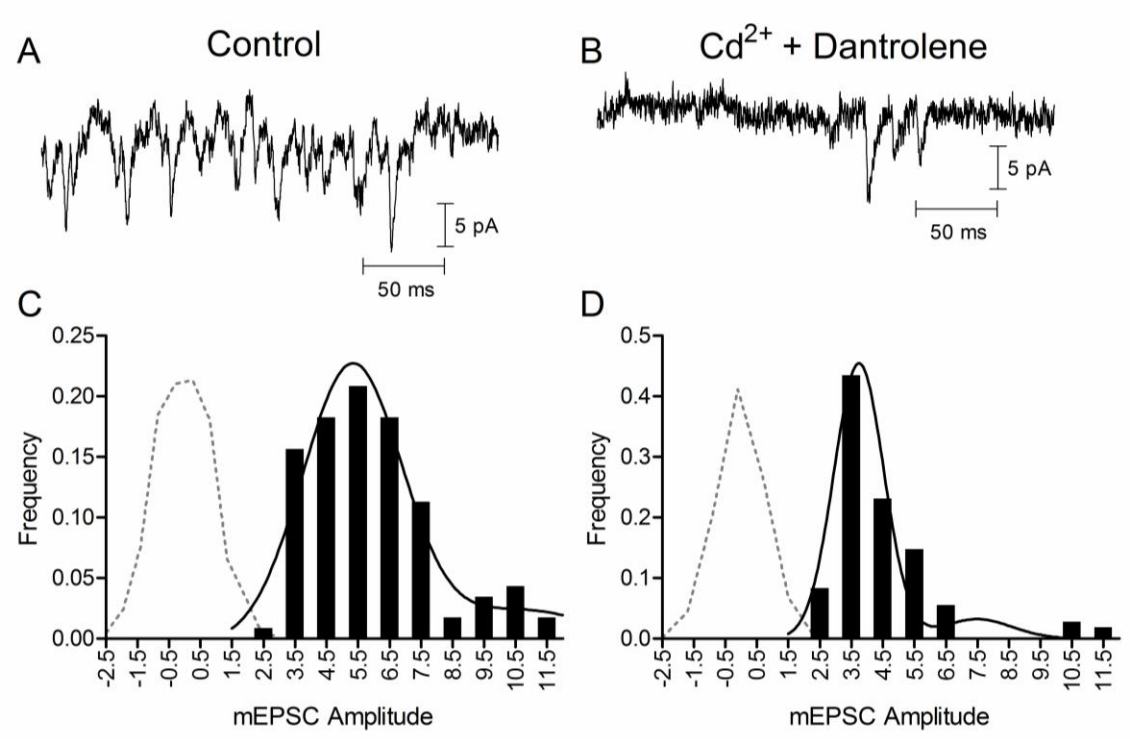

Figure 4: mEPSCs persisted after blocking Ca^{2+} channels with Cd^{2+} (100 mM) and CICR with dantrolene (10 mM).

mEPSCs were measured by whole-cell patch clamp recording in horizontal cells (HCs). Representative traces showing mEPSCs in control conditions (A) and following application of Cd^{2+} plus dantrolene in the same cell (B). (C) and (D) show mEPSC amplitude histograms from the same cell. The dashed lines show the baseline noise histograms. Distributions were fit with a binomially-constrained multiple Gaussian curve. Control data were fit with an amplitude (± S.D.) of 5.01 ± 1.12 pA, n = 2 release sites and release probability of 0.168 yielding a quantal content of m = 1.21 vesicles/release site. Cd^{2+} plus dantrolene data were fit with an amplitude of 3.74 ± 0.79 pA, 2 release sites, and release probability of 0.167 yielding a quantal content of 1.09 vesicles/release site. Control: 115 events. Cd^{2+}plus dantrolene: 108 events.

We examined potential sources of Ca^{2+} that might support spontaneous baseline release. We focus first on mEPSC frequency and consider effects of these agents on mEPSC amplitude later. The lowest mEPSC frequency was observed in Cd^{2+} plus dantrolene (19.0 ± 4.15 Hz; N = 7 HCs). Application of Cd^{2+} alone without dantrolene reduced frequency to a lesser extent (36.0 ± 7.42 Hz, P = 0.08, N = 8 HCs). To test the possibility that spontaneous release might be mediated by Ca^{2+} influx through other types of Ca^{2+}-permeable channels that are not blocked by Cd^{2+}, we applied 0 Ca^{2+} solution plus EGTA (1 mM) to ensure removal of residual Ca^{2+} from the extracellular solution. With 0 Ca^{2+} plus EGTA, the frequency of mEPSCs was reduced significantly relative to control (Fig. 5A, 27.4 ± 6.28 Hz, P < 0.05, N = 5 HCs), but remained slightly higher than that seen with Cd^{2+} plus dantrolene. This suggests that influx through other Ca^{2+}-permeable channels did not contribute significantly to spontaneous release. Consistent with this, adding Gd^{3+} (30 µM) to block store-operated channels in the presence of Cd^{2+} also did not further reduce mEPSC frequency (37.0 ± 11.49 Hz, P = 0.94, N = 6 HCs).

An alternative mechanism by which extracellular Ca^{2+} could trigger spontaneous release is through activation of Ca^{2+}-sensing receptors (Vyleta & Smith, 2011). We tested a positive allosteric modulator for Ca^{2+}-sensing receptors, calindol (5 µM), and observed no significant effect on mEPSC frequency (KS test, P = 0.81, N = 6) or amplitude (KS test, P = 0.70, N = 6). Furthermore, this mechanism does not explain the persistence of mEPSCs in 0 Ca^{2+} extracellular solution. These results indicate that spontaneous HC mEPSCs are not the result of activating Ca^{2+}-sensing receptors in photoreceptors.

The residual release seen in Cd^{2+} plus dantrolene shows that there is a component of baseline vesicle release from photoreceptors that does not require Ca^{2+} influx through membrane channels. However, it is possible that the basal level of intracellular Ca^{2+} is sufficient to drive vesicle release, especially at photoreceptor synapses that employ an exocytotic Ca^{2+} sensor exhibiting a threshold of only ~400 nM Ca^{2+} and a low Ca^{2+} cooperativity of 1-2 (Thoreson et al., 2004; Duncan et al., 2010). Increasing intracellular Ca^{2+} buffering with EGTA-AM or BAPTA-AM can reduce the frequency of spontaneous miniature postsynaptic currents (Xu et al., 2009; Goswami et al., 2012; Schneider et al., 2015). If basal Ca^{2+} triggers spontaneous HC mEPSCs, we expected to see a decrease in mEPSC frequency relative to control when we increased intracellular buffering by incubating retinas in EGTA-AM (100 µM) for 2 hours. After EGTA-AM incubation, the frequency of mEPSCs was no different from control untreated slices (Fig. 5A, 56.69 ± 10.60 Hz, P = 0.92, N = 6 HCs). Addition of Cd^{2+} plus dantrolene to slices incubated in EGTA-AM did not reduce mEPSC frequency (Fig. 5A- 56.05 ± 12.53 Hz, P = 0.97, N = 6 HCs) suggesting that the spontaneous mEPSCs observed under these conditions were Ca^{2+}-independent. Nanodomains of Ca^{2+} were unlikely to be the cause of the remaining release, because Cd^{2+} blocked influx through Ca^{2+} channels.

As mentioned earlier, in addition to lowering release frequency, Cd^{2+} plus dantrolene reduced mEPSC amplitude from 5.64 ± 0.35 pA (N = 17 HCs) to 4.45 ± 0.36 pA (Fig. 5, P < 0.001 paired t-test, N = 7 HCs). Amplitude was also reduced in 0 Ca^{2+} extracellular solution to 4.7 ± 0.35 pA (N = 5 HCs) although this reduction did not reach statistical significance (P = 0.08 paired t-test). After incubation with EGTA-AM, mEPSCs showed an amplitude of 5.20 ± 0.30 pA (Fig. 5B- N = 6 HCs), which was not significantly different from control (P = 0.50). After incubation with EGTA-AM followed by application

of Cd^{2+} plus dantrolene, mEPSCs also exhibited a mean amplitude of 5.60 ± 0.52 pA (Fig. 5B- N = 6 HCs) that did not differ significantly from control (P = 0.96). The decline in mEPSC amplitude appeared to parallel effects on frequency (Fig. 4). One potential contributor to this decline in amplitude is that lower release frequency promotes detection of smaller events, thus skewing the distribution downward. While this likely contributed to some of the amplitude changes, there was also a genuine reduction in the number of large events in the presence of Cd^{2+} plus dantrolene. This can be seen, for example, by comparing the example traces show in Fig. 4. We investigate the source of this amplitude reduction further in the next set of experiments.

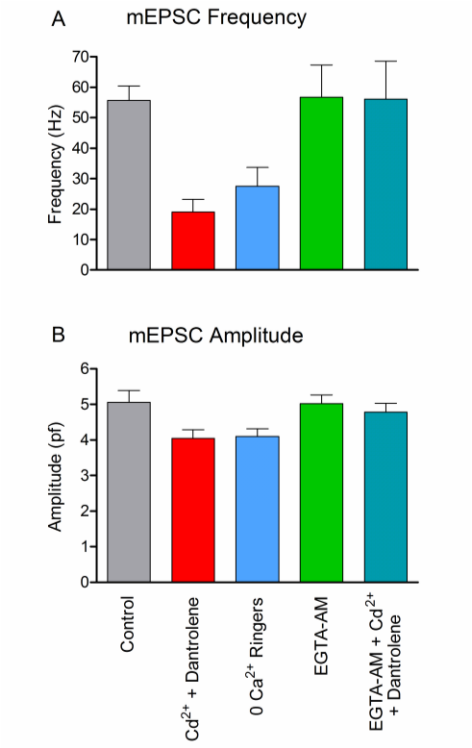

Figure 5: HC mEPSCs are lower in frequency and amplitude when Ca^{2+} influx and efflux are inhibited.

mEPSCs were recorded in HCs voltage clamped at -60 mV. (A) HC mEPSCs in control conditions exhibited a frequency of 55.7 ± 4.66 (N = 17 HCs). Application of Cd^{2+} (100 µM) plus dantrolene (10 µM) reduced the frequency of mEPSCs to 19.0 ± 4.15 Hz (N = 7 HCs). This was significantly lower than in control conditions ($P < 0.001$), but also remained significantly non-zero ($P < 0.05$, one-sided t-test). In 0 Ca^{2+} extracellular solution with EGTA (1 mM) to buffer any residual Ca^{2+}, mEPSCs showed a frequency of 27.4 ± 6.28 Hz (N = 5 HCs), significantly lower than control ($P < 0.05$), but significantly non-zero ($P < 0.05$, one-sided t-test). After incubation with EGTA-AM (100 µM) for 2 hours to increase buffering of intracellular Ca^{2+}, mEPSCs had a frequency of 56.7 ± 10.6 Hz (N = 6 HCs), which was not significantly different from control ($P = 0.92$). Application of Cd^{2+} plus dantrolene to slices incubated in EGTA-AM (100 µM) did not reduce frequency (56.1 ± 12.5 Hz; N = 6 HCs). (B) In control conditions, mEPSCs had an amplitude of 5.64 ± 0.35 pA (N = 17 HCs). In Cd^{2+} plus dantrolene, mEPSCs had a significantly smaller amplitude of 4.45 ± 0.36 pA ($P < 0.001$, N = 7 HCs). In 0 Ca^{2+} extracellular solution, mEPSCs had an amplitude of 4.71 ± 0.35 pA ($P = 0.08$ paired t-test compared to control, N = 5 HCs). After incubation with EGTA-AM, mEPSCs had an amplitude of 5.20 ± 0.30 pA (N = 6 HCs). After incubation with EGTA-AM followed by application of Cd^{2+} plus dantrolene, mEPSCs had an amplitude of 5.60 ± 0.52 pA (N = 6 HCs). Increasing intracellular Ca^{2+} buffering with EGTA-AM did not change mEPSC frequency ($P = 0.92$ EGTA-AM, $P = 0.97$ EGTA-AM + Cd^{2+} + dantrolene) or amplitude ($P = 0.50$ EGTA-AM, $P = 0.96$ EGTA-AM + Cd^{2+} + dantrolene) relative to control.

2.3b mEPSCs result from glutamate release by rods and cones

The release of glutamate-filled vesicles activates glutamate transporters on presynaptic photoreceptors producing anion currents that can be used to detect release events (Picaud et al., 1995; Szmajda & Devries, 2011). To enhance glutamate transporter anion currents, we recorded from rods and cones using a patch pipette containing thiocyanate as the primary anion (Szmajda & Devries, 2011). In rods voltage clamped at -70 mV with this pipette solution, we observed spontaneous inward currents as illustrated in Fig. 6. As expected for transporter anion currents, presynaptic events were blocked by the glutamate transport inhibitor, TBOA (100 µM, N = 4 rods, Fig. 6A). The spontaneous events in rods had much slower kinetics than those in horizontal cells with rise times averaging 7.95 ± 0.33 ms and decay times averaging 6.67 ± 0.90 ms (N = 7 rods). As illustrated in Fig. 6B, application of Cd^{2+} (100 µM) significantly reduced the frequency of rod presynaptic events relative to control conditions (9.1 ± 0.65 Hz control; 6.3 ± 0.79 Hz Cd^{2+}; paired t-test P = 0.02, N = 7 rods). This result is consistent with the reduction in frequency of HC mEPSCs found in Cd^{2+}. The amplitude of rod presynaptic events in Cd^{2+} was also reduced significantly relative to control conditions (7.56 ± 1.06 pA control; 5.66 ± 0.96 pA Cd^{2+}; paired t-test P < 0.001, N = 7 rods). Similar to HC mEPSCs, application of Cd^{2+} abolished larger events in rods, leaving only smaller events as illustrated in Fig. 6B. This indicates that the smaller size of mEPSCs observed in recordings from HCs is due to reduced presynaptic release of glutamate and not post-synaptic factors such as inhibition of glutamate receptors by Cd^{2+}. These data indicate that when rods are voltage-clamped at -70 mV where few if any Ca^{2+} channels should be open, baseline release involves both larger Ca^{2+}-dependent and smaller Ca^{2+}-independent release events.

HCs in salamander retina receive inputs from both rods and cones (Zhang et al., 2006), so we determined whether cones were also capable of Ca^{2+}-independent release of vesicles. As with rods, we observed quantal presynaptic glutamate anion currents in cones voltage-clamped at -70 mV under control conditions (Fig. 6C). This finding supports the assumption that spontaneous mEPSCs in HCs are the result of release from both rods and cones. The kinetics of presynaptic events in cones were even slower than those in rods (rise 9.15 ± 0.23 ms, P = 0.016; decay 14.8 ± 1.27 ms, P < 0.001, N = 6 cones), which may reflect differences in the locations of glutamate transporters relative to release sites (Vandenbranden et al., 2000; Hasegawa et al., 2006; Rowan et al., 2010). Presynaptic events in cones were also abolished when TBOA was applied (data not shown). As in rods, Cd^{2+} (100 µM) completely blocked the cone Ca^{2+} current (N = 6 cones; not shown) but presynaptic events persisted (Fig. 6C). In cones, evoked release appears to occur only at ribbon sites (Snellman et al., 2011). The presence of quantal anion currents in cones after blockade of Ca^{2+} channels is therefore consistent with spontaneous release occurring at ribbons although it is possible that Ca^{2+}-independent release might also involve non-ribbon sites that do not participate in evoked release. Similar to both rods and HCs, the average amplitude of cone presynaptic events was also reduced after Cd^{2+} was applied (6.87 ± 0.58 pA control; 5.32 ± 0.54 pA Cd^{2+}; paired t-test P = 0.037, N = 5 cones). There was not a significant change in frequency of cone presynaptic events (9.7 ± 0.75 Hz control; 10.1 ± 2.00 Hz Cd^{2+}; paired t-test P = 0.80, N = 5 cones). Like rods, these data suggest there are both larger Ca^{2+}-dependent and smaller Ca^{2+}-independent components to spontaneous release from cones at -70 mV. The lack of a significant change in frequency suggests that there are few large Ca^{2+}-dependent events in cones and that their loss has smaller effects on frequency than average amplitude.

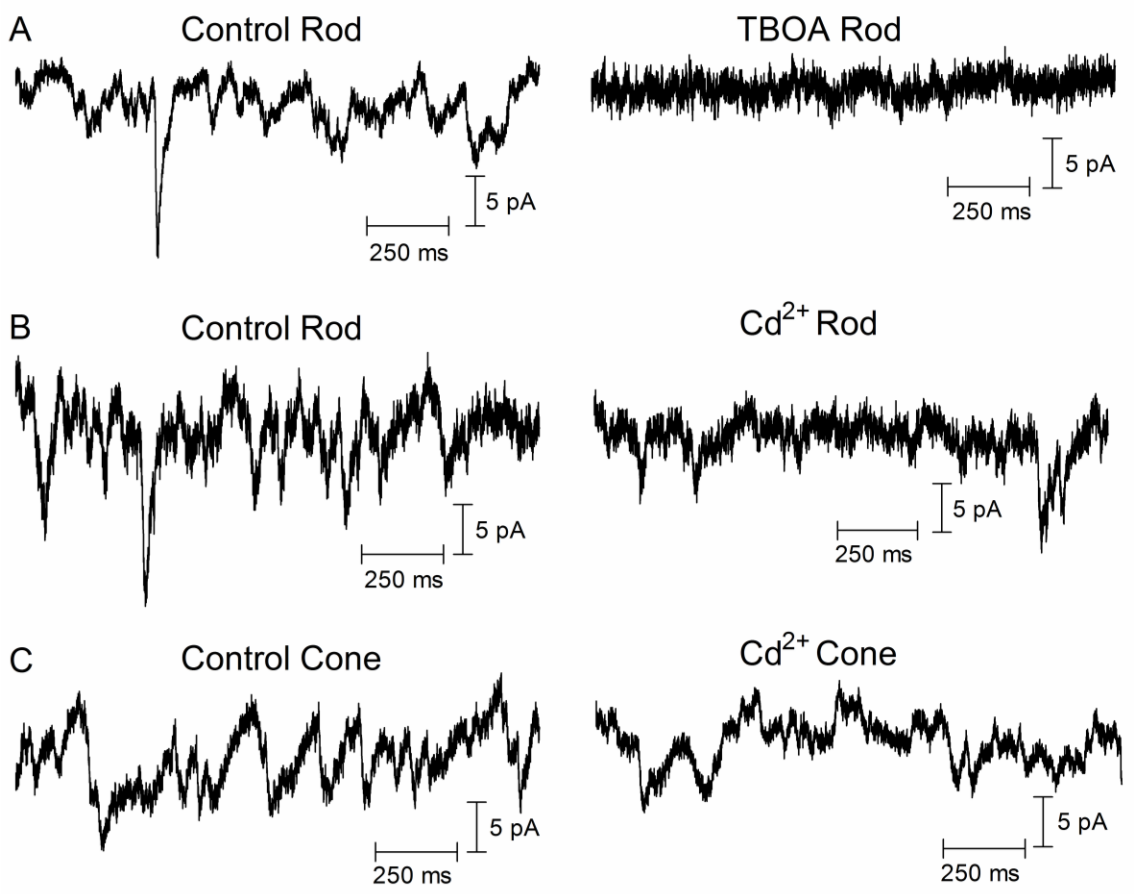

Figure 6: Presynaptic release events detected by glutamate transporter anion currents in rod and cone photoreceptors.

(A) Presynaptic release events in rods voltage clamped at -70 mV were blocked by inhibiting the glutamate transporter with TBOA (100 µM). (B) Application of Cd^{2+} (100 µM) reduced the frequency and amplitude of presynaptic events but did not eliminate them. (C) Release events in cones voltage clamped at -70 mV were also reduced in amplitude by application of Cd^{2+} (100 µM).

2.3c Independence of vesicle pool involved in spontaneous and evoked release

The finding that Ca^{2+}-independent spontaneous mEPSCs were smaller in amplitude than Ca^{2+}-dependent mEPSCs suggests that they may arise from different vesicle populations. To test this idea further, we inhibited the vesicular ATPase with bafilomycin to inhibit glutamate refilling of vesicles. We then compared evoked EPSCs and baseline mEPSCs during bafilomycin application. To evoke EPSCs, we obtained paired whole cell recordings from a rod and post-synaptic HC and then stimulated the rod with a depolarizing voltage step (-70 to -10 mV, 100 ms) at one-minute intervals. As illustrated in Fig. 7A, a depolarizing voltage step applied to rods typically evoked an initial fast EPSC followed by slower EPSC components. The initial fast component has been shown to be due to release from synaptic ribbons (Chen et al., 2013, 2014). The second slower component is primarily due to non-ribbon release driven by CICR (Chen et al, 2014). Slow EPSC components also involve release from neighboring rods evoked by the flow of depolarizing current through gap junctions (Cadetti et al., 2006; Chen et al., 2014). Release by this mechanism was limited in our experiments by hyperpolarizing neighboring rods with application of a bright background light (Chen et al., 2014). Fig. 7C and D plot the amplitude of the fast, ribbon-mediated component (C) and the second, slower, non-ribbon component (D) as a function of time. In control conditions, EPSCs exhibited rundown during paired recording, with the faster ribbon-mediated EPSC component showing a more rapid rundown than the slower component. Applying bafilomycin (7 mM) caused a slight, but not statistically significant, acceleration of rundown in both fast and slow EPSC components. On the other hand, bafilomycin caused a larger and statistically significant decline in both the frequency (Fig. 7E) and amplitude (Fig. 7F) of baseline mEPSCs measured in the absence of stimulation. After 10 min. of bafilomycin treatment, mEPSC frequency had declined by 40% and amplitude

by 19%. The decline in amplitude is likely due to incomplete re-filling of vesicles following their turnover (Cavelier & Attwell, 2007). Based on the reductions in mEPSC amplitude and frequency, if the pools involved in spontaneous and evoked release mixed thoroughly, then one would predict that treatment with bafilomycin should have reduced EPSCs and mEPSCs by a similar percentage.

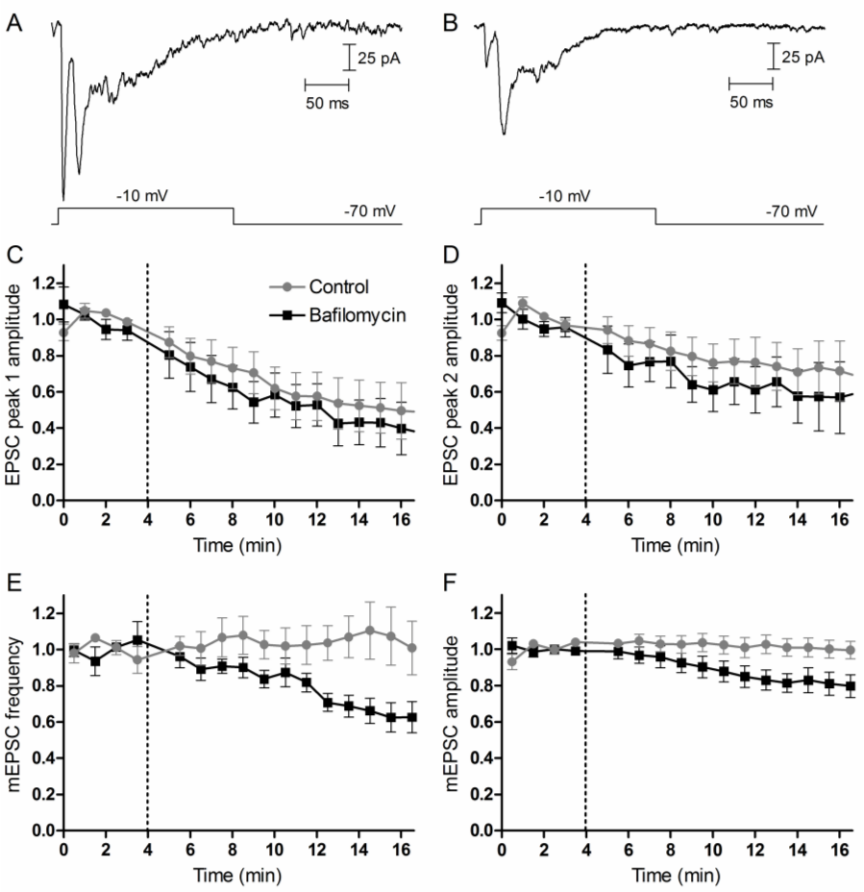

Figure 7: Using the vesicular ATPase inhibitor bafilomycin to block refilling of vesicles with glutamate causes different rates of decline in EPSCs and mEPSCs.

(A) A representative HC EPSC in control conditions evoked by a 200-ms depolarizing step from -70 to -10 mV in a paired rod. There is an initial fast EPSC due to release from ribbons followed by a second slower peak due to non-ribbon release (Chen et al., 2014). (B) EPSC evoked in the same rod/HC pair 15 min after application of bafilomycin (7 µM). There was a decrease in amplitude of both EPSC peaks. (C) Decline in amplitude of the fast, ribbon-mediated EPSC peak in control conditions and following bafilomycin application. Bafilomycin was applied at 4 minutes (dashed vertical lines). (D) Decline in amplitude of the 2nd EPSC peak in control conditions and following bafilomycin application. Both the 1st and 2nd EPSC peaks declined in control conditions due to rundown. The decrease in EPSC amplitude was slightly but not significantly accelerated by bafilomycin (peak 1: P = 0.65, N = 9 rod/HC pairs bafilomycin, N = 8 rod/HC pairs control; peak 2: P = 0.44, N = 8 rod/HC pairs bafilomycin, N = 8 rod/HC pairs control). (E) HC mEPSC frequency declined significantly during application of bafilomycin (P = 0.03, N = 7 HCs bafilomycin, N = 8 HCs control). (F) HC mEPSC amplitude declined significantly during application of bafilomycin (P = 0.03, N = 7 HCs bafilomycin, N = 8 HCs control).

2.3d Spontaneous release can occur at ribbon and non-ribbon sites

Since evoked release appears to occur only at ribbons in cones (Snellman et al., 2011), the persistence of spontaneous events in cones following application of Cd^{2+} suggests that Ca^{2+}-independent release can occur at ribbons. In rods, evoked release can occur at both ribbon and non-ribbon sites (Chen et al., 2013; Zampighi et al. 2011). We therefore examined the sites of release in rods using total internal reflection fluorescence (TIRF) microscopy. To visualize individual release events, vesicles within rod terminals were loaded with a 10-kD dextran-conjugated pH-sensitive form of rhodamine (pHrodo). This dye fluoresces in the acidic conditions within the vesicle, but its fluorescence is quickly quenched when exposed to the slightly alkaline extracellular medium. We used a short incubation period of 3 minutes with the dye to load only 1-3% of the vesicles and thus visualize individual vesicle fusion events (Chen et al., 2013).

We first measured spontaneous release events in the presence of Cd^{2+} (100 µM) plus dantrolene (10 µM) to block influx through Ca^{2+} channels and efflux from internal stores, matching the condition in which HC mEPSC frequency was the lowest. With Cd^{2+} plus dantrolene we observed spontaneous vesicle release events at sites throughout rod terminals (Fig. 8A), rather than being clustered together as occurs when release occurs principally at ribbon release sites (Chen et al., 2013, 2014).

Ca^{2+} channels are clustered at ribbons and so, to locate ribbon sites, we identified hot spots of Ca^{2+} influx using the Ca^{2+}-sensitive dye fluo-5F (Chen et al., 2013). Use of ribbon-targeted fluorescent peptides was a less reliable way of identifying ribbons (Chen et al. 2013). Because we were unable to identify hot spots of Ca^{2+} influx after blocking Ca^{2+} channels with Cd^{2+}, we instead visualized the location of spontaneous release events that occurred in rod terminals voltage-clamped at -70 mV (Fig. 8B). Evidence from glutamate transporter currents indicates that spontaneous

release events consisted of both Ca^{2+}-dependent and Ca^{2+}-independent release. We applied a 50-ms voltage step to -10 mV to trigger a brief influx of Ca^{2+} so that we could locate hot spots of Ca^{2+} influx at ribbons (Chen et al., 2013). Fig. 8C replots data from Chen et al. (2013) showing the distance of individual vesicle fusion events evoked by the depolarizing voltage step from the nearest Ca^{2+} hot spot, which can be used as a proxy for the ribbon location. These data showed that release evoked by 50-ms steps tended to cluster close to ribbons. We analyzed data from these same cells to determine the distance from the nearest Ca^{2+} hot spot for spontaneously occurring baseline release events that preceded the voltage step. As shown in Fig 8C, these baseline, unstimulated release events tended to occur farther away from Ca^{2+} entry sites than release events stimulated by a 50-ms step (KS test $P < 0.001$) suggesting that many spontaneous release events occurred at non-ribbon sites.

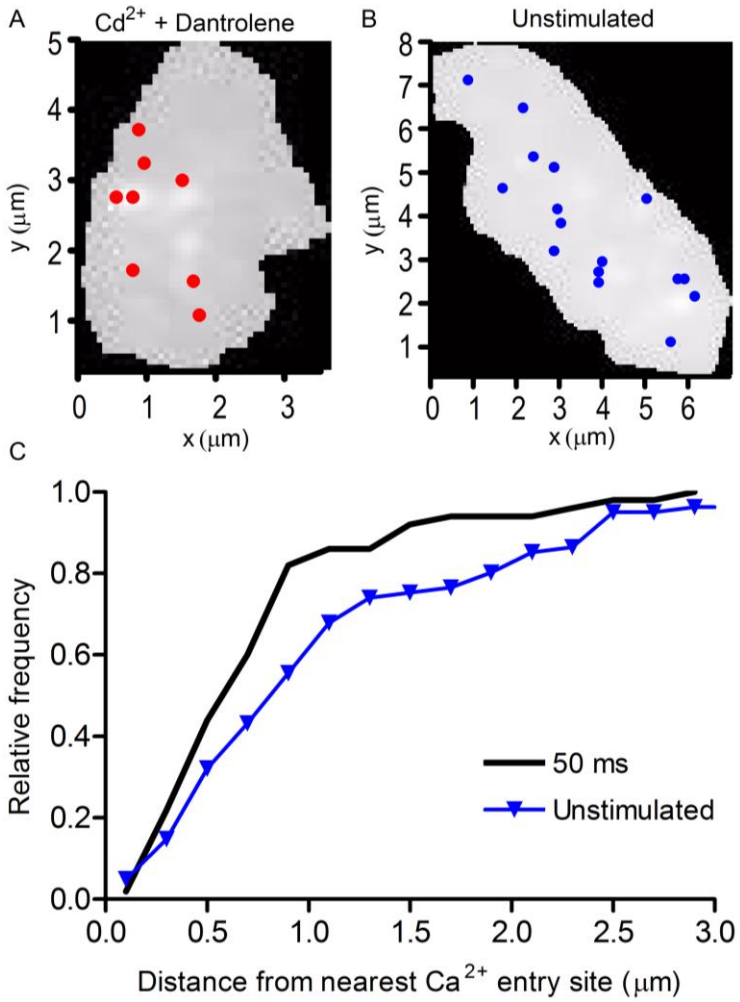

Figure 8: Spatial distribution of spontaneous release events visualized by TIRF microscopy in rod terminals where vesicles were loaded with 10 kD dextran-conjugated pHrodo.

(A) Map of spontaneous release events occurring in the presence of Cd^{2+} (100 µM) and dantrolene (10 µM). The gray region shows the footprint of the rod terminal membrane pressed against the coverslip. Ca^{2+}-independent spontaneous release events did not appear to be clustered at any particular location but occurred throughout the terminal. (B) A map of release sites in a different rod that was voltage-clamped at -70 mV also shows spontaneous release events occurring throughout the rod terminal. (C) Exocytosis events following a 50-ms voltage step from -70 to -10 mV to evoke exocytosis occur closer to Ca^{2+} entry sites at ribbons (data replotted from Chen et al., 2013) than events occurring in un-stimulated rods. Baseline release events in unstimulated rods occurred more often further away from Ca^{2+} entry sites than depolarization-evoked release indicating that spontaneous release events can occur at non-ribbon sites (KS test $P < 0.001$, N = 50 events- 50 ms, N = 81 events- unstimulated).

2.4 Discussion

2.4a Mechanisms of baseline release

Vertebrate photoreceptors do not exhibit fast sodium-dependent action potentials but instead vary their membrane potential continuously with changes in light intensity and the state of adaptation. The resting membrane potential of about -40 mV in darkness drives continuous release of vesicles. Our study delineates three components to this continuous release: 1) Ca^{2+}-dependent, evoked release driven by the sustained activation of L-type Ca^{2+} channels that diminishes when photoreceptors are hyperpolarized by light, 2) Ca^{2+}-dependent spontaneous release that occurs even when photoreceptors are hyperpolarized to -70 mV where L-type Ca^{2+} channels are generally thought to remain in the closed state, and 3) Ca^{2+}-independent spontaneous release that persists even after inhibiting Ca^{2+} influx with Cd^{2+} or Ca^{2+}-free extracellular solution. Our data suggest that the mEPSCs that remain after reduction of synaptic Ca^{2+} are likely due to a Ca^{2+}-independent release mechanism that does not require Ca^{2+} influx, Ca^{2+} release from intracellular stores, or high basal levels of intracellular Ca^{2+}. However, in the light-adapted state of the retinas that we studied, much of the baseline release was likely due to Ca^{2+}-dependent spontaneous release.

The reduction in amplitude of HC mEPSCs and quantal currents in photoreceptors by Cd^{2+} suggests that Ca^{2+}-independent events are smaller than Ca^{2+}-dependent release events. Their smaller size suggests that Ca^{2+}-independent spontaneous release involves different vesicles than either evoked or spontaneous Ca^{2+}-dependent release. Bafilomycin caused a more rapid decline in spontaneous mEPSCs, which in this case consisted of both Ca^{2+}-dependent and Ca^{2+}-independent release, than

in evoked EPSCs, supporting the idea that vesicles involved in evoked and at least one form of baseline release may originate from different vesicle pools.

Some studies suggest that different molecular mechanisms mediate evoked and spontaneous release, whereas others suggest that the same mechanisms may mediate both (Deitcher et al., 1998; Deak et al., 2006; Glitsch, 2008; Smith et al., 2012; Kaeser & Regehr, 2014). The initial hypothesis to explain the origins of spontaneous release was that it might occur through SNARE-mediated membrane fusion driven by Ca^{2+}-independent, thermodynamic changes in SNARE conformation. But it has also been proposed that a special Ca^{2+} sensor such as Doc2 may mediate Ca^{2+}-dependent spontaneous release (Groffen et al., 2010). Doc2 might also be involved in Ca^{2+}-independent spontaneous release (Pang et al., 2011). Although its molecular identity remains unclear, the sensor that mediates exocytosis at photoreceptor synapses exhibits high Ca^{2+} affinity and low cooperativity (Thoreson et al., 2004; Duncan et al., 2010), properties that are similar to the sensor thought to mediate asynchronous and spontaneous release at other synapses (Lou et al., 2005; Sun et al., 2007). It has also been suggested that distinct SNARE proteins, such as the noncanonical SNAREs VAMP7 (Hua et al., 2011) and Vti1a (Ramirez et al., 2012), may mediate spontaneous release (Hua et al., 1998; Scheuber et al., 2006). Differences in SNARE configurations caused by different SNARE isoforms or associated proteins might alter the preference for spontaneous or evoked release (Maximov et al., 2009; Buhl et al., 2013) by altering domain structure of the SNARE complex (Weber et al., 2010). For example, the expression of complexin 3/4 subtypes at ribbon synapses constrains ongoing spontaneous release from bipolar cells (Vaithianathan et al., 2013, 2015).

2.4b Sources of Ca^{2+}-independent spontaneous release

Post-synaptic recordings from HCs, which receive both rod and cone inputs, and presynaptic recordings from both photoreceptor types, indicate that Ca^{2+}-independent spontaneous release can occurred in both rods and cones. Our TIRF results show that when Ca^{2+} channels were blocked with Cd^{2+}, release from rods occurs throughout the terminal, consistent with release at non-ribbon sites. We also observed Ca^{2+}-independent release in cones, where only ribbon release has been shown (Snellman et al., 2011). Taken together, these results suggest that Ca^{2+}-independent release can occur at both ribbon and non-ribbon sites.

At bipolar cell ribbon synapses, as well as other ribbon (Glowatzki & Fuchs, 2002) and conventional synapses (Wadiche & Jahr, 2001; Raghavachari & Lisman, 2004), release of vesicles can occur in coordinated bursts involving more than one vesicle. Consistent with the presence of coordinated release of multiple vesicles in photoreceptors, we found that amplitude histograms of mEPSCs during baseline release could be fit with a multiple Gaussian function when the integrals of the Gaussian were constrained to a binomial distribution (Freed & Liang, 2014). Ca^{2+}-independent spontaneous mEPSCs and mEPSCs in baseline control conditions that were largely due to Ca^{2+}-dependent release both exhibited a similar quantal content averaging ~1.1 vesicles/release event. These data suggest that a small fraction of baseline release events may be due to the coordinated release of multiple vesicles. By comparison, the average quantal content of spontaneous mEPSCs in retinal ganglion cells originating from bipolar cell release averaged ~1.4 quanta/release event (Singer et al., 2004; Freed & Liang, 2014). If different mechanisms were employed for the release of Ca^{2+}-dependent and Ca^{2+}-independent mEPSCs, then one would expect to see a difference in the propensity for coordinated multivesicular release. Thus, the finding of equivalent quantal content in both conditions suggests they involve similar mechanisms of release.

TIRF results indicate that spontaneous release in rods occurs with a greater frequency at non-ribbon sites than evoked release, but the sites of Ca^{2+}-independent and Ca^{2+}-dependent spontaneous release did not differ dramatically. Together, these results suggest that the differences in amplitude between Ca^{2+}-dependent and Ca^{2+}-independent mEPSCs are likely to arise from differences between the vesicles themselves, not differences in the sites or mechanisms of release.

2.4c Functional impact of spontaneous release

A number of functions have been proposed for spontaneous release, including maintenance of synaptic connections and potentiation of post-synaptic receptors (McKinney el al., 1999; Kombian et al., 2000; Carter & Regehr, 2002; Sutton et al., 2006). Photoreceptor synapses do not show any evidence for synaptic potentiation. Furthermore, the frequency of Ca^{2+}-dependent release, even when photoreceptors are hyperpolarized to -70 mV, should be sufficient for post-synaptic cells to recognize that connections to presynaptic photoreceptors are still present. Thus, the function, if any, for Ca^{2+}-independent spontaneous release remains unclear.

While its functional significance remains unclear, one functional consequence of Ca^{2+}-independent spontaneous release is to increase noise at photoreceptor synapses. Ca^{2+}-independent spontaneous mEPSCs in HCs showed an average frequency of 19 Hz in the presence of Cd^{2+} and dantrolene, but the rate of release at any individual presynaptic release site is far lower. Although there are not similar numbers for HCs, Lasansky (1978) reported that each OFF-bipolar cell received 30-50 contacts from 10-15 photoreceptors. Horizontal cells have larger light responses and larger receptive fields than OFF-bipolar cells, so HCs are likely to receive at least as many contacts as OFF bipolar cells. In cones, there appear to be ~15-20 release sites at the base of each

ribbon (Bartoletti et al., 2010). In rods, the readily releasable pool averages a slightly larger number of ~24 vesicles/ribbon (Van Hook & Thoreson, unpublished). If we assume that each HC, like each OFF BP, receives 30-50 ribbon contacts and that each ribbon has 20 release sites at its base, then input into a horizontal cell may arise from 600-1000 separate release sites. Given a total frequency of 19 Hz, this suggests a frequency at each release site of only 0.02-0.03 Hz or one release event every 30-50 s. Ribbon release sites in cones are replenished within about 1 s (Van Hook et al., 2014) suggesting that individual release sites are capable of sustaining release at a frequency of 15-24 vesicles/s/ribbon or ~1 Hz at each release site, almost 1000x greater than the spontaneous rate. A rate of 15-24 vesicles/s/ribbon is consistent with previous estimates of release in darkness (Ashmore & Copenhagen, 1983; Sheng et al., 2007). Assuming that 1200 release sites contact each HC, these data suggest that HC mEPSCs could occur at a rate of 1200 Hz in darkness. This high rate would support a steady inward current of ~20-30 pA in darkness given an individual mEPSC peak amplitude of 5 pA and duration of ~5 ms. This is similar to the amplitude of OFF bipolar cell light responses in salamander retina (Gao et al., 2000; Thoreson et al., 2003). However, dark-adapted HCs sometimes exhibit a light-evoked change in membrane current exceeding 300 pA suggesting that they receive ten times as many synaptic inputs (Yang et al., 1998; Thoreson et al., 2003). By under-estimating the number of photoreceptor contacts per horizontal cell and not including non-ribbon release sites where considerable spontaneous release can occur in rods, the actual frequency of spontaneous release per release site in photoreceptors is likely to be at least tenfold lower than 1 release event every 30-50 seconds. This would approach the frequency at other synapses where spontaneous release has been estimated to occur as little as once every 1,000 s at each site (Kaeser & Regehr, 2014). Such a low frequency of spontaneous release would contribute little synaptic noise. The post-synaptic impact of spontaneous mEPSCs may

be further minimized by the smaller size of Ca^{2+}-independent mEPSCs. The impact of a single mEPSC would also be small because the low input resistance of most HCs would result in only a small change in voltage for a given current change.

Chapter 3[1]

Rapid kinetics of endocytosis at rod photoreceptor synapses depends upon endocytic load and calcium

Abstract

Release from rods is triggered by the opening of L-type Ca^{2+} channels that lie beneath synaptic ribbons. After exocytosis, vesicles are retrieved by compensatory endocytosis. Previous work showed that endocytosis is dynamin-dependent in rods but dynamin-independent in cones. We hypothesized that fast endocytosis in rods may also differ from cones in its dependence upon the amount of Ca^{2+} influx and/or endocytic load. We measured exocytosis and endocytosis from membrane capacitance (C_m) changes evoked by depolarizing steps in voltage clamped rods from tiger salamander retinal slices. Similar to cones, the time constant for endocytosis in rods was quite fast, averaging <200 ms. We manipulated Ca^{2+} influx and the amount of vesicle release by altering the duration and voltage of depolarizing steps. Unlike cones, endocytosis kinetics in rods slowed after increasing Ca^{2+} channel activation with longer step durations or more strongly depolarized voltage steps. Endocytosis kinetics also slowed as Ca^{2+} buffering was decreased by replacing BAPTA (10 or 1 mM) with the slower Ca^{2+} buffer EGTA (5 or 0.5 mM) in the pipette solution. These data provide further evidence that endocytosis mechanisms differ in rods and cones and suggest that endocytosis in rods is regulated by both endocytic load and local Ca^{2+} levels.

[1] The material presented in this chapter was previously published: Cork KM, Thoreson WB. (2014). Rapid kinetics of endocytosis at rod photoreceptor synapses depends upon endocytic load and calcium. *Visual Neuroscience* 31(3):227-35.

3.1 Introduction

To maintain signal transmission, neurons must sustain release of synaptic vesicles for long periods of time (Beutner et al., 2001; Wu et al., 2007; Alabi & Tsien, 2012). This process requires tight coupling between exocytosis and endocytosis (Rieke & Schwartz, 1996; Gundelfinger et al., 2003; Haucke et al., 2011), with vesicles retrieved via compensatory endocytosis after their release (Pysh & Wiley, 1974; Miller & Heuser, 1984; LoGiudice & Matthews, 2007; Wu et al., 2007; Barg & Machado, 2008; Smith et al., 2008; Xue & Mei, 2011). Tight temporal coupling between exocytosis and endocytosis is especially important in rod photoreceptors. At conventional synapses release occurs phasically in response to action potentials (Waites & Garner, 2011), but rods respond to changes in light and dark by graded changes in membrane potential that modulate the continuous release of vesicles (Dowling, 2012). In darkness, rods have a depolarized membrane potential of ca. -40 mV that promotes continued activation of L-type Ca^{2+} channels and sustained release of vesicles. To facilitate ongoing release, rods contain a specialized protein active zone structure known as the ribbon, which tethers releasable vesicles close to Ca^{2+} channels (Sterling & Matthews, 2005; Schmitz, 2009). Unlike mammalian rods that have a single ribbon per rod terminal (Sterling & Matthews, 2005), there are an average of 7 ribbons per terminal in salamander rods (Townes-Anderson et al., 1985). Measurements in both salamander and mouse retina suggest that synaptic vesicles are released from rods at a rate of 18 vesicles/second/ribbon in darkness (Berntson & Taylor 2003; Sheng et al. 2007). At this rate, the entire cytoplasmic pool of vesicles would be depleted within 5-10 minutes after the onset of darkness without compensatory endocytosis (Sheng et al. 2007; Zampighi et al, 2011). Thus, even though a very large number of vesicles participate in release from rods (ca.

75,000 per rod in salamander retina; Sheng et al., 2007), endocytosis remains essential for maintaining ongoing release.

The properties of endocytosis have been studied directly in only a few neuronal cell types. Retinal bipolar cells are one of the most thoroughly characterized. Studies in bipolar cells show that multiple mechanisms of endocytosis with different kinetics are involved in retrieving vesicles after their release (von Gersdorff & Matthews, 1994*b*). A slow phase of endocytosis, with a time constant of approximately 10 s, was shown to be clathrin-dependent (Jockush et al., 2005). In clathrin-mediated endocytosis, a clathrin protein lattice coats the exterior of the vesicle prior to endoctyosis. Another faster component of endocytosis, with a time constant of approximately 1 s, was not clathrin-dependent (Jockush et al., 2005), but did involve endophilin (Llobet et al. 2011). This fast component was not due to a kiss-and-run endocytosis mechanism, in which a transient pore connects the vesicle to the plasma membrane without full collapse fusion (Zenisek et al., 2002; Llobet et al., 2003). Both clathrin-dependent and clathrin-independent modes of endocytosis typically involve the GTPase dynamin (LoGiudice et al., 2009; Wan & Heidelberger, 2011). However, a GTP-independent mode of endocytosis has also been observed in bipolar cells (Heidelberger, 2001) as well as other neurons (Xu et al. 2008; Chung et al., 2010). A third mechanism, bulk endocytosis, was identified under conditions of strong and prolonged stimulation (Holt et al., 2003; Coggins et al., 2007). In this mechanism, portions of the synaptic membrane are retrieved less selectively forming large endosomes.

In photoreceptors, both coated vesicles (Gray & Pease, 1971; Schaeffer & Raviola, 1978) and clathrin (Sherry & Heidelberger, 2005; Wahl et al., 2013; Fuchs et al., 2014) are found in perisynaptic regions adjacent to ribbons. Other endocytic proteins including dynamin, syndapin, amphiphysin, endophilin, and calcineurin are also found in

this region of rod terminals (Ullrich & Sudhof, 1994; Sherry & Heidelberger, 2005; Wahl et al., 2013; Fuchs et al., 2014). Rods and cones exhibit both fast and slow components of endocytosis (Rieke & Schwartz, 1996; Rabl et al. 2005; Innocenti & Heidelberger, 2008; Van Hook & Thoreson, 2012). Cones have an ultrafast component of endocytosis, with a time constant of ~250 ms, much more rapid than the fast component in bipolar cells (Van Hook & Thoreson, 2012). Fast endocytosis in cones was not slowed by inhibition of dynamin with dynasore or GTPγS, whereas endocytosis in rods was decreased by these same inhibitors (Van Hook & Thoreson, 2012). This result indicates that different mechanisms mediate endocytosis in rods and cones.

In the present study, we characterized endocytosis in rods further and observed an ultrafast component of retrieval with an average time constant of <200 ms following a brief depolarizing test step. Unlike cones, the kinetics of endocytosis in rods slowed with increasing release and decreasing Ca^{2+} buffering suggesting that endocytosis in rods is regulated by both endocytic load and local Ca^{2+} levels.

3.2 Materials and methods

3.2a Retinal slice

Slices were prepared from the retina of aquatic tiger salamanders (*Ambystoma tigrinum*; both sexes, 18-25 cm length; Charles Sullivan, Nashville, TN) using methods described by Van Hook and Thoreson (2013). Experimental procedures were approved by the University of Nebraska Medical Center's Institutional Animal Care and Use Committee. Animals were maintained at 4-8ºC on a 12 h:12 h light-dark cycle. Salamanders were sacrificed 1-2 hours after the beginning of subjective night by rapid decapitation and hemisection of the head with heavy shears followed immediately by pithing. Then, the eyes were enucleated and the anterior segment of the eye and the lens were removed. The resultant eyecup was placed vitreal side down onto a nitrocellulose membrane (5 x 10 mm; type AAWP, 0.8 µm pores; Millipore). The tissue was cut into 125 µm slices using a razor blade tissue slicer (Stoelting Co.). Slices were rotated 90 degrees and anchored to the recording chamber using vacuum grease. The recording chamber was placed on an upright fixed stage microscope (E600FN; Nikon) equipped with a long-working distance, 60X, 1.0 NA water-immersion objective. Tissue was superfused at ~1 ml/min with an oxygenated amphibian saline solution containing the following (in mM): 111 NaCl, 2.5 KCl, 1.8 $CaCl_2$, 0.5 $MgCl_2$, 5 glucose, and 10 HEPES (pH 7.8; 240-245 mOsm).

3.2b Electrophysiology

Recording pipettes were fabricated from borosilicate glass pipettes (1.2 mm outer diameter, 0.9 mm inner diameter, with internal filament; World Precisions Instruments)

using a Narishige PP-830 vertical puller to produce tips of ~2 μm in diameter and resistance values between 12-20 MΩ. The shaft of each recording pipette was coated with dental wax to reduce stray capacitance. Pipettes were positioned with Huxley–Wall micromanipulators, so that the tip of the pipette contacted the rod cell body, which was identified morphologically. After establishing a giga-ohm seal, the patch was ruptured with gentle suction. The pipette solution contained (in mM): 40 Cs glutamate, 50 Cs gluconate, 10 TEACl, 3.5 NaCl, 1 $CaCl_2$, 1 $MgCl_2$, 10 MgATP, 0.5 GTP, 1 BAPTA, and 10 HEPES (pH 7.2; 235-240 mOsm). BAPTA was included to rapidly buffer Ca^{2+} and minimize Ca^{2+}-dependent conductances. In some experiments, we used 10 mM BAPTA, 5 mM EGTA, or 0.5 mM EGTA in place of the 1 mM BAPTA. The 0.5 mM EGTA solution was made without the 1 mM $CaCl_2$. TEA and Cs are included to block K^+ channels, improving voltage clamp and Ca^{2+} current (I_{Ca}) measurements. Rods were voltage clamped with an Optopatch patch-clamp amplifier (Cairn Research), which was controlled using an Axon Instruments Digidata 1322A interface (Molecular Devices) and pClamp 9.2 software (Axon/Molecular Devices). We excluded rods that required holding currents >200 pA in order to maintain a membrane potential of -70 mV. Membrane resistance, series resistance, and membrane capacitance (C_m) averaged 223.0 ± 16.8 MΩ, 34.5 ± 1.8 MΩ, and 31.2 ± 1.4 pF, respectively (N = 21).

Changes in C_m were used to measure exocytosis and endocytosis. Vesicle exocytosis was evoked by applying a depolarizing voltage step to the rod. Measurements of C_m were made using the phase-tracking circuitry of the lock-in amplifier integrated into the Optopatch patch clamp amplifier (Johnson et al., 2002; Rabl et al., 2006; Bartoletti et al., 2010; Van Hook & Thoreson 2012). The membrane potential was varied sinusoidally (500-600 Hz, 30 mV peak-to-peak) about a holding potential of -70 mV. Series resistance and membrane capacitance controls were

adjusted to cancel the sinusoidal output current of the lock-in amplifier. To limit possible C_m measurement artefacts that can be caused by conductance changes and allow time for the phase angle feedback circuitry to settle, capacitance recordings were suspended during the voltage step and for 30 ms afterwards. Recordings that showed pronounced poststimulus changes in access resistance were excluded. The net change in C_m is due to exocytosis of vesicles minus any compensatory endocytic retrieval. The kinetics of endocytosis were characterized by the time constant for a single exponential fit to the decline in C_m after stimulation (T_{endo}) or for the time required for the increase in C_m to decline by 50% (t_{50}).

In a few experiments, we obtained simultaneous paired whole cell recordings from rods and horizontal cells in retinal slices. Rod recordings were obtained as described for capacitance experiments. Rods were voltage clamped at -70 mV and stimulated with 200 ms voltage steps to -10 mV. Horizontal cells were voltage clamped at -60 mV with an Axopatch 200B amplifier. Horizontal cell pipettes were filled with a solution containing the following (in mM): 90 Cs gluconate, 10 TEACl, 3.5 NaCl, 1 $CaCl_2$, 1 $MgCl_2$, 10 MgATP, 0.5 GTP, 5 EGTA, and 10 HEPES (pH 7.2; 235-240 mOsm). Paired recording techniques are described in detail by Van Hook & Thoreson (2013).

3.2c Analysis

Capacitance traces were analyzed with pClamp 10 software. Data were analyzed using GraphPad Prism 4 to determine the mean ± SEM. Statistical significance of differences between experimental conditions was determined using two-tailed independent or paired Student's *t* tests with $P < 0.05$.

3.3 Results

3.3a Fast endocytosis in rods

To study endocytosis in rods, we used capacitance recording techniques. Membrane capacitance provides a direct, high temporal resolution method for measuring changes in membrane surface area that result from the exocytosis and endocytosis of vesicles. Depolarizing test steps applied to voltage clamped rods typically evoked rapid endocytic retrieval of membrane. Fig. 9 illustrates the response of a rod to a 100 ms step from -70 to -10 mV. This strong stimulus maximally triggers opening of the L-type Ca^{2+} channels beneath the ribbon, allowing an influx of Ca^{2+} that drives vesicle release (Thoreson et al., 2004; Rabl et al., 2006). The step evoked an inward I_m followed by an outward tail current after the step (Fig. 9: I_m). An increase in membrane capacitance due to exocytosis was observed when measurements were resumed 30 ms after the step. Capacitance declined thereafter due to endocytosis (Fig. 9: C_m).

We measured the kinetics of endocytosis in two ways. First, we determined τ_{endo} from a single exponential fit to the decline in C_m (gray line, Fig. 9). Fitting the records with two exponentials did not improve the fit. For 5 out of the 6 step durations tested, fitting the average trace with a two exponential function produced a negative value for the amplitude and/or the time constant. When fits were constrained to positive values for amplitude and time constant, fits were not improved significantly by addition of a second exponential component (paired comparison of the sum of squared errors for fits to average waveforms with 5-200 ms steps, $P = 0.38$, $N = 6$). Although there is evidence that slower endocytic components also contribute to retrieval with longer steps (Rieke & Schwartz, 1996; Thoreson et al., 2004), these results suggest that a single kinetic process dominated endocytosis with the relatively short steps used in our experiments.

We often observed a brief plateau before capacitance began to decline. Because of this plateau, we also characterized endocytosis by the time required for the amplitude of the capacitance increase to decline by 50% (t_{50}). The t_{50} values were typically longer than τ_{endo}, because they included this initial plateau (Fig. 9).

The kinetics of endocytosis following a 100 ms step were quite rapid (τ_{endo} = 174.4 ± 33.54 ms, N = 13; t_{50} = 192.9 ± 23.77 ms, N = 14; 100 ms; -70 to -10 mV). Cones often exhibited an endocytic overshoot, in which C_m went below baseline after stimulation before returning to the pre-stimulation level (Van Hook & Thoreson, 2012). By contrast, in rods we did not see convincing evidence for such an overshoot even with 200 ms steps. Some individual records appeared to show endocytic overshoot but when we averaged multiple records to reduce the influence of baseline noise, we observed no evidence for an endocytic overshoot in rods. A similar method of analysis in cones using averaged records persisted in demonstrating endocytic overshoot (Van Hook & Thoreson, 2012).

A 100 ms step to -10 mV evoked a capacitance increase averaging 76 fF. The diameter of a single vesicle in rods averages 45 nm, equivalent to a C_m of 57 aF (Thoreson et al., 2004), suggesting 1333 vesicles were released during the step. Salamander rods possess an average of 7 ribbons/terminal (Townes-Anderson et al., 1985) and each ribbon has an average of 710 vesicles, yielding a total ribbon pool of 4,970 vesicles (Thoreson et al., 2004). In mammalian rods, 17% of the ribbon pool is docked in contact with the plasma membrane (Sterling & Matthews, 2005). Assuming a similar proportion in salamander, this suggests an immediately releasable pool of 845 vesicles. Many vesicles were also probably released from non-ribbon sites (Chen et al., 2013).

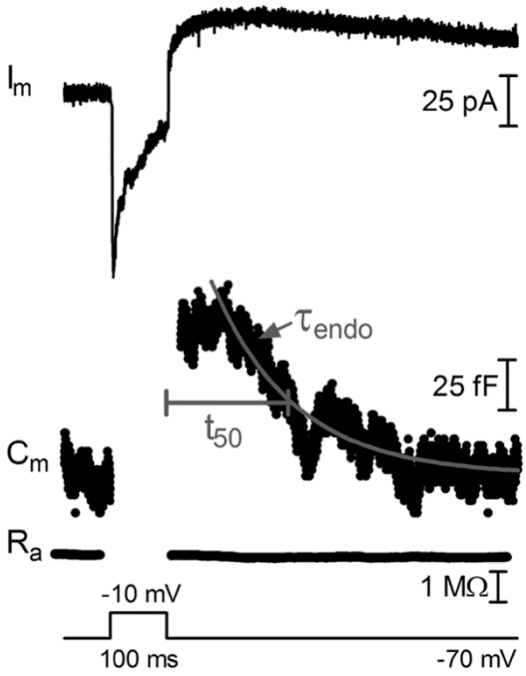

Figure 9: Fast endocytosis in rods.

Whole-cell capacitance recordings from a rod in a salamander retinal slice preparation. Changes in membrane current (I_m), membrane capacitance (C_m), and access resistance (R_a) evoked by a 100 ms depolarizing step to -10 mV from a mean holding potential of -70 mV. The increase in C_m caused by fusion of synaptic vesicles was followed, after a brief delay, by a decline in capacitance due to compensatory endocytosis. C_m and R_a measurements were suspended during the step and for 30 ms afterwards. The light gray trace shows an exponential fit (T_{endo}) to the decline with a time constant of 142 ms. Endocytosis kinetics were also measured by determining the time at which the capacitance increase had declined by 50% (t_{50}), which was 213 ms in this example. (Cork & Thoreson, 2014)

We performed a number of control experiments to confirm that capacitance increases represented synaptic exocytosis. 1) Depletion of the releasable pool of vesicles by a 1 s pulse train (25 ms steps to -10 mV at 13.3 Hz) abolished the capacitance increase evoked by a subsequent depolarizing test pulse. The left trace in Fig. 10A shows a capacitance increase evoked by a depolarizing test step (25 ms to -10 mV) prior to the train. Immediately after the train, the response was abolished (center trace, Fig. 10A). The depolarization-evoked capacitance increase subsequently recovered after waiting >1 min for replenishment of the releasable pool of vesicles (right trace, Fig. 10A). 2) Capacitance increases were not consistently correlated with the presence or absence of tail currents following depolarizing steps. Fig. 10B (left traces) shows a recording in which depolarization (25 ms to -10 mV) evoked both a capacitance increase and a brief inward tail current. Application of the same depolarizing step later in the same cell evoked a similar tail current but no capacitance increase (Fig. 10B, center traces). Subsequent application of a 200 ms step evoked a large inward tail current, but also did not evoke a capacitance increase (Fig. 10B, right traces). This indicates that the small tail current evoked by the 25 ms step applied earlier in the same cell was not responsible for the observed capacitance increase (Fig. 10B, left traces). The absence of capacitance increases in the two later traces was presumably due to rundown of exocytosis (Linton et al., 2010). In some cells, we observed outward rather than inward tail currents. These were also not consistently correlated with capacitance increases. Together these experiments showed that, in the absence of any significant change in the resistance trace, tail currents were not responsible for capacitance increases. However, if tail currents were accompanied by large changes in the resistance trace (e.g., the 200 ms record in Fig. 10B, right trace), we excluded those records out of concern that such

large changes in resistance might induce artefacts that could influence capacitance measurements. 3) As expected for exocytosis, there was rundown in the amplitudes of capacitance responses over time (average slope significantly non-zero, P = 0.0015), averaging -5.5 ± 1.3 fF/min (N = 13) for cells stimulated with 10 ms steps (-70 to -10 mV). 4) Depolarization-evoked capacitance increases were unchanged after blocking $I_{Cl(Ca)}$ with niflumic acid (10 ms steps: 0.1 mM t_{50} = 142.7 ± 24.02 ms, N = 8; control t_{50} = 115.6 ± 6.85 ms, N = 58; P = 0.19). Two results from earlier studies provide further evidence that depolarization-evoked capacitance increases in rods are due to exocytosis: 1) The amount of exocytosis measured from capacitance increases was linearly correlated with the amount of release measured by postsynaptic currents in paired recordings from rods and horizontal cells (Rabl et al., 2005). 2) In a model photoreceptor cell, large changes in membrane resistance did not produce a capacitance increase (Rabl et al., 2005).

We tested whether properties of the phase lock amplifier might influence the measured kinetics of endocytosis. Changing the gain of the phase tracking feedback circuitry (by changing the amplifier gain) changed the rise time of depolarization-evoked capacitance increases, quickening it with higher gains, but did not significantly alter endocytosis kinetics (10 ms steps: gain 2 t_{50} = 83.44 ± 5.02 ms, N = 8; gain 5 t_{50} = 86.43 ± 16.68 ms, N = 8; P = 0.88). Slowing the frequency of the sine wave used for capacitance measurements from 500 to 300 Hz also did not significantly alter endocytosis kinetics or amplitude (25 ms steps: 500 Hz t_{50} = 126.6 ± 22.28 ms, amplitude = 100.6 ± 21.11 fF, N = 5; 300 Hz t_{50} = 137.4 ± 25.23 ms, amplitude = 79.9 ± 12.18 fF, N = 5; t_{50} P = 0.62; amplitude P = 0.42). Finally, we obtained similar time constants for endocytosis following 50 ms steps whether we used the phase tracking hardware of the Optopatch amplifier (T_{endo} = 169.5 ± 28.82 ms, N = 15) or the software-

based, dual sine-wave protocol incorporated into JClamp (Scisoft) (Santos-Sacchi, 2004) and implemented with a Multiclamp 700A amplifier (Molecular Devices) (T_{endo} = 176 $\pm$ 37 ms, N = 4).

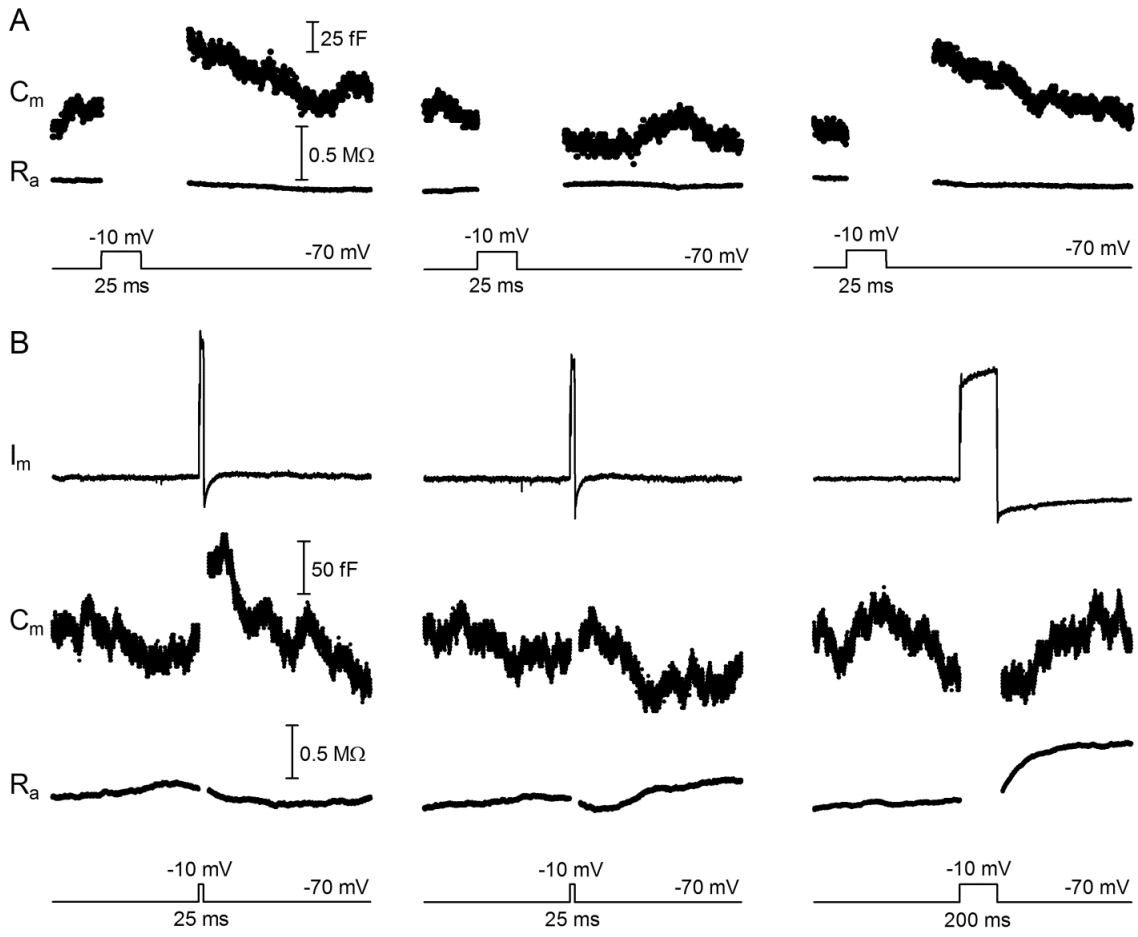

Figure 10: Capacitance changes were not due to conductance or amplifier artifacts.

A) Emptying the releasable pool of vesicles with a 1 s pulse train (25 ms steps to -10 mV at 13.3 Hz) abolished the depolarization-evoked capacitance increase. Three responses recorded in the same cell show the membrane capacitance (C_m) and access resistance (R_a) evoked by a test step (25 ms to -10 mV) prior to the pulse train (left traces), immediately after the pulse train when the vesicle pool was depleted (center traces), and following subsequent recovery of the releasable vesicle pool (right traces). This result is consistent with capacitance increases being due to vesicle exocytosis. B) Capacitance responses are not due to tail currents. A step depolarization (25 ms step to -10 mV) induced a capacitance increase and brief inward tail current (left traces). The same test step applied later in the same cell evoked a similar tail current but did not evoke a capacitance increase (center traces). Subsequent application of a 200 ms test step evoked a large tail current but no capacitance increase (right traces). The absence of a capacitance increase in later records was presumably due to rundown of exocytosis. (Cork & Thoreson, 2014)

3.3b Role of calcium in endocytic load

Next, we tested two factors that are commonly found to regulate the kinetics of endocytosis: the amount of Ca^{2+} influx and the endocytic load (the amount of membrane that needs to be retrieved) (Wu et al., 2014). To do so, we varied Ca^{2+} influx and endocytic load by changing the duration and strength of voltage steps. Longer durations and larger voltage steps promote greater influx of Ca^{2+} and also trigger more exocytosis, and thus a greater endocytic load. The single cell and average traces illustrate that as the step duration increased, the time for the C_m to return to baseline after the step also increased (Fig. 11). Both T_{endo} and t_{50} values increased for steps from 5 to 50 ms and then remained about the same with 100 and 200 ms steps (Fig. 12A-B). Steps longer than 200 ms stimulated large tail currents that were accompanied by large resistance changes that made capacitance measurements of the endocytosis kinetics unreliable.

In addition to longer values for T_{endo}, slowing of the kinetics of endocytosis also involved a lengthening of the plateau in the capacitance trace prior to endocytic retrieval. This plateau tended to increase in length with increasing test step duration (5 ms = 56.1 ± 6.27 ms, N = 14; 10 ms = 54.4 ± 3.12 ms, N = 49; 25 ms = 58.9 ± 8.25 ms, N = 20; 50 ms = 88.8 ± 8.58 ms, N = 14; 100 ms = 106.8 ± 14.72 ms, N = 13; 200 ms = 103.5 ± 15.99 ms, N = 11). Because Ca^{2+} influx increases with longer duration steps, these results are consistent with evidence that endocytosis can be inhibited by high Ca^{2+} concentrations and thereby delay the capacitance decline (von Gersdorff & Matthews, 1994*a*; Wan et al., 2008; Leitz & Kavalali, 2011). However, another possible explanation for lengthening of the plateau is that endocytosis may be balanced by release that continues after the end of the voltage step (e.g., Singer and Diamond, 2006; von Gersdorff et al., 1998). To examine that possibility we obtained paired whole cell recordings from rods and horizontal cells. We stimulated the rod with a depolarizing

voltage step to -10 mV for 200 ms and recorded the excitatory postsynaptic current (EPSC) evoked in the postsynaptic horizontal cell. Fig. 11C shows an EPSC from a single rod/horizontal cell pair as well as the average EPSC from 22 cell pairs. The EPSC persisted for an average of 72.7 ± 13.3 ms (N = 22) after the end of the step. This is slightly shorter than the average plateau duration in the capacitance response evoked by 200 ms steps measured with the same pipette solution (5 mM EGTA; 109.4 ± 19.2 ms, N = 7; P = 0.17), suggesting that continued release may also contribute to lengthening of the plateau with increasing step duration.

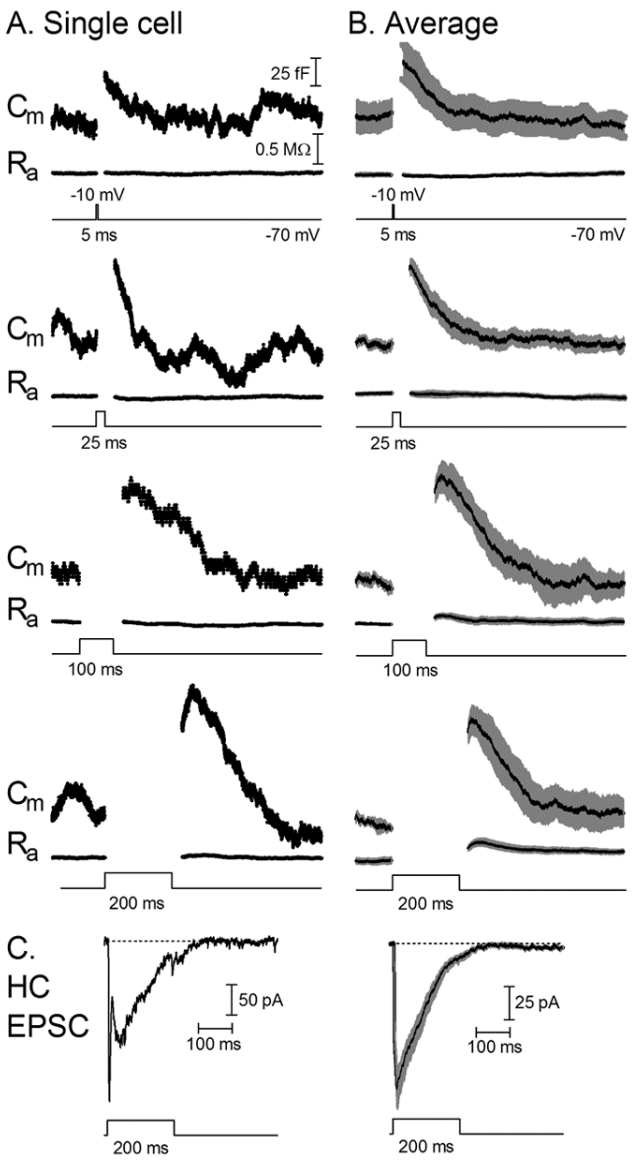

Figure 11: The kinetics of endocytosis slowed with longer duration test steps.

Representative traces from an individual cell (A), all responses from the same cell) and average traces from multiple cells (B) with different duration steps: 5, 25, 100, and 200 ms (-70 to 10 mV). Average traces show the mean in black and SEM in gray (5 ms N = 15, 25 ms N = 21, 100 ms N = 14, 200 ms N = 13). Endocytosis kinetics slowed with longer steps. (C) Excitatory post-synaptic currents evoked in a horizontal cell by stimulation of rods with a depolarizing step (200 ms, -70 to -10 mV). The trace at the left shows an example from a single cell pair and the trace at the right shows the post-synaptic response averaged from 22 cell pairs. (Cork & Thoreson, 2014)

Ca^{2+} influx and endocytic load were also varied by changing the strength of 50 ms depolarizing steps. The voltage step was increased from -40 mV, which is near the threshold for opening of L-type Ca^{2+} channels in rods, up to -10 mV. The voltage needed for maximal Ca^{2+} channel activation is near -20 mV. As the probability of Ca^{2+} channel openings increased, the Ca^{2+} influx and endocytic load also increased. As with increasing step duration, increasing the strength of the voltage step resulted in a slowing of the kinetics of endocytosis as represented by increasing t_{50} values (Fig. 12C).

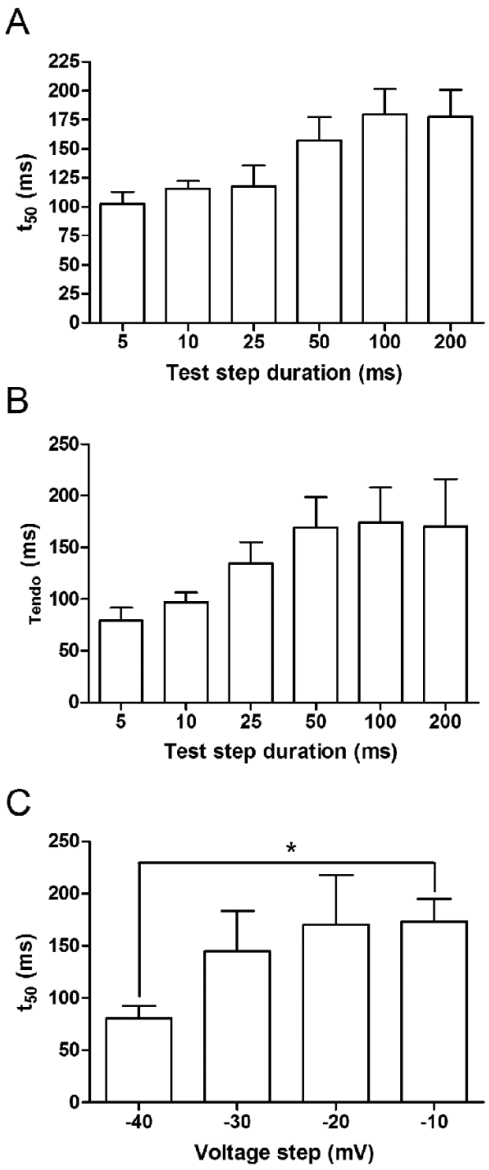

Figure 12: Effects of test step duration and amplitude on endocytosis kinetics.

With longer step durations (5, 10, 25, 50, 100, 200 ms) there was a similar increase in both t_{50} (A) and T_{endo} (B) values. (t_{50}: 5 ms = 102.4 ± 10.33 ms, N = 15; 10 ms = 115.6 ± 6.85 ms, N = 58; 25 ms = 117.9 ± 17.97 ms, N = 20; 50 ms = 157.0 ± 20.19 ms, N = 14; 100 ms = 179.5 ± 21.72 ms, N = 13; 200 ms = 177.4 ± 23.33 ms, N = 11) (T_{endo}: 5 ms = 79.20 ± 12.39 ms, N = 15; 10 ms = 96.89 ± 9.036 ms, N = 54; 25 ms = 134.4 ± 20.72 ms, N = 21; 50 ms = 169.5 ± 28.82 ms, N = 15; 100 ms = 174.4 ± 33.54 ms, N = 13; 200 ms = 170.3 ± 45.96 ms, N = 12). (C) With increasing voltage steps (-70 to -40, -30, -20, and -10 mV; 50 ms) there was an increase in the t_{50} of endocytosis (-40 mV = 80.50 ± 12.17 ms, N = 8; -30 mV = 145.0 ± 38.62 ms, N = 8; -20 mV = 170.5 ± 47.32 ms, N = 11; -10 mV = 172.9 ± 22.03 ms, N = 28; -40 vs. -10 mV, $P < 0.05$). (Cork & Thoreson, 2014)

To assess whether the kinetics of endocytosis depend upon the amount of Ca^{2+} influx, we changed intracellular Ca^{2+} buffering to vary the local Ca^{2+} levels near release sites. In our standard pipette solution we used 1 mM BAPTA, which is a relatively rapid chelator of Ca^{2+} and confines Ca^{2+} to within 100 nm of open Ca^{2+} channels (Van Hook & Thoreson, 2012). We compared this to stronger buffering with 10 mM BAPTA, which abolished endocytosis entirely in mature calyx of Held neurons (Yamashita et al., 2010). We also used the slower Ca^{2+} chelator EGTA at 5 and 0.5 mM concentrations, which allows Ca^{2+} to spread further away from sites of Ca^{2+} entry. These different buffering conditions should produce significant differences in Ca^{2+} concentration at more distant regions of the terminal where endocytosis occurs (Logiudice et al., 2009; Wahl et al., 2013; Fuchs et al. 2014).

For a given Ca^{2+} buffer the amount of release increased with longer step durations up to 200 ms (Fig. 13A). In addition, at a given step duration, decreasing the amount of Ca^{2+} buffering from 10 mM BAPTA to 0.5 EGTA tended to increase the t_{50} value of endocytosis (Fig. 13B). Fast endocytosis persisted with use of 10 mM BAPTA, although the amount of exocytosis was diminished. With weak intracellular Ca^{2+} buffering using 0.5 mM EGTA, test steps longer than 50 ms evoked large tail currents that prevented accurate capacitance measurements. The lengthening of t_{50} values with the shift from a high concentration of the fast buffer BAPTA to a low concentration of the slow buffer EGTA suggests that elevation of cytosolic Ca^{2+} slows endocytosis.

Decreasing Ca^{2+} buffering also increased the amplitude of exocytotic capacitance responses (Fig. 13A), perhaps by stimulating greater release at sites relatively far from the ribbon (Chen et al., 2013, 2014). We therefore tested whether the kinetics of membrane retrieval might also be influenced by endocytic load by plotting t_{50} values against the amount of release (endocytic load) for the different test conditions described

above: different durations, voltage steps, and Ca^{2+} chelators. As shown in Fig. 13C, there was a linear correlation between the slowing of endocytosis and the increase in endocytic load ($r^2 = 0.66$; Fig. 13C) over a range of experimental conditions. This correlation between endocytic load and kinetics held even under conditions where perisynaptic Ca^{2+} levels should be quite different due to the use of different Ca^{2+} buffers. This suggests that endocytic load also regulates the kinetics of endocytosis in rods.

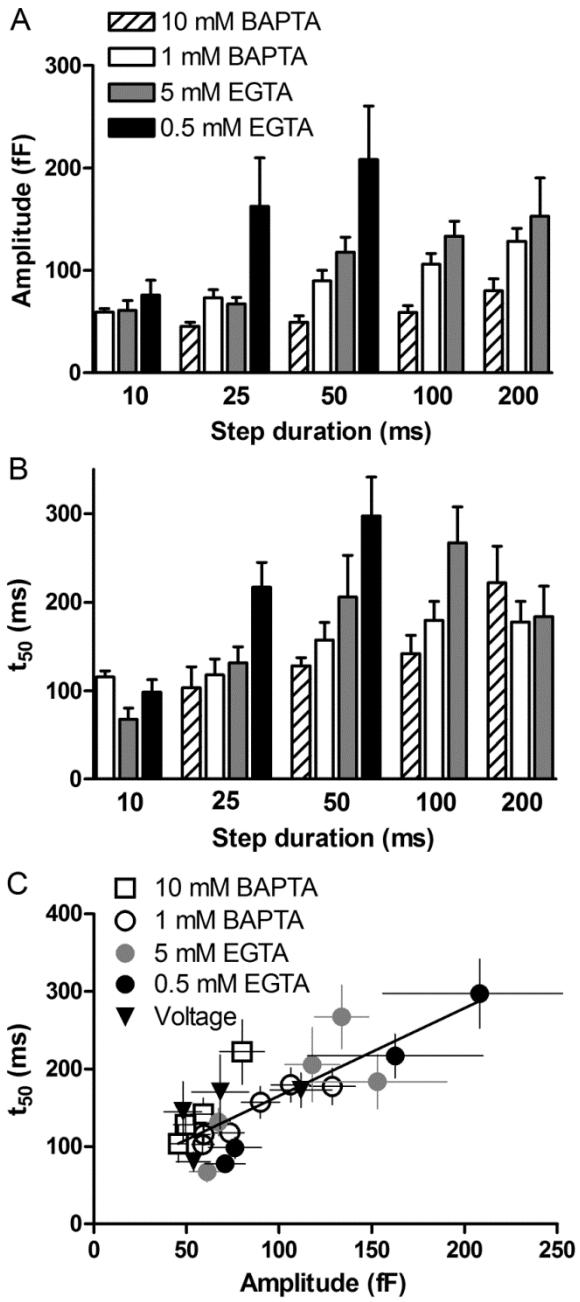

Figure 13: Changes in step duration and Ca^{2+} buffering altered the kinetics of endocytosis.

(A) The amplitude of capacitance increases observed with different test step durations and intracellular Ca^{2+} buffers (10 mM BAPTA, 1 mM BAPTA, 5 mM EGTA, and 0.5 mM EGTA). (B) Average t_{50} for steps of increasing duration measured using the same intracellular Ca^{2+} buffers. (C) There was a linear correlation between t_{50} and the amplitude of exocytosis, which is proportional to endocytic load ($r^2 = 0.66$; slope significantly nonzero, $P < 0.0001$). (Cork & Thoreson, 2014)

3.4 Discussion

Our results indicate that endocytosis in rods involves “ultrafast” retrieval with time constants of less than 300 ms and an onset delay that lengthened with greater release. The rates of retrieval observed in rods were much faster than the fast endocytic component observed in many neurons including bipolar cells (Neves & Lagnado, 1999; Wan & Heidelberger 2011), the calyx of Held (Sun & Wu, 2001), and frog auditory hair cells (Cho et al., 2011). However, ultrafast endocytosis has been observed previously in cones (Van Hook & Thoreson, 2013); mammalian inner hair cells (Beutner et al., 2001), hippocampal neurons (Gandhi & Stevens, 2003; Watanabe et al., 2013*a*), neuromuscular junction (Watanabe et al., 2013*b*), and neuroendocrine cells (Thomas et al., 1994; Artalaejo et al., 1995; Hsu & Jackson, 1996). Kiss-and-run fusion is one potential mechanism for ultrafast endocytosis, but unlike ultrafast endocytosis in rods (Van Hook and Thoreson, 2012) kiss-and-run fusion is not thought to be sensitive to dynamin inhibitors. Furthermore, imaging of single vesicle fusion events suggested that most fusion events in rods involve full collapse of vesicles (Chen et al., 2013).

Most cell types, including bipolar cells and the calyx of Held, exhibit at least two kinetic components to membrane retrieval (von Gersdorff & Matthews, 1994*b*; Neves & Lagnado, 1999; Wu et al., 2005; Dittman & Ryan, 2009). We found that endocytosis in rods following steps up to 200 ms in duration was better fit by a single exponential. Nevertheless, previous studies in enzymatically isolated rods and with longer test steps have shown evidence for a second slower component of retrieval (Rieke & Schwartz, 1996; Thoreson et al., 2004). The presence of clathrin and related endocytic proteins in rod terminals is also consistent with the presence of a slower component of retrieval by

clathrin-mediated endocytosis (Wahl et al., 2013; Fuchs et al., 2014). It is possible that small, slow components of endocytosis may have been obscured by unrelated slow baseline capacitance changes in our recordings. In addition, slow retrieval is typically more prominent after longer steps that stimulate greater Ca^{2+} influx and greater release. In our experiments, such long steps stimulated large Ca^{2+}-activated tail currents and large resistance changes that made measurements of endocytosis unreliable.

Both the amount of preceding exocytosis (endocytic load) and cytosolic Ca^{2+} levels have been shown to promote endocytosis (Yamashita, 2012; Wu et al., 2014). Increases in Ca^{2+} speed endocytosis in many cell types (Wu et al., 2014), but increasing Ca^{2+} influx can also slow endocytosis (Hsu & Jackson, 1996 ; Wu & Betz, 1996 ; Sun & Wu, 2001 ; Sun et al., 2002 ; Oltedal & Hartveit, 2010 ; Cho et al., 2011). Slowing of endocytosis may be caused by global elevation of cytosolic Ca^{2+}, whereas enhancement of endocytosis may be triggered by localized elevation of synaptic Ca^{2+} (Wu & Wu, 2014). In retinal bipolar cells, Ca^{2+} slows the time constant of the slow mode of endocytosis (von Gersdorff & Matthews, 1994*a*; Wan et al., 2008), but can also increase contributions from fast endocytosis without altering the fast time constant (Neves et al., 2001). Mammalian inner hair cells show a similar enhanced contribution from fast endocytosis with increasing Ca^{2+} influx (Beutner et al., 2001; Neef et al., 2014). We found that shifting from high concentrations of the fast Ca^{2+} buffer BAPTA to low concentrations of the slower Ca^{2+} buffer EGTA, which promotes greater increases in perisynaptic Ca^{2+}, was accompanied by a slowing of endocytosis in rods. While this suggests that Ca^{2+} regulates endocytosis kinetics in rods, greater Ca^{2+} influx also stimulates greater release. Unlike other neurons that show a marked cooperativity between Ca^{2+} influx and release, the amount of exocytosis in rods increases linearly with the amount of Ca^{2+} influx (Thoreson et al., 2004). This makes it especially difficult to

distinguish the contributions of endocytic load and intracellular Ca^{2+} in shaping endocytosis kinetics in rods. However, we found that the slowing of endocytosis paralleled increases in endocytic load over a variety of different conditions, including conditions where perisynaptic Ca^{2+} levels should differ considerably (Fig. 13). This is similar to data from other cell types showing that slowing of endocytosis is linearly related to the amount of preceding exocytosis (Sankaranarayanan & Ryan, 2000; Wu et al., 2005; Renden & von Gersdorff, 2007). Slowing of endocytosis with greater release may be due to saturation of endocytic capacity (Wu et al., 2014). Taken together, our results suggest that both Ca^{2+} and endocytic load play a role in regulating endocytosis in rods, similar to other systems (Wu et al., 2014).

The present results provide further evidence that endocytosis mechanisms differ in rod and cone photoreceptors. Endocytosis in both cell types involves ultrafast retrieval. However, ultrafast endocytosis in rods is dynamin-dependent, whereas it is dynamin-independent in cones (Van Hook & Thoreson, 2012). Furthermore, we found that endocytosis in rods slowed with greater Ca^{2+}-triggered release, whereas the time constant of membrane retrieval in cones was independent of both Ca^{2+} and endocytic load. Cones also showed an endocytic overshoot that appeared to be absent from rods (Van Hook & Thoreson, 2012). The molecular mechanisms responsible for rod/cone differences in endocytosis remain to be elucidated. It is possible that rod-cone differences in endocytosis may relate to rod-cone differences in the sites at which release occurs. Release from cones occurs almost exclusively at ribbons (Snellman et al., 2011), whereas a significant amount of release from rods can occur at non-ribbon locations (Chen et al., 2013, 2014). It is plausible that vesicles released at ribbon sites may be retrieved by different mechanisms than vesicles released at non-ribbon sites. Differences in retrieval at ribbon and non-ribbon release sites might also contribute to

differences in kinetics observed within rods under different experimental conditions. In rods, shorter steps and Ca^{2+} increases that remain confined near the ribbon favor more ribbon release, whereas longer steps and greater spread of intraterminal Ca^{2+} favor more non-ribbon release (Chen et al., 2013, 2014). Thus, the faster kinetics of endocytosis observed in rods with shorter steps and stronger Ca^{2+} buffering might reflect a faster retrieval mechanism for ribbon release compared to non-ribbon release.

Exocytosis in rods is continually balanced by endocytosis (Rieke & Schwartz, 1996). Ongoing endocytosis is essential at the rod synapse in order to maintain synaptic signaling, especially during darkness when there is continuous vesicle release for hours at a time. The fast rate of endocytosis may facilitate this balance by helping to rapidly clear previously exocytosed proteins from release sites, readying them for a subsequent round of release (Neher, 2010).

Chapter 4

Summary of exocytosis and endocytosis

The studies in Chapters 2 and 3 characterized exocytosis and endocytosis. Exocytosis and endocytosis are fundamental cellular processes vital to the function of many cell types. Exocytosis allows cells to release molecules to signal to neighboring cells or to interact with the environment. Exocytosis allows cells to secrete many different proteins including enzymes, peptide hormones, and antibodies (Lo Cicero et al., 2015). Exocytosis can also release other molecules including lipids and RNA. In addition, exocytosis delivers proteins to the cell membrane, for example during antigen presentation and recycling of plasma membrane-bound receptors. After exocytosis, endocytosis retrieves the vesicle membrane from the cellular membrane. The endocytosis process that follows exocytosis maintains the structure of the cell and allows for its ongoing function.

These studies focused on the function of exocytosis and endocytosis photoreceptor neurons. Neurons contain synaptic vesicles filled with neurotransmitter. When the neuron is stimulated, synaptic vesicles at the active zone undergo exocytosis thereby releasing neurotransmitter into the synaptic cleft. The neurotransmitter then binds to receptors on the post synaptic neuron, passing the signal downstream. In neurons, the coupling of exocytosis and endocytosis is necessary to maintain the vesicle pool for ongoing signaling. If vesicles were not returned to the synapse after exocytosis via endocytosis, there would not be sufficient vesicles available to be released in response to subsequent stimulation. This would impede the neurons' ability to rapidly and reliably transfer information downstream within the neuronal network. The coupling of exocytosis and endocytosis in neurons also maintains the structure of the synapse.

Proteins localized at the synapse that comprise the cytomatrix at the active zone are vital for neuronal signaling. As exocytosis occurs, the vesicular membrane fuses with the presynaptic membrane. Endocytosis then removes the vesicular membrane restoring the structure of the presynaptic membrane. Without endocytosis the presynaptic membrane would expand and protein localization would be disrupted.

Exocytosis and endocytosis are linked process. The mechanisms involved in the coupling between exocytosis and endocytosis are not currently well characterized and may differ between different types and kinetic components of exocytosis and endocytosis (Haucke et al., 2011). Intracellular Ca^{2+} concentration is a likely contributor to exocytosis and endocytosis coupling. High Ca^{2+} concentrations trigger evoked exocytosis of vesicles. Chapter 2 showed that Ca^{2+} can also trigger spontaneous exocytosis in rod and cone photoreceptors. Chapter 3 demonstrated that the kinetics of endocytosis depend upon the intracellular Ca^{2+} concentration. Coupling of exocytosis and endocytosis by Ca^{2+} provides functional benefits. Intracellular Ca^{2+} is tightly regulated by buffering, extrusion, and sequestration. Therefore, Ca^{2+} can serve as a spatially and temporally constrained mediator of exocytosis and endocytosis. The increase in intracellular Ca^{2+} is proportional to the degree of neuronal stimulation, so Ca^{2+} could serve to link the amount of exocytosis and endocytosis to the activity state of the cell. The gradient of Ca^{2+} within the terminal may allow for differential regulation of exocytosis and endocytosis. The rapid influx of Ca^{2+} following opening of Ca^{2+} channels produces a high concentration of Ca^{2+} at the active zone where vesicles are docked prior to exocytosis. This Ca^{2+} then diffuses within the synaptic terminal and can then regulate endocytosis that occurs after exocytosis in the perisynaptic region around the active zone. Proteins involved in exocytosis and endocytosis including synaptotagmin, synaptobrevin synaptophysin, and dynamin serve as a physical link between the two

processes (Yao et al., 2011; Wu et al., 2014). Ca^{2+} can also play a role in protein-mediated coupling, as many proteins involved in exocytosis and endocytosis can bind Ca^{2+}, triggering changes in their conformation and function. Future work can help clarify the mechanisms that link exocytosis and endocytosis. One method by which these two processes can be studied is by selectively inhibiting endocytosis in order to determine the functional impact on continued exocytosis.

Appendices

Appendix A: Abbreviations

Abbreviation	Term
BAPTA	1,2-bis(o-aminophenoxy)ethane-N,N,N',N'-tetraacetic acid
$[Ca^{2+}]$	concentration of calcium ions
cGMP	cyclic guanosine monophosphate
C_m	membrane capacitance
EAATs	excitatory amino acid transporters
EGTA	ethylene glycol-bis(β-aminoethyl ether)-N,N,N’,N’-tetraacetic acid
GABA	gamma-aminobutyric acid
GDP	guanosine diphosphate
GTP	guanosine triphosphate
GTPγS	guanosine 5'-O-[gamma-thio]triphosphate
mEPSC	miniature excitatory postsynaptic current
mM	millimolar
mV	millivolt
MΩ	megaohm

NAD	nicotinamide adenine dinucleotide
NSF	N-ethylmaleimide sensitive fusion protein
pF	picofarad
pHrodo	10 kD-dextra-conjugated, pH-sensitive form of rhodamine
SNAP-25	synaptosomal associated protein-25
SNARE	soluble NSF attachment protein receptor
t_{50}	time for the increase in C_m following stimulation to decline by 50%
T_{endo}	single exponential fit to the decline in C_m
TIRFM	total internal reflection fluorescence microscopy
VGCCs	voltage-gated Ca^{2+} channels

Appendix B: References

Alabi AA, Tsien RW. (2012). Synaptic vesicle pools and dynamics. *Cold Spring Harbor Perspectives in Biology* 4:a013680.

Artalejo CR, Henley JR, McNiven MA, Palfrey HC. (1995). Rapid endocytosis coupled to exocytosis in adrenal chromaffin cells involves Ca^{2+}, GTP, and dynamin but not clathrin. *Proceedings of the National Academy of Sciences USA* 92:8328-8332.

Ashmore JF, Copenhagen DR. (1983). An analysis of transmission from cones to hyperpolarizing bipolar cells in the retina of the turtle. *The Journal of Physiology* 340:569-97.

Atasoy D, Ertunc M, Moulder KL, Blackwell J, Chung C, Su J, Kavalali ET. (2008). Spontaneous and evoked glutamate release activates two populations of NMDA receptors with limited overlap. *The Journal of Neuroscience* 28(40):10151-66.

Babai N, Morgans CW, Thoreson WB. (2010). Calcium-induced calcium release contributes to synaptic release from mouse rod photoreceptors. *Neuroscience* 165(4):1447-56.

Babai N, Thoreson WB. (2009). Horizontal cell feedback regulates calcium currents and intracellular calcium levels in rod photoreceptors of salamander and mouse retina. *The Journal of Physiology* 587(Pt 10):2353-64.

Ball SL, Powers PA, Shin HS, Morgans CW, Peachey NS, Gregg RG. (2002). Role of the beta(2) subunit of voltage-dependent calcium channels in the retinal outer plexiform layer. *Investigative Ophthalmology & Visual Science* 43(5):1595-603.

Barg S, Machado JD. (2008). Compensatory endocytosis in chromaffin cells. *Acta Physiologica (Oxford)* 192:195-201.

Barnes S, Kelly MEM. (2000). Calcium Channels at the Photoreceptor Synapse. In: Madame Curie Bioscience Database, Landes Bioscience.

Bartoletti TM, Babai N, Thoreson WB. (2010). Vesicle pool size at the salamander cone ribbon synapse. *Journal of Neurophysiology* 103:419-423.

Bartoletti TM, Jackman SL, Babai N, Mercer AJ, Kramer RH, Thoreson WB. (2011). Release from the cone ribbon synapse under bright light conditions can be controlled by the opening of only a few Ca(2+) channels. *Journal of Neurophysiology* 106(6):2922-35.

Berntson A, Taylor WR. (2003). The unitary event amplitude of mouse retinal on-cone bipolar cells. *Visual Neuroscience* 20:621-626.

Beutner D, Voets T, Neher E, Moser T. (2001). Calcium dependence of exocytosis and endocytosis at the cochlear inner hair cell afferent synapse. *Neuron* 29:681-690.

Buhl LK, Jorquera RA, Akbergenova Y, Huntwork-Rodriguez S, Volfson D, Littleton JT. (2013). Differential regulation of evoked and spontaneous neurotransmitter release by C-terminal modifications of complexin. *Molecular and Cellular Neuroscience* 52:161-72.

Bunt AH. (1971). Enzymatic digestion of synaptic ribbons in amphibian retinal photoreceptors. *Brain Research* 25(3):571-7.

Burris C, Klug K, Ngo IT, Sterling P, Schein S. (2002). How Müller glial cells in macaque fovea coat and isolate the synaptic terminals of cone photoreceptors. *Journal of Comparative Neurology* 453(1):100-11.

Cadetti L, Bartoletti TM, Thoreson WB. (2008). Quantal mEPSCs and residual glutamate: how horizontal cell responses are shaped at the photoreceptor ribbon synapse. *European Journal of Neuroscience* 27(10):2575-86.

Cadetti L, Bryson EJ, Ciccone CA, Rabl K, Thoreson WB. (2006). Calcium-induced calcium release in rod photoreceptor terminals boosts synaptic transmission during maintained depolarization. *European Journal of Neuroscience* 23(11):2983-90.

Cadetti L, Tranchina D, Thoreson WB. (2005). A comparison of release kinetics and glutamate receptor properties in shaping rod-cone differences in EPSC kinetics in the salamander retina. *The Journal of Physiology* 569(Pt 3):773-88.

Calkins DJ, Tsukamoto Y, Sterling P. (1996). Foveal cones form basal as well as invaginating junctions with diffuse ON bipolar cells. *Vision Research* 36(21):3373-81.

Carter AG, Regehr WG. (2002). Quantal events shape cerebellar interneuron firing. *Nature Neuroscience* 5(12):1309-18.

Carter-Dawson LD, LaVail MM. (1979). Rods and cones in the mouse retina. I. Structural analysis using light and electron microscopy. *Journal of Comparative Neurology* 188(2):245-62.

Cavelier P, Attwell D. (2007). Neurotransmitter depletion by bafilomycin is promoted by vesicle turnover. *Neuroscience Letters* 412(2):95-100.

Chapman ER. (2008). How does synaptotagmin trigger neurotransmitter release? *Annual Review of Biochemistry* 77:615-41.

Chen M, Krizaj D, Thoreson WB. (2014). Intracellular calcium stores drive slow non-ribbon vesicle release from rod photoreceptors. *Frontiers in Cellular Neuroscience* 8(20):1-16.

Chen M, Van Hook MJ, Zenisek D, Thoreson WB. (2013). Properties of ribbon and non-ribbon release from rod photoreceptors revealed by visualizing individual synaptic vesicles. *The Journal of Neuroscience* 33:2071-2086.

Cho S, Li GL, von Gersdorff H. (2011). Recovery from short-term depression and facilitation is ultrafast and Ca^{2+} dependent at auditory hair cell synapses. *The Journal of Neuroscience* 31:5682-5692.

Choi SY, Jackman S, Thoreson WB, Kramer RH. (2008). Light regulation of Ca^{2+} in the cone photoreceptor synaptic terminal. *Visual Neuroscience* 25(5-6):693-700.

Chung C, Barylko B, Leitz J, Liu X, Kavalali ET. (2010). Acute dynamin inhibition dissects synaptic vesicle recycling pathways that drive spontaneous and evoked neurotransmission. *The Journal of Neuroscience* 30:1363-1376.

Clark D, Dedova I, Cordwell S, Matsumoto I. (2006). A proteome analysis of the anterior cingulate cortex gray matter in schizophrenia. *Molecular Psychiatry* 11(5):459-70, 423.

Coggins MR, Grabner CP, Almers W, Zenisek D. (2007). Stimulated exocytosis of endosomes in goldfish retinal bipolar neurons. *The Journal of Physiology* 584:853-865.

Connaughton V. (2007). Glutamate and Glutamate Receptors in the Vertebrate Retina. *The Organization of the Retina and Visual System*.

Connaughton VP, Graham D, Nelson R. (2004). Identification and morphological classification of horizontal, bipolar, and amacrine cells within the zebrafish retina. *Journal of Comparative Neurology* 477:371–385.

Cork KM, Thoreson WB. (2014). Rapid kinetics of endocytosis at rod photoreceptor synapses depends upon endocytic load and calcium. *Visual Neuroscience* 31(3):227-35.

Cuenca N, Haverkamp S, Kolb H. (2000). Choline acetyltransferase is found in terminals of horizontal cells that label with GABA, nitric oxide synthase and calcium binding proteins in the turtle retina. *Brain Research* 878:228–239.

David C, McPherson PS, Mundigl O, de Camilli P. (1996). A role of amphiphysin in synaptic vesicle endocytosis suggested by its binding to dynamin in nerve terminals. *Proceedings of the National Academy of Sciences* 93(1):331-5.

.

Deak F, Shin OH, Kavalali ET, Sudhof TC. (2006). Structural determinants of synaptobrevin 2 function in synaptic vesicle fusion. *The Journal of Neuroscience* 26:6668–6676.

Deitcher DL, Ueda A, Stewart BA, Burgess RW, Kidokoro Y, Schwarz TL. (1998). Distinct requirements for evoked and spontaneous release of neurotransmitter are revealed by mutations in the Drosophila gene neuronal-synaptobrevin. *The Journal of Neuroscience* 18(6):2028-39.

Deterre P, Bigay J, Forquet F, Robert M, Chabre M. (1988). cGMP phosphodiesterase of retinal rods is regulated by two inhibitory subunits *Proceedings of the National Academy of Sciences* 85(8):2424-8.

DeVries SH. (2000). Bipolar cells use kainate and AMPA receptors to filter visual information into separate channels. *Neuron* 28(3):847-56.

DeVries SH, Li W, Saszik S. (2006). Parallel processing in two transmitter microenvironments at the cone photoreceptor synapse. *Neuron* 50(5):735-48.

DeVries SH, Schwartz EA. (1999). Kainate receptors mediate synaptic transmission between cones and 'Off' bipolar cells in a mammalian retina. *Nature* 397(6715):157-60.

Dittman J, Ryan TA. (2009). Molecular circuitry of endocytosis at nerve terminals. *Annual Review Cell Developmental Biology* 25:133-160.

Dong CJ, McReynolds JS. (1991). The relationship between light, dopamine release and horizontal cell coupling in the mudpuppy retina. *The Journal of Physiology* 440:291-309.

Dowling, JE. (1987). The Retina, Harvard University Press.

Dowling, JE. (2012). The retina: an approachable part of the brain. Belknap Press, Cambridge, MA.

Dowling JE, Werblin FS. (1969). Organization of retina of the mudpuppy, Necturus maculosus. I. Synaptic structure. *Journal of Neurophysiology* 32(3):315-38.

Duncan G, Rabl K, Gemp I, Heidelberger R, Thoreson WB. (2010). Quantitative analysis of synaptic release at the photoreceptor synapse. *Biophysical Journal* 98(10):2102-10.

Edqvist PH, Lek M, Boije H, Lindbäck SM, Hallböök F. (2008). Axon-bearing and axon-less horizontal cell subtypes are generated consecutively during chick retinal development from progenitors that are sensitive to follistatin. *BMC Developmental Biology* 8:46.

Eliasof S, Arriza JL, Leighton BH, Amara SG, Kavanaugh MP. (1998). Localization and function of five glutamate transporters cloned from the salamander retina. *Vision Research* 38(10):1443-54

Emptage NJ, Reid CA, Fine A. (2001). Calcium stores in hippocampal synaptic boutons mediate short-term plasticity, store-operated Ca^{2+} entry, and spontaneous transmitter release. *Neuron* 29(1):197-208.

English JA, Dicker P, Föcking M, Dunn MJ, Cotter DR. (2009). 2-D DIGE analysis implicates cytoskeletal abnormalities in psychiatric disease. *Proteomics* 9(12):3368-82.

Erdmann KS, Mao Y, McCrea HJ, Zoncu R, Lee S, Paradise S, Modregger J, Biemesderfer D, Toomre D, De Camilli P. (2007). A role of the Lowe syndrome protein OCRL in early steps of the endocytic pathway. *Developmental Cell* 13(3):377-90.

Euler T, Haverkamp S, Schubert T, Baden T. (2014). Retinal bipolar cells: elementary building blocks of vision. *Nature Reviews Neuroscience* 15(8):507-19.

Fain GL. (2006). Why photoreceptors die (and why they don't). *Bioessays* 28(4):344-54.

Freed MA, Liang Z. (2014). Synaptic noise is an information bottleneck in the inner retina during dynamic visual stimulation. *The Journal of Physiology* 592(Pt 4):635-51.

Fu Y. (2010). Phototransduction in Rods and Cones. T*he Organization of the Retina and Visual System*. University of Utah Health Sciences Center.

Fuchs M, Brandstätter JH, Regus-Leidig H. (2014). Evidence for a Clathrin-independent mode of endocytosis at a continuously active sensory synapse. *Frontiers in Cellular Neuroscience* 25;8:60.

Gandhi SP, Stevens CF. (2003). Three modes of synaptic vesicular recycling revealed by single-vesicle imaging. *Nature* 423:607-613.

Gao F, Maple BR, Wu SM. (2000). I4AA-Sensitive chloride current contributes to the center light responses of bipolar cells in the tiger salamander retina. *Journal of Neurophysiology* 83(6):3473-82.

Glowatzki E, Fuchs PA. (2002). Transmitter release at the hair cell ribbon synapse. *Nature Neuroscience* 5(2):147-54.

Goswami SP, Bucurenciu I, Jonas P. (2012). Miniature IPSCs in hippocampal granule cells are triggered by voltage-gated Ca^{2+} channels via microdomain coupling. *The Journal of Neuroscience* 32:14294–304.

Gray EG, Pease HL. (1971). On understanding the organisation of the retinal receptor synapses. *Brain Research* 35:1-15.

Graydon CW, Zhang J, Oesch NW, Sousa AA, Leapman RD, Diamond JS. (2014). Passive diffusion as a mechanism underlying ribbon synapse vesicle release and resupply. *The Journal of Neuroscience* 34(27):8948-62.

Groffen AJ, Martens S, Díez Arazola R, Cornelisse LN, Lozovaya N, de Jong AP, Goriounova NA, Habets RL, Takai Y, Borst JG, Brose N, McMahon HT, Verhage M. (2010). Doc2b is a high-affinity Ca^{2+} sensor for spontaneous neurotransmitter release. *Science* 327(5973):1614-8.

Gundelfinger ED, Kessels MM, Qualmann B. (2003). Temporal and spatial coordination of exocytosis and endocytosis. *Nature Review Molecular Cell Biology* 4:127-139.

Hankins, MW. (1995). Horizontal cell coupling and its regulation. *Neurobiology and Clinical Aspects of the Outer Retina* pp 195-220.

Hansen N, Grünewald B, Weishaupt A, Colaço MN, Toyka KV, Sommer C, Geis C. (2013). Human Stiff person syndrome IgG-containing high-titer anti-GAD65 autoantibodies induce motor dysfunction in rats. *Experimental Neurology* 239:202-9.

Harold D, Abraham R, Hollingworth P, Sims R, Gerrish A, Hamshere ML, et al. (2009). Genome-wide association study identifies variants at CLU and PICALM associated with Alzheimer's disease. *Nature Genetics* 41(10):1088-93.

Harsanyi K, Mangel SC. (1993). Modulation of cone to horizontal cell transmission by calcium and pH in the fish retina. *Visual Neuroscience* 10(1):81-91.

Hasegawa J, Obara T, Tanaka K, Tachibana M. (2006). High-density presynaptic transporters are required for glutamate removal from the first visual synapse. *Neuron* 50(1):63-74.

Haucke V, Neher E, Sigrist SJ. (2011). Protein scaffolds in the coupling of synaptic exocytosis and endocytosis. *Nature Reviews Neuroscience* 12:127-138.

Haverkamp S, Grünert U, Wässle H. (2000). The cone pedicle, a complex synapse in the retina. *Neuron* 27(1):85-95.

Heidelberger R. (2001). ATP is required at an early step in compensatory endocytosis in synaptic terminals. *The Journal of Neuroscience* 21:6467-7644.

Heidelberger R, Sterling P, Matthews G. (2002). Roles of ATP in depletion and replenishment of the releasable pool of synaptic vesicles. *Journal of Neurophysiology* 88(1):98-106.

Heidelberger R, Thoreson WB, Witkovsky P. (2005). Synaptic transmission at retinal ribbon synapses. *Progress in Retinal and Eye Research* 24(6):682-720.

Hilfiker S, Pieribone VA, Czernik AJ, Kao HT, Augustine GJ, Greengard P. (1999). Synapsins as regulators of neurotransmitter release. *Philosophical Transactions of the Royal Society B: Biological Sciences* 354(1381):269-79.

Holt M, Cooke A, Wu MM, Lagnado L. (2003). Bulk membrane retrieval in the synaptic terminal of retinal bipolar cells. *The Journal of Neuroscience* 23:1329-1339.

Holt M, Cooke A, Neef A, Lagnado L. (2004). High mobility of vesicles supports continuous exocytosis at a ribbon synapse. *Current Biology* 14(3):173-83.

Hsu SF, Jackson MB. (1996). Rapid exocytosis and endocytosis in nerve terminals of the rat posterior pituitary. *The Journal of Physiology* 494:539-553.

Hua SY, Raciborska DA, Trimble WS, Charlton MP. (1998). Different VAMP/synaptobrevin complexes for spontaneous and evoked transmitter release at the crayfish neuromuscular junction *Journal of Neurophysiology* 80(6):3233-46.

Hua Z, Leal-Ortiz S, Foss SM, Waites CL, Garner CC, et al. (2011). v-SNARE composition distinguishes synaptic vesicle pools. *Neuron* 71:474–87.

Innocenti B, Heidelberger R. (2008). Mechanisms contributing to tonic release at the cone photoreceptor ribbon synapse. *Journal of Neurophysiology* 99:25-36.

Jackman SL, Choi SY, Thoreson WB, Rabl K, Bartoletti TM, Kramer RH. (2009). Role of the synaptic ribbon in transmitting the cone light response. *Nature Neuroscience* 12(3):303-10.

Jockusch WJ, Praefcke GJ, McMahon HT, Lagnado L. (2005). Clathrin-dependent and clathrin-independent retrieval of synaptic vesicles in retinal bipolar cells. *Neuron* 46:869-878.

Johnson JE Jr, Perkins GA, Giddabasappa A, Chaney S, Xiao W, White AD, Brown JM, Waggoner J, Ellisman MH, Fox DA. (2007). Spatiotemporal regulation of ATP and Ca^{2+} dynamics in vertebrate rod and cone ribbon synapses. *Molecular Vision* 13:887-919.

Johnson SL, Thomas MV, Kros CJ. (2002). Membrane capacitance measurement using patch clamp with integrated self-balancing lock-in amplifier. *Pflugers Archive* 443:653-663.

Kaeser PS, Regehr WG. (2014). Molecular mechanisms for synchronous, asynchronous, and spontaneous neurotransmitter release. *Annual Review of Physiology* 76:333-63.

Kandel H, Adhikari P, Shrestha GS, Ruokonen EL, Shah DN. (2012). Visual function in patients on ethambutol therapy for tuberculosis. *Journal of Ocular Pharmacology Ther*apy 28(2):174-8.

Katz, B. (1969). The Release of Neural Transmitter Substances. *The Sherrington Lectures* Thomas, Springfield, IL.

Kavalali ET. (2015). The mechanisms and functions of spontaneous neurotransmitter release. *Nature Reviews Neuroscience* 16(1):5-16.

Kawano T, Indo Y, Nakazato H, Shimadzu M, Matsuda I. (1998). Oculocerebrorenal syndrome of Lowe: three mutations in the OCRL1 gene derived from three patients with different phenotypes. *American Journal of Medical Genetics* 77(5):348-55.

Keating DJ. (2008). Mitochondrial dysfunction, oxidative stress, regulation of exocytosis and their relevance to neurodegenerative diseases *Journal of Neurochemistry* 104(2):298-305.

Kim HG, Miller RF. (1993). Properties of synaptic transmission from photoreceptors to bipolar cells in the mudpuppy retina. *Journal of Neurophysiology* 69(2):352-60.

Koike C, Numata T, Ueda H, Mori Y, Furukawa T (2010). TRPM1: a vertebrate TRP channel responsible for retinal ON bipolar function. *Cell Calcium* 48: 95-101.

Kolb H, Fernandez E, Schouten J, Ahnelt P, Linberg KA, Fisher SK. (1994). Are there three types of horizontal cell in the human retina? *Journal of Comparative Neurology* 343:370–386.

Kombian SB, Hirasawa M, Mouginot D, Chen X, Pittman QJ. (2000). Short-term potentiation of miniature excitatory synaptic currents causes excitation of supraoptic neurons. *Journal of Neurophysiology* 83(5):2542-53.

Krishna VR, Knievel K, Ladha S, Sivakumar K. (2012). Lower extremity predominant stiff-person syndrome and limbic encephalitis with amphiphysin antibodies in breast cancer. *Journal of Clinical Neuromuscular Disease* 14(2):72-4.

Krizaj D. (2005). Serca isoform expression in the mammalian retina. *Experimental Eye Research* 81(6):690-9

Krizaj D. (2012). Calcium stores in vertebrate photoreceptors. *Advances in Experimental Medicine and Biology* 740:873-89.

Krizaj D, Bao JX, Schmitz Y, Witkovsky P, Copenhagen DR. (1999). Caffeine-sensitive calcium stores regulate synaptic transmission from retinal rod photoreceptors. *The Journal of Neuroscience* 19(17):7249-61.

Krizaj D, Copenhagen DR. (1998). Compartmentalization of calcium extrusion mechanisms in the outer and inner segments of photoreceptors. *Neuron* 21(1):249-56.

Krizaj D, Copenhagen DR. (2002). Calcium regulation in photoreceptors. *Frontiers in Bioscience* 7:d2023-44.

Krizaj D, Demarco SJ, Johnson J, Strehler EE, Copenhagen DR. (2002). Cell-specific expression of plasma membrane calcium ATPase isoforms in retinal neurons. *Journal of Comparative Neurology* 451(1):1-21.

Krizaj D, Lai FA, Copenhagen DR. (2003). Ryanodine stores and calcium regulation in the inner segments of salamander rods and cones. *The Journal of Physiology* 547(Pt 3):761-74.

Kuromi H, Kidokoro Y. (2005). Exocytosis and endocytosis of synaptic vesicles and functional roles of vesicle pools: lessons from the Drosophila neuromuscular junction. *Neuroscientist* 11(2):138-47.

Kwok MC, Holopainen JM, Molday LL, Foster LJ, Molday RS. (2008). Proteomics of photoreceptor outer segments identifies a subset of SNARE and Rab proteins implicated in membrane vesicle trafficking and fusion. *Molecular and Cellular Proteomics* 7(6):1053-66.

Lasansky A. (1973). Organization of the outer synaptic layer in the retina of the larval tiger salamander. *Philosophical Transactions of the Royal Society B: Biological Sciences* 265(872):471-89.

Lasansky A. (1978). Contacts between receptors and electrophysiologically identified neurones in the retina of the larval tiger salamander. *The Journal of Physiology* 285:531-42.

Lee A, Wang S, Williams B, Hagen J, Scheetz TE, Haeseleer F. Characterization of Cav1.4 complexes (α11.4, β2, and α2δ4) in HEK293T cells and in the retina. (2015). *The Journal of Biological Chemistry* 290(3):1505-21.

Leitz J, Kavalali ET. (2011). Ca^{2+} influx slows single synaptic vesicle endocytosis. *The Journal of Neuroscience* 31:16318-16326.

Lindstrom SH, Ryan DG, Shi J, DeVries SH. (2014). Kainate receptor subunit diversity underlying response diversity in retinal off bipolar cells. *The Journal of Physiology* 592(Pt 7):1457-77.

Linton JD, Holzhausen LC, Babai N, Song H, Miyagishima KJ, Stearns GW, Lindsay K, Wei J, Chertov AO, Peters TA, Caffe R, Pluk H, Seeliger MW, Tanimoto N, Fong K, Bolton L, Kuok DL, Sweet IR, Bartoletti TM, Radu RA, Travis GH, Zagotta WN, Townes-Anderson E, Parker E, Van der Zee CE, Sampath AP, Sokolov M, Thoreson WB, Hurley JB. (2010). Flow of energy in the outer retina in darkness and in light. *Proceedings of the National Academy of Sciences USA* 107:8599-8604.

Llobet A, Beaumont V, Lagnado L. (2003). Real-time measurement of exocytosis and endocytosis using interference of light. *Neuron* 40:1075–1086.

Llobet A, Gallop JL, Burden JJ, Camdere G, Chandra P, Vallis Y, Hopkins CR, Lagnado L, McMahon HT. (2011). Endophilin drives the fast mode of vesicle retrieval in a ribbon synapse. *The Journal of Neuroscience* 31:8512-8519.

Lo Cicero A, Stahl PD, Raposo G. (2015). Extracellular vesicles shuffling intercellular messages: for good or for bad. *Current Opinion in Cell Biology* 35:69-77.

LoGiudice L, Matthews G. (2007). Endocytosis at ribbon synapses. *Traffic* 8:1123-1128.

LoGiudice L, Sterling P, Matthews G. (2009). Vesicle recycling at ribbon synapses in the finely branched axon terminals of mouse retinal bipolar neurons. *Neuroscience* 164:1546-56.

Lou X, Scheuss V, Schneggenburger R. (2005). Allosteric modulation of the presynaptic Ca2+ sensor for vesicle fusion. *Nature* 435:497–501.

Maple BR, Werblin FS, Wu SM. (1994). Miniature excitatory postsynaptic currents in bipolar cells of the tiger salamander retina. *Vision Research* 34(18):2357-62.

Mariani AP. (1987). Neuronal and synaptic organization of the outer plexiform layer of the pigeon retina. *The American Journal of Anatomy* 179:25–39.

Masland RH. (2012). The tasks of amacrine cells. *Visual Neuroscience* 29(1):3-9.

Matthews G, Fuchs P. (2010) The diverse roles of ribbon synapses in sensory neurotransmission. *Nature Reviews Neuroscience* 11(12):812-22.

Maximov A, Tang J, Yang X, Pang ZP, Südhof TC. (2009). Complexin controls the force transfer from SNARE complexes to membranes in fusion. *Science* 323:516–21.

McKinney RA, Capogna M, Dürr R, Gähwiler BH, Thompson SM. (1999). Miniature synaptic events maintain dendritic spines via AMPA receptor activation. *Nature Neuroscience* 2(1):44-9.

McMahon HT, Boucrot E. (2011). Molecular mechanism and physiological functions of clathrin-mediated endocytosis. *Nature Reviews Molecular Cell Biology* 12(8):517-33.

Melom JE, Akbergenova Y, Gavornik JP, Littleton JT. (2013). Spontaneous and evoked release are independently regulated at individual active zones. *The Journal of Neuroscience* 33(44):17253-63.

Mercer AJ, Rabl K, Riccardi GE, Brecha NC, Stella SL Jr, Thoreson WB. (2011). Location of release sites and calcium-activated chloride channels relative to calcium

channels at the photoreceptor ribbon synapse. *Journal of Neurophysiology* 105(1):321-35.

Mercer AJ, Thoreson WB. (2011). The dynamic architecture of photoreceptor ribbon synapses: cytoskeletal, extracellular matrix, and intramembrane proteins. *Visual Neuroscience* 28(6):453-71.

Miller RF, Gottesman J, Henderson D, Sikora M, Kolb H. (2001). Pre- and postsynaptic mechanisms of spontaneous, excitatory postsynaptic currents in the salamander retina. *Progress in Brain Research* 131:241-53.

Miller TM, Heuser JE. (1984). Endocytosis of synaptic vesicle membrane at the frog neuromuscular junction. *The Journal of Cell Biology* 98:685-698.

Molnar T, Barabas P, Birnbaumer L, Punzo C, Kefalov V, Križaj D. (2012). Store-operated channels regulate intracellular calcium in mammalian rods. *The Journal of Physiology* 590(Pt 15):3465-81.

Morgans CW, Brandstätter JH, Kellerman J, Betz H, Wässle H. (1996). A SNARE complex containing syntaxin 3 is present in ribbon synapses of the retina. *The Journal of Neuroscience* 16(21):6713-21.

Morgans CW, Brown RL, Duvoisin RM. (2010). TRPM1: the endpoint of the mGluR6 signal transduction cascade in retinal ON-bipolar cells. *Bioessays* 32:609-614.

Morgans CW, El Far O, Berntson A, Wässle H, Taylor WR. (1998). Calcium extrusion from mammalian photoreceptor terminals. *The Journal of Neuroscience* 18(7):2467-74.

Nachman-Clewner M, St Jules R, Townes-Anderson E. (1999). L-type calcium channels in the photoreceptor ribbon synapse: localization and role in plasticity. *Journal of Comparative Neurology* 415(1):1-16.

Neef J, Jung S, Wong AB, Reuter K, Pangrsic T, Chakrabarti R, Kügler S, Lenz C, Nouvian R, Boumil RM, Frankel WN, Wichmann C, Moser T. (2014). Modes and regulation of endocytic membrane retrieval in mouse auditory hair cells. *The Journal of Neuroscience* 34:705-716.

Neher E. (2010). What is Rate-Limiting during Sustained Synaptic Activity: Vesicle Supply or the Availability of Release Sites. *Frontiers in Synaptic Neuroscience* 2:144.

Neves G, Lagnado L. (1999). The kinetics of exocytosis and endocytosis in the synaptic terminal of goldfish retinal bipolar cells. *The Journal of Physiology* 515:181-202.

Neves G, Gomis A, Lagnado L. (2001). Calcium influx selects the fast mode of endocytosis in the synaptic terminal of retinal bipolar cells. *Proceedings of the National Academy of Sciences USA* 98:15282-15287.

Nosková L, Stránecký V, Hartmannová H, Přistoupilová A, Barešová V, Ivánek R, Hůlková H, Jahnová H, van der Zee J, Staropoli JF, Sims KB, Tyynelä J, Van Broeckhoven C, Nijssen PC, Mole SE, Elleder M, Kmoch S. (2011). Mutations in DNAJC5, encoding cysteine-string protein alpha, cause autosomal-dominant adult-onset neuronal ceroid lipofuscinosis. *The American Journal of Human Genetics* 89(2):241-52.

O'Brien JJ, Li W, Pan F, Keung J, O'Brien J, Massey SC. (2006). Coupling between A-type horizontal cells is mediated by connexin 50 gap junctions in the rabbit retina. *The Journal of Neuroscience* 26(45):11624-36.

Oltedal L, Hartveit E. (2010). Transient release kinetics of rod bipolar cells revealed by capacitance measurement of exocytosis from axon terminals in rat retinal slices *The Journal of Physiology* 588:1469-1487.

Pang ZP, Bacaj T, Yang X, Zhou P, Xu W, Südhof TC. (2011). Doc2 supports spontaneous synaptic transmission by a Ca(2+)-independent mechanism. *Neuron* 70(2):244-51.

Pelassa I, Zhao C, Pasche M, Odermatt B, Lagnado L. (2014). Synaptic vesicles are "primed" for fast clathrin-mediated endocytosis at the ribbon synapse. *Frontiers in Molecular Neuroscience* 7:91.

Peled ES, Newman ZL, Isacoff EY. (2014). Evoked and spontaneous transmission favored by distinct sets of synapses. *Current Biology* 24(5):484-93.

Pennington K, Beasley CL, Dicker P, Fagan A, English J, Pariante CM, Wait R, Dunn MJ, Cotter DR. (2008). Prominent synaptic and metabolic abnormalities revealed by proteomic analysis of the dorsolateral prefrontal cortex in schizophrenia and bipolar disorder. *Molecular Psychiatry* 13(12):1102-17.

Peters JH, McDougall SJ, Fawley JA, Smith SM, Andresen MC. (2010). Primary afferent activation of thermosensitive TRPV1 triggers asynchronous glutamate release at central neurons. *Neuron* 65:657–69.

Picaud S, Larsson HP, Wellis DP, Lecar H, Werblin F. (1995). Cone photoreceptors respond to their own glutamate release in the tiger salamander. *Proceedings of the National Academy of Sciences* 92(20):9417-21.

Piccolino M, Byzov AL, Kurennyi DE, Pignatelli A, Sappia F, Wilkinson M, Barnes S. (1996). Low-calcium-induced enhancement of chemical synaptic transmission from photoreceptors to horizontal cells in the vertebrate retina. *Proceedings of the National Academy of Sciences* 93(6):2302-6.

Piccolino M, Pignatelli A. (1996). Calcium-independent synaptic transmission: artifact or fact? *Trends in Neuroscience* 19(4):120-5.

Prabakaran S, Swatton JE, Ryan MM, Huffaker SJ, Huang JT, Griffin JL, Wayland M, Freeman T, Dudbridge F, Lilley KS, Karp NA, Hester S, Tkachev D, Mimmack ML, Yolken RH, Webster MJ, Torrey EF, Bahn S. (2004). Mitochondrial dysfunction in schizophrenia: evidence for compromised brain metabolism and oxidative stress. *Molecular Psychiatry* (7):684-97, 643.

Prescott ED, Zenisek D. (2005). Recent progress towards understanding the synaptic ribbon. *Current Opinion in Neurobiology* 15(4):431-6.

Puthussery T, Percival KA, Venkataramani S, Gayet-Primo J, Grünert U, Taylor WR. (2014). Kainate receptors mediate synaptic input to transient and sustained OFF visual pathways in primate retina. *The Journal of Neuroscience* 34(22):7611-21.

Pysh JJ, Wiley RG. (1974). Synaptic vesicle depletion and recovery in cat sympathetic ganglia electrically stimulated in vivo. Evidence for transmitter secretion by exocytosis. *The Journal of Cell Biology* 60:365-374.

Qin N, Yagel S, Momplaisir ML, Codd EE, D'Andrea MR. (2002). Molecular cloning and characterization of the human voltage-gated calcium channel alpha(2)delta-4 subunit. *Molecular Pharmacology* 62(3):485-96.

Rabl K, Cadetti L, Thoreson WB. (2005). Kinetics of exocytosis is faster in cones than in rods. *The Journal of Neuroscience* 25:4633-4640.

Rabl K, Cadetti L, Thoreson WB. (2006). Paired-pulse depression at photoreceptor synapses. *The Journal of Neuroscience* 26:2555-2563.

Raghavachari S, Lisman JE. (2004). Properties of quantal transmission at CA1 synapses*. Journal of Neurophysiology* 92(4):2456-67.

Ramirez DM, Khvotchev M, Trauterman B, Kavalali ET. (2012). Vti1a identifies a vesicle pool that preferentially recycles at rest and maintains spontaneous neurotransmission. *Neuron* 73:121–34.

Ramsey DJ, Ramsey KM, Vavvas DG. (2013) Genetic advances in ophthalmology: the role of melanopsin-expressing, intrinsically photosensitive retinal ganglion cells in the circadian organization of the visual system. *Seminars in Ophthalmology* 28(5-6):406-21.

Rao-Mirotznik R, Buchsbaum G, Sterling P. (1998). Transmitter concentration at a three-dimensional synapse. *Journal of Neurophysiology* 80(6):3163-72.

Rauen T, Wiessner M, Sullivan R, Lee A, Pow DV. (2004). A new GLT1 splice variant: cloning and immunolocalization of GLT1c in the mammalian retina and brain. *Neurochemistry International* 45(7):1095-106.

Raviola E, Gilula NB. (1975). Intramembrane organization of specialized contacts in the outer plexiform layer of the retina. A freeze-fracture study in monkeys and rabbits. *The Journal of Cell Biology* 65(1):192-222.

Rea R, Li J, Dharia A, Levitan ES, Sterling P, Kramer RH. (2004). Streamlined synaptic vesicle cycle in cone photoreceptor terminals. *Neuron* 41(5):755-66.

Renden R, von Gersdorff H. (2007). Synaptic vesicle endocytosis at a CNS nerve terminal: faster kinetics at physiological temperatures and increased endocytic capacity during maturation. *Journal of Neurophysiology* 98:3349-3359.

Rieke F, Schwartz EA. (1996). Asynchronous transmitter release: control of exocytosis and endocytosis at the salamander rod synapse. *The Journal of Physiology* 493:1-8.

Rizo J, Rosenmund C. (2008). Synaptic vesicle fusion. *Nature Structural & Molecular Biology* 15(7):665-74.

Robles E, Laurell E, Baier H. (2014). The retinal projectome reveals brain-area-specific visual representations generated by ganglion cell diversity. *Current Biology* 24(18):2085-96.

Rowan MJ, Ripps H, Shen W. (2010). Fast glutamate uptake via EAAT2 shapes the cone-mediated light offset response in bipolar cells. *The Journal of Physiology* 588(Pt 20):3943-56.

Saito T, Guan F, Papolos DF, Lau S, Klein M, Fann CS, Lachman HM. (2001). Mutation analysis of SYNJ1: a possible candidate gene for chromosome 21q22-linked bipolar disorder. *Molecular Psychiatry* 6(4):387-95.

Sankaranarayanan S, Ryan TA. (2000). Real-time measurements of vesicle-SNARE recycling in synapses of the central nervous system. *Nature Cell Biology* 2:197-204.

Santos-Sacchi J. (2004). Determination of cell capacitance using the exact empirical solution of partial differential Y/partial differential Cm and its phase angle. *Biophysical Journal* 87:714-727.

Sampath AP, Rieke F. (2004) Selective transmission of single photon responses by saturation at the rod-to-rod bipolar synapse. *Neuron* 41(3):431-43.

Scanziani M, Capogna M, Gähwiler BH, Thompson SM. (1992). Presynaptic inhibition of miniature excitatory synaptic currents by baclofen and adenosine in the hippocampus. *Neuron* 9(5):919-27.

Schaeffer SF, Raviola E. (1978). Membrane recycling in the cone cell endings of the turtle retina. *The Journal of Cell Biology* 79:802-825.

Schein S, Ahmad KM. (2005). A clockwork hypothesis: synaptic release by rod photoreceptors must be regular. *Biophysical Journal* 89(6):3931-49.

Scheuber A, Rudge R, Danglot L, Raposo G, Binz T, Poncer JC, Galli T. (2006). Loss of AP-3 function affects spontaneous and evoked release at hippocampal mossy fiber synapses. *Proceedings of the National Academy of Sciences* 103(44):16562-7.

Schmitz F. (2009). The making of synaptic ribbons: how they are built and what they do. *Neuroscientist* 15:611-624.

Schmitz F, Königstorfer A, Südhof TC. (2000). RIBEYE, a component of synaptic ribbons: a protein's journey through evolution provides insight into synaptic ribbon function. *Neuron* 28(3):857-72.

Schnapf JL, Copenhagen DR. (1982). Differences in the kinetics of rod and cone synaptic transmission. *Nature* 296(5860):862-4.

Schnapf JL, Kraft TW, Nunn BJ, Baylor DA. (1988). Spectral sensitivity of primate photoreceptors. *Visual Neuroscience* 1(3):255-61.

Schneider R, Hosy E, Kohl J, Klueva J, Choquet D, Thomas U, Voigt A, Heine M. (2015). Mobility of calcium channels in the presynaptic membrane. *Neuron* 86(3):672-9.

Seshadri S, Fitzpatrick AL, Ikram MA, DeStefano AL, Gudnason V, Boada M, et al. (2010). Genome-wide analysis of genetic loci associated with Alzheimer disease. *JAMA* 303(18):1832-40.

Shen W, Finnegan SG, Slaughter MM. (2004). Glutamate receptor subtypes in human retinal horizontal cells. *Visual Neuroscience* 21(1):89-95.

Sheng Z, Choi SY, Dharia A, Li J, Sterling P, Kramer RH. (2007). Synaptic Ca^{2+} in darkness is lower in rods than cones, causing slower tonic release of vesicles. *The Journal of Neuroscience* 27:5033-5042.

Sherry DM, Heidelberger R. (2005). Distribution of proteins associated with synaptic vesicle endocytosis in the mouse and goldfish retina. *Journal of Comparative Neurology* 484:440-457.

Sherry DM, Mitchell R, Standifer KM, du Plessis B. (2006). Distribution of plasma membrane-associated syntaxins 1 through 4 indicates distinct trafficking functions in the synaptic layers of the mouse retina. *BMC Neuroscience* 7:54.

Shoshan-Barmatz V, Orr I, Martin C, Vardi N. (2005). Novel ryanodine-binding properties in mammalian retina. *The International Journal of Biochemistry & Cell Biology* 37(8):1681-95.

Shoshan-Barmatz V, Zakar M, Shmuelivich F, Nahon E, Vardi N. (2007). Retina expresses a novel variant of the ryanodine receptor. *European Journal of Neuroscience* 26(11):3113-25.

Shoudai K, Peters JH, McDougall SJ, Fawley JA, Andresen MC. (2010). Thermally active TRPV1 tonically drives central spontaneous glutamate release. *The Journal of Neuroscience* 30:14470–75.

Singer JH, Diamond JS. (2006). Vesicle depletion and synaptic depression at a mammalian ribbon synapse. *Journal of Neurophysiology* 95(5):3191-8.

Singer JH, Lassova L, Vardi N, Diamond JS. (2004). Coordinated multivesicular release at a mammalian ribbon synapse. *Nature Neuroscience* 7:826–833.

Smith R, Brundin P, Li JY. (2005) Synaptic dysfunction in Huntington's disease: a new perspective*. Cellular and Molecular Life Sciences* 62(17):1901-12.

Smith SM, Chen W, Vyleta NP, Williams C, Lee CH, Phillips C, Andresen MC. (2012). Calcium regulation of spontaneous and asynchronous neurotransmitter release. *Cell Calcium* 52(3-4):226-33.

Smith SM, Renden R, von Gersdorff H. (2008). Synaptic vesicle endocytosis: fast and slow modes of membrane retrieval. *Trends in Neurosciences* 31:559-568.

Snellman J, Mehta B, Babai N, Bartoletti TM, Akmentin W, Francis A, Matthews G, Thoreson W, Zenisek D. (2011). Acute destruction of the synaptic ribbon reveals a role for the ribbon in vesicle priming. *Nature Neuroscience* 14:1135-1141.

Sterling P, Matthews G. (2005). Structure and function of ribbon synapses. *Trends in Neurosciences* 28:20-29.

Sun J, Pang ZP, Qin D, Fahim AT, Adachi R, Südhof TC. (2007). A dual-Ca2+-sensor model for neurotransmitter release in a central synapse. *Nature* 450:676–82.

Sun JY, Wu LG. (2001). Fast kinetics of exocytosis revealed by simultaneous measurements of presynaptic capacitance and postsynaptic currents at a central synapse. *Neuron* 30:171-182.

Sun JY, Wu XS, Wu LG. (2002). Single and multiple vesicle fusion induce different rates of endocytosis at a central synapse. *Nature* 417:555-559.

Suryanarayanan A, Slaughter MM. (2006). Synaptic transmission mediated by internal calcium stores in rod photoreceptors. *The Journal of Neuroscience* 26(6):1759-66.

Sutton MA, Ito HT, Cressy P, KempAC, Woo JC, Schuman EM. (2006). Miniature neurotransmission stabilizes synaptic function via tonic suppression of local dendritic protein synthesis. *Cell* 125(4):785-99.

Szikra T, Krizaj D. (2006). The dynamic range and domain-specific signals of intracellular calcium in photoreceptors. *Neuroscience* 141(1):143-55.

Szikra T, Krizaj D. (2007). Intracellular organelles and calcium homeostasis in rods and cones. *Visual Neuroscience* 24(5):733-43.

Szmajda BA, Devries SH. (2011). Glutamate spillover between mammalian cone photoreceptors. *The Journal of Neuroscience* 31(38):13431-41.

Tang PH, Kono M, Koutalos Y, Ablonczy Z, Crouch RK. (2013). New insights into retinoid metabolism and cycling within the retina. *Progress in Retinal and Eye Research* 32:48-63. Thomas P, Lee AK, Wong JG, Almers W. (1994). A triggered mechanism retrieves membrane in seconds after Ca($^{2+}$)-stimulated exocytosis in single pituitary cells. *The Journal of Cell Biology* 124:667-675.

Thoreson WB. (2010). Physiology of Photoreceptor Synapses and Other Ribbon Synapses. *Encyclopedia of Eye* vol. 3, pp. 444-450.

Thoreson WB, Mangel SC. (2012). Lateral interactions in the outer retina. *Progress in Retinal and Eye Research* 31(5):407-41.

Thoreson WB, Nitzan R, Miller RF. (1997). Reducing extracellular Cl^- suppresses dihydropyridine-sensitive Ca^{2+} currents and synaptic transmission in amphibian photoreceptors. *Journal of Neurophysiology* 77(4):2175-90.

Thoreson WB, Rabl K, Townes-Anderson E, Heidelberger R. (2004). A highly Ca^{2+}-sensitive pool of vesicles contributes to linearity at the rod photoreceptor ribbon synapse. *Neuron* 42:595-605.

Thoreson WB, Stella SL Jr, Bryson EI, Clements J, Witkovsky P. (2002). D2-like dopamine receptors promote interactions between calcium and chloride channels that diminish rod synaptic transfer in the salamander retina. *Visual Neuroscience* 19(3):235-47.

Thoreson WB, Tranchina D, Witkovsky P. (2003). Kinetics of synaptic transfer from rods and cones to horizontal cells in the salamander retina. *Neuroscience* 122(3):785-98.

Thoreson WB, Witkovsky P. (1999). Glutamate receptors and circuits in the vertebrate retina. *Progress in Retinal and Eye Research* 18(6):765-810.

Tian M, Xu CS, Montpetit R, Kramer RH. (2012). Rab3A mediates vesicle delivery at photoreceptor ribbon synapses. *The Journal of Neuroscience* 32(20):6931-6.

tom Dieck S, Altrock WD, Kessels MM, Qualmann B, Regus H, Brauner D, Fejtová A, Bracko O, Gundelfinger ED, Brandstätter JH. (2005). Molecular dissection of the photoreceptor ribbon synapse: physical interaction of Bassoon and RIBEYE is essential for the assembly of the ribbon complex. *The Journal of Cell Biology* 168(5):825-36.

Townes-Anderson E, MacLeish PR, Raviola E. (1985). Rod cells dissociated from mature salamander retina: ultrastructure and uptake of horseradish peroxidase. *The Journal of Cell Biology* 100:175-188

Ullrich B, Südhof TC. (1994). Distribution of synaptic markers in the retina: implications for synaptic vesicle traffic in ribbon synapses. *Journal of Physiology Paris* 88:249-257.

Ungar D, Hughson FM. (2003). SNARE protein structure and function. *Annual Review of Cell and Developmental Biology* 19:493-517.

Ungar F, Piscopo I, Letizia J, Holtzman E. (1984). Uptake of calcium by the endoplasmic reticulum of the frog photoreceptor. *The Journal of Cell Biology* 98(5):1645-55.

Vaithianathan T, Henry D, Akmentin W, Matthews G. (2015). Functional roles of complexin in neurotransmitter release at ribbon synapses of mouse retinal bipolar neurons. *The Journal of Neuroscience* 35(9):4065-70.

Vaithianathan T, Zanazzi G, Henry D, Akmentin W, Matthews G. (2013). Stabilization of spontaneous neurotransmitter release at ribbon synapses by ribbon-specific subtypes of complexin. *The Journal of Neuroscience* 33(19):8216-26.

Vandenbranden CA, Yazulla S, Studholme KM, Kamphuis W, Kamermans M. (2000). Immunocytochemical localization of the glutamate transporter GLT-1 in goldfish (Carassius auratus) retina. *Journal of Comparative Neurology* 423(3):440-51.

Van Hook MJ, Parmelee CM, Chen M, Cork KM, Curto C, Thoreson WB. (2014). Calmodulin enhances ribbon replenishment and shapes filtering of synaptic transmission by cone photoreceptors. *The Journal of General Physiology* 144(5):357-78.

Van Hook MJ, Thoreson WB. (2012). Rapid synaptic vesicle endocytosis in cone photoreceptors of salamander retina. *The Journal of Neuroscience* 32:18112-18123.

Van Hook MJ, Thoreson WB. (2013). Simultaneous whole-cell recordings from photoreceptors and second-order neurons in an amphibian retinal slice preparation. *Journal of Visualized Experiments* 76: e50007.

Van Hook MJ, Thoreson WB. (2014). Molecular Mechanisms of Photoreceptor Synaptic Transmission. *Vertebrate Photoreceptors* pp 167-198.

von Gersdorff H, Matthews G. (1994)*a*. Inhibition of endocytosis by elevated internal calcium in a synaptic terminal. *Nature* 370:652-655.

von Gersdorff H, Matthews G. (1994)*b*. Dynamics of synaptic vesicle fusion and membrane retrieval in synaptic terminals. *Nature* 367:735-739.

von Gersdorff H, Sakaba T, Berglund K, Tachibana M. (1998). Submillisecond kinetics of glutamate release from a sensory synapse. *Neuron* 1998 21(5):1177-88.

Vyleta NP, Smith SM. (2011). Spontaneous glutamate release is independent of calcium influx and tonically activated by the calcium-sensing receptor. *The Journal of Neuroscience* 31:4593–4606.

Wadiche JI, Jahr CE. (2001). Multivesicular release at climbing fiber-Purkinje cell synapses. *Neuron* 32(2):301-13.

Wahl S, Katiyar R, Schmitz F. (2013). A local, periactive zone endocytic machinery at photoreceptor synapses in close vicinity to synaptic ribbons. *The Journal of Neuroscience* 33:10278-10300.

Waites CL, Garner CC. (2011). Presynaptic function in health and disease. *Trends in Neurosciences* 34:326-337.

Wan QF, Heidelberger R. (2011). Synaptic release at mammalian bipolar cell terminals. *Visual Neuroscience* 28:109-119.

Wan QF, Nixon E, Heidelberger R. (2012). Regulation of presynaptic calcium in a mammalian synaptic terminal. *Journal of Neurophysiology* 108(11):3059-67.

Wan QF, Vila A, Zhou ZY, Heidelberger R. (2008). Synaptic vesicle dynamics in mouse rod bipolar cells. *Visual Neuroscience* 25:523-533.

Watanabe S, Rost BR, Camacho-Pérez M, Davis MW, Söhl-Kielczynski B, Rosenmund C, Jorgensen EM. (2013a). Ultrafast endocytosis at mouse hippocampal synapses. *Nature* 504:242-247.

Watanabe S, Liu Q, Davis MW, Hollopeter G, Thomas N, Jorgensen NB, Jorgensen EM (2013b). Ultrafast endocytosis at Caenorhabditis elegans neuromuscular junctions. *Elife* 2:e00723.

Weber JP, Reim K, Sørensen JB. (2010). Opposing functions of two sub-domains of the SNARE-complex in neurotransmission*. The EMBO Journal* 29:2477–2490.

Williams C, Chen W, Lee CH, Yaeger D, Vyleta NP, Smith SM. (2012). Coactivation of multiple tightly coupled calcium channels triggers spontaneous release of GABA. *Nature Neuroscience* 15:1195–97.

Wu LG, Betz WJ. (1996). Nerve activity but not intracellular calcium determines the time course of endocytosis at the frog neuromuscular junction. *Neuron* 17:769-779.

Wu LG, Hamid E, Shin W, Chiang HC. (2014) Exocytosis and endocytosis: modes, function, and coupling mechanisms. *Annual Review of Physiology* 76: 301-331.

Wu LG, Ryan TA, Lagnado L. (2007). Modes of vesicle retrieval at ribbon synapses, calyx-type synapses, and small central synapses. *The Journal of Neuroscience* 27:11793-117802.

Wu SM, Gao F, Maple BR. (2000). Functional architecture of synapses in the inner retina: segregation of visual signals by stratification of bipolar cell axon terminals. *The Journal of Neuroscience* 20(12):4462-70.

Wu W, Xu J, Wu XS, Wu LG. (2005). Activity-dependent acceleration of endocytosis at a central synapse. *The Journal of Neuroscience* 25:11676-11683.

Wu XS, Wu LG. (2014). The yin and yang of calcium effects of synaptic vesicle endocytosis. *The Journal of Neuroscience* 34: 2652-2659.

Wycisk KA, Budde B, Feil S, Skosyrski S, Buzzi F, Neidhardt J, Glaus E, Nürnberg P, Ruether K, Berger W. (2006). Structural and functional abnormalities of retinal ribbon synapses due to Cacna2d4 mutation. *Investigative Ophthalmology & Visual Science* 47(8):3523-30.

Xin D, Bloomfield SA. (1999). Dark- and light-induced changes in coupling between horizontal cells in mammalian retina. *Journal of Comparative Neurology* 405(1):75-87.

Xu J, McNeil B, Wu W, Nees D, Bai L, Wu LG. (2008). GTP-independent rapid and slow endocytosis at a central synapse. *Nature Neuroscience* 11:45-53.

Xu J, Pang ZP, Shin OH, Südhof TC. (2009). Synaptotagmin-1 functions as a Ca2+ sensor for spontaneous release. *Nature Neuroscience* 12(6):759-66.

Xu JW, Slaughter MM. (2005). Large-conductance calcium-activated potassium channels facilitate transmitter release in salamander rod synapse. *The Journal of Neuroscience* 25(33):7660-8.

Xue L, Mei YA. (2011). Synaptic vesicle recycling at the calyx of Held. *Acta Pharmacologica Sinica* 32:280-287.

Yamashita T. (2012). Ca^{2+}-dependent regulation of synaptic vesicle endocytosis. *Neuroscience Research* 73:1-7.

Yamashita T, Eguchi K, Saitoh N, von Gersdorff H, Takahashi T. (2010) Developmental shift to a mechanism of synaptic vesicle endocytosis requiring nanodomain Ca^{2+}. *Nature Neuroscience* 13:838-844.

Yang JH, Maple B, Gao F, Maguire G, Wu SM. (1998). Postsynaptic responses of horizontal cells in the tiger salamander retina are mediated by AMPA-preferring receptors. *Brain Research* 797(1):125-34.

Yang JH, Wu SM. (1997). Characterization of glutamate transporter function in the tiger salamander retina. *Vision Research* 37(7):827-38.

Yang XL. (2004). Characterization of receptors for glutamate and GABA in retinal neurons. *Progress in Neurobiology* 73(2):127-50.

Yao J, Kwon SE, Gaffaney JD, Dunning FM, Chapman ER. (2011). Uncoupling the roles of synaptotagmin I during endo- and exocytosis of synaptic vesicles. *Nature Neuroscience* 15(2):243-9.

Zampighi GA, Schietroma C, Zampighi LM, Woodruff M, Wright EM, Brecha NC. (2011). Conical tomography of a ribbon synapse: structural evidence for vesicle fusion. *PLOS ONE* 6(3):e16944.

Zenisek D. (2008). Vesicle association and exocytosis at ribbon and extraribbon sites in retinal bipolar cell presynaptic terminals. *Proceedings of the National Academy of Sciences* 105(12):4922-7.

Zenisek D, Matthews G. (2000). The role of mitochondria in presynaptic calcium handling at a ribbon synapse. *Neuron* 25(1):229-37.

Zenisek D, Steyer JA, Feldman ME, Almers W. (2002). A membrane marker leaves synaptic vesicles in milliseconds after exocytosis in retinal bipolar cells. *Neuron* 35:1085–1097.

Zhang AJ, Zhang J, Wu SM. (2006). Electrical coupling, receptive fields, and relative rod/cone inputs of horizontal cells in the tiger salamander retina. *Journal of Comparative Neurology* 499(3):422-31

Zhang YQ, Henderson MX, Colangelo CM, Ginsberg SD, Bruce C, Wu T, Chandra SS. (2012). Identification of CSPα clients reveals a role in dynamin 1 regulation. *Neuron* 74(1):136-50.

Züchner S, Noureddine M, Kennerson M, Verhoeven K, Claeys K, De Jonghe P, Merory J, Oliveira SA, Speer MC, Stenger JE, Walizada G, Zhu D, Pericak-Vance MA, Nicholson G, Timmerman V, Vance JM. (2005). Mutations in the pleckstrin homology domain of dynamin 2 cause dominant intermediate Charcot-Marie-Tooth disease. *Nature Genetics* 37(3):289-94.

Appendix C: Peer-Reviewed Publications

Van Hook MJ, Parmelee CM, Chen M, **Cork KM**, Curto C, Thoreson WB. Calmodulin enhances ribbon replenishment and shapes filtering of synaptic transmission by cone photoreceptors. Journal of General Physiology, 2014 Nov;144(5):357-78.

Cork, KM & Thoreson, WB. Rapid kinetics of endocytosis at rod photoreceptor synapses depends upon endocytic load and calcium. Visual Neuroscience, 2014 May; 31(3):227-35.

Thoreson WB, Mercer AJ, **Cork KM**, Szalewski RJ. Lateral mobility of L-type calcium channels in synaptic terminals of retinal bipolar cells. Molecular Vision. January 7, 2013; 19:16-24.